Eustatic and Tectonic Controls on the Development of the Stratigraphic Architecture of the Cayman Islands, British West Indies

by

Cole Alexander McCormick

A thesis submitted in partial fulfillment of the requirements for the degree of

Master of Science

Department of Earth and Atmospheric Sciences
University of Alberta

Abstract

The Paleogene to Neogene carbonate sedimentary successions that form the cores of each of the Cayman Islands, which are located within 150 km of each other, developed on isolated banks that were surrounded by deep oceanic water. Although each of the Cayman Islands has experienced uniform changes in eustatic sea level, each island is situated atop separate fault blocks that have undergone independent tectonic histories. Cayman Brac for example, was uplifted and tilted between the late Pliocene and ~125 ka, whereas evidence from the stratigraphic framework and $^{87}Sr/^{86}Sr$ isotope ratios suggests that Grand Cayman has been subsiding since the early Miocene. Accordingly, by comparing the successions on each of the Cayman Islands, the impacts of eustasy can be decoupled from the impacts of tectonism.

Each of the cores of the Cayman Islands is comprised by the Bluff Group that includes the Brac Formation (Lower Oligocene), Cayman Formation (Middle Miocene), and Pedro Castle Formation (Pliocene). On western and central Grand Cayman, the Brac Formation is at least 69 m thick, the Cayman Formation is 45 m - 129 m thick, and the Pedro Castle Formation is 0 m - 22 m thick. Six facies have been identified in the Brac Formation (assigned to facies associations FA1 and FA2), whereas nine facies have been identified in the Cayman Formation (assigned to facies associations FA3 and FA4). Antecedent topography on the Brac Unconformity, which forms the upper boundary of the Brac Formation and is located from 72 m - 129 m below sea level, restricted bank circulation and influenced the deposition of the sediments that now form FA3 of the Cayman Formation. FA3, which is 12 m - 73 m thick, consists of a deepening-upwards succession of benthic foraminifera, red algae, bivalve and domal coral grainstone and rudstone that onlapped and filled paleo-topographic lows on the underlying Brac Unconformity. FA4, which is 26 m - 47 m thick with minimal variability, consists of a shallowing-upwards succession of branching coral, rhodolith, green algae, and bivalve wackestone and floatstone. FA3 has an average porosity of 32.5%, an average maximum horizontal permeability (K_{max}) of 2379 mD, and an average vertical permeability (K_{vert}) of 1586 mD, whereas FA4 has an average porosity of 9.3%, an average K_{max} of 1044 mD, and an average K_{vert} of 44.2 mD.

Dedication

This thesis is dedicated to my grandfather, *Gordon W. Friedrick*, who I attribute largely my passion for science and the natural environment. My grandfather, who had to leave the University of Saskatchewan at the age of 19 (1946) to work on the farm, embodies what it means to be a life-long learner. To this day, at the age of 93, he is still curious about the world that surrounds him and shows that you do not necessarily need a degree to be well-educated.

Acknowledgements

I am immeasurably indebted to Dr. Brian Jones, not only for his advice and input towards this thesis, but also for his mentorship throughout my undergraduate degree. Meeting Brian in 2014, when I enrolled in his course on carbonate sedimentology and diagenesis, was indispensable for the passion I have for carbonates, my desired career path, and the eventual topics for both my B.Sc. and M.Sc. thesis projects under his supervision.

I would also like to express my thanks towards Industrial Services and Equipment Ltd. and the Water Authority, Cayman Islands for drilling the wells and assisting Dr. Jones in collecting the samples that were used in this study. I wish to thank the staff in the Department of Earth and Atmospheric Sciences at the University of Alberta, who were instrumental in their assistance with sample preparation and analyses: Diane Caird and Katie Nichols for running the XRD analyses, Walter Harley and Mark Labbe for preparing the thin sections, and Dr. Robert Creaser for running the $^{87}Sr/^{86}Sr$ isotope ratio analyses.

Lastly, I would like to acknowledge the financial support that was provided for this thesis and express gratitude towards the American Association of Petroleum Geologists Foundation (Harold J. Funkhouser Memorial Grant to C. A. McCormick) and the Natural Sciences and Engineering Research Council of Canada (grant ZA635 to Dr. B. Jones).

Table of Contents

Chapter 1: Introduction 1

1.1. Location 1

1.2. Tectonic Setting 2

1.3. Study Area 3

1.4. Stratigraphic Framework 5

1.4.1. Bluff Group - Brac Formation 7

1.4.2. Bluff Group - Cayman Formation 8

1.4.3 Bluff Group - Pedro Castle Formation 9

1.4.4 Ironshore Formation 10

1.4.5. Formational Boundaries 11

1.5. Objectives 12

1.6. Methods 13

Chapter 2: Unconformities in the Paleogene - Neogene Succession on Grand Cayman 15

2.1. Brac Unconformity 15

2.1.1. $^{87}Sr/^{86}Sr$ Isotope Ratio Characterization of the Brac Unconformity 17

2.1.2. Position of the Brac Unconformity on Grand Cayman 22

2.2. Cayman Unconformity 23

2.3. Pedro Castle Unconformity 23

Chapter 3: Facies in the Paleogene - Neogene Succession on Grand Cayman 25

3.1. Facies in the Brac Formation 25

3.1.1. Brac Formation - Facies Association 1 (FA1) 27

3.1.2. Brac Formation - Facies Association 2 (FA2) 29

3.2. Facies in the Cayman Formation 31

3.2.1. Cayman Formation - Facies Association 3 (FA3) 33

3.2.2. Cayman Formation - Facies Association 4 (FA4) 36

3.3. Facies in the Pedro Castle Formation 41

Chapter 4: Facies Architecture and Reservoir Quality on Grand Cayman 42

4.1. Facies Architecture - Western and Central Grand Cayman 42

4.1.1. Formational Boundaries and Thicknesses 42

4.1.2. Facies Architecture in the Brac Formation 44

4.1.3. Facies Architecture in the Cayman Formation 46

4.1.4. Facies Architecture in the Pedro Castle Formation 47

4.2. Reservoir Quality - Western and Central Grand Cayman 48

4.2.1. Porosity and Permeability in the Brac Formation 50

4.2.2. Porosity and Permeability in the Cayman Formation 52

Chapter 5: Interpretation 55

5.1. Paleo-environmental Interpretation of Facies Associations 55

5.1.1. Brac Formation - Facies Association 1 57

5.1.2. Brac Formation - Facies Association 2 59

5.1.3. Cayman Formation - Facies Association 3 60

5.1.4. Cayman Formation - Facies Association 4 62

5.1.5. Pedro Castle Formation 63

5.2. Evolution of the Paleogene - Neogene Carbonate Bank on Grand Cayman 65

5.2.1. Age Constraints in the Paleogene - Neogene Succession 65

5.2.2. Facies Association Boundaries 67

5.2.3. Comparison of Cayman Stratigraphy to Paleo-Eustatic Curves 70

5.2.4. Paleogene - Neogene Bank Architecture 74

Chapter 6: Discussion 78

Chapter 7: Conclusions 82

References 83

List of Tables

Table 1: Table of facies and facies associations in the Brac Formation on Grand Cayman. 28

Table 2: Table of facies and facies associations in the Cayman Formation on Grand Cayman. 34

List of Appendices

Appendix 1: List of samples and data from the wells on western and central Grand Cayman used for this study (see Fig. 2A, 2C for locations), including the maximum depth reached from drilling. 94

Appendix 2: Depth to the top of each formation, facies association, and unconformity identified in this study on western and central Grand Cayman. 95

Appendix 3: List of all $^{87}Sr/^{86}Sr$ isotope ratios used for this study from the wells on western and central Grand Cayman, including the showing sample locations and depths, as well as the 2 standard error for the analysis. 96

List of Figures

Fig. 1. Location and tectonic setting of the Cayman Islands. 2

Fig. 2. Geological maps of Grand Cayman and Cayman Brac. 4

Fig. 3. Stratigraphic succession on the Cayman Islands. 6

Fig. 4. Surface exposures of the Cayman Unconformity and the Brac Unconformity. 16

Fig. 5. Core photo and petrographic photos of the Brac Unconformity in well SHT-4. 18

Fig. 6: $^{87}Sr/^{86}Sr$ isotope ratio vs. depth profile for wells on Grand Cayman. 20

Fig. 7: N - S and W - E cross sections on Grand Cayman. 21

Fig. 8: Litholog of well SHT-4 including the mineralogy and $^{87}Sr/^{86}Sr$ isotope ratios. 26

Fig. 9: Facies 1A core and petrographic photos from SHT-4. 29

Fig. 10: Facies 1B core and petrographic photos from SHT-4. 30

Fig. 11: Facies 2A core and petrographic photos from SHT-4. 31

Fig. 12: Facies 2B core and petrographic photos from SHT-4. 32

Fig. 13: Facies 3A core and petrographic photos from SHT-4. 35

Fig. 14: Facies 3B core and petrographic photos from well LV-2. 36

Fig. 15: Facies 3D core and petrographic photos from LV-2. 37

Fig. 16: Facies 3E core photos from LV-2. 38

Fig. 17: Facies 4A core and petrographic photos from SHT-4. 38

Fig. 18: Facies 4B core and petrographic photos from SHT-4. 39

Fig. 19: Facies 4B core and petrographic photos from wells WMF-1 and LV-2. 40

Fig. 20: Facies 4C core and petrographic photos from SHT-4. 40

Fig. 21: Facies 4C core and petrographic photos from LV-2. 41

Fig. 22: N - S cross section of the facies architecture on western Grand Cayman. 43

Fig. 23: W - E cross section of the facies architecture on west-central Grand Cayman. 43

Fig. 24: Variable dolomitization of the Brac Formation in the wells from the CUC area. 45

Fig. 25: Porosity vs. depth profile in wells SHT-4 and LV-2. 49

Fig. 26: Porosity and permeability plots for the Brac Formation. 51

Fig. 27: Porosity and permeability plots for the Cayman Formation. 53

Fig. 28: Depositional environment schematic for shallow-water carbonate banks. 56

Fig. 29: Diagram showing the distribution of facies in a restricted bank during transgression. 62

Fig. 30: Interpreted sea level curve from the facies and unconformities on Grand Cayman. 66

Fig. 31: Correlation of the succession on Grand Cayman to paleo-eustatic curves. 71

Fig. 32: Idealized diagram showing the minimum subsidence history of Grand Cayman. 72

Fig. 33: Evolution of Grand Cayman from the early Oligocene to modern times. 75

Chapter 1: Introduction

1.1. Location

The Cayman Islands (Fig. 1A) are a British overseas territory in the northwest part of the Caribbean Sea. Grand Cayman (81°24'W, 19°32'N), which is located approximately 325 km southwest of Cuba and 435 km northwest of Jamaica, is the largest of the Cayman Islands with a land surface area of 196 km^2. Cayman Brac (79°80'W, 19°72'N) and Little Cayman (80°04'W, 19°69'N) are approximately 130 km northeast of Grand Cayman; the land surface areas of which are 38 km^2 and 28.5 km^2, respectively.

The Cayman Islands are relatively isolated in the Caribbean Sea and, therefore, the climate is predominantly governed by the sea. This results in a seasonally variable, sub-humid, tropical climate, with wet seasons (summer) and dry seasons (winter). The Cayman Islands are situated at the center of the northeast trade winds belt, and experience relatively stable weather patterns. Seasonal temperatures on Grand Cayman ranges from 11.2°C - 36.5°C (Burton, 1994). Grand Cayman experiences semidiurnal tides, with an average tidal range of 26 cm (Burton, 1994). There is a variation in precipitation across Grand Cayman, with seasonal precipitation increasing from east to west (Ng et al. 1992).

Each of the Cayman Islands has a granodiorite basement that is overlain by volcanic rocks and capped by a succession of carbonate sedimentary rocks (Holcombe et al. 1973; Perfit and Heezen, 1978). The total thickness of the carbonate succession on Grand Cayman is unknown; however, wells drilled in 1956 were still penetrating limestone at a depth of 401 m when drilling ceased (Emery and Milliman, 1980). The stratigraphic architecture of the Cayman Islands reflects 'relative sea level' changes, which is the combined effect of local tectonism and global eustacy (*sensu* Catuneanu et al. 2009, 2011). There are no surface streams or siliciclastic sediments on the islands, because groundwater percolates through the porous bedrock. Instead, relative sea level highstands led to the deposition of the sediments that now form the succession, whereas subaerial erosion during relative sea level lowstands gave rise to the development of unconformities that define the boundaries between the formations (Jones and Hunter, 1994a, 1994b).

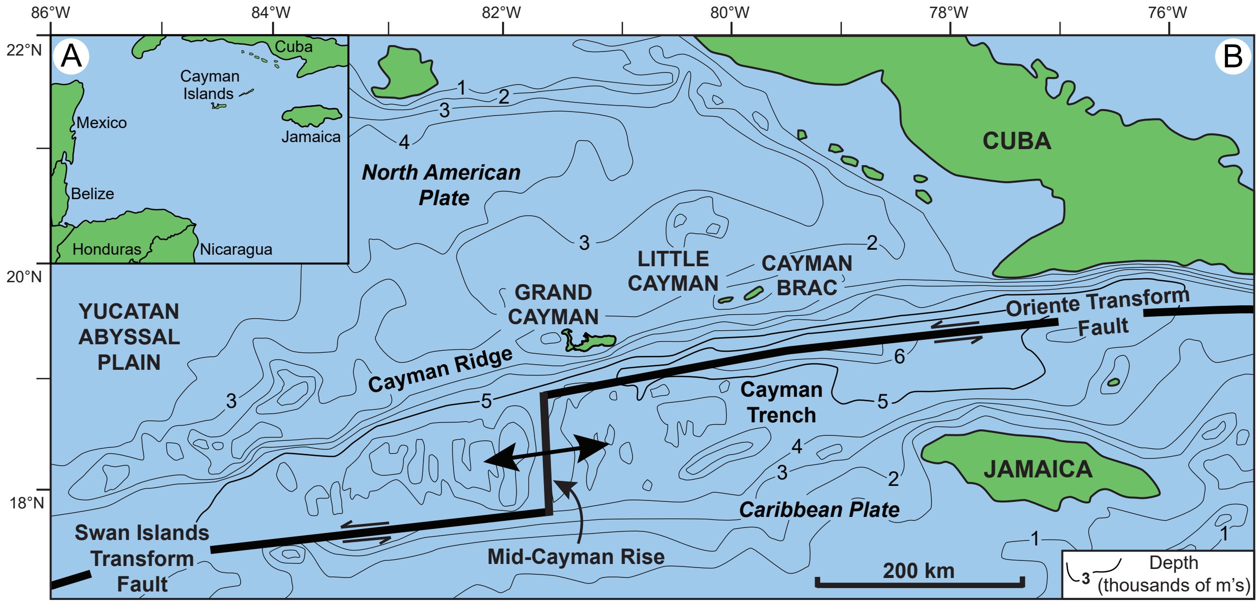

Fig. 1. (A) Location of the Cayman Islands; (B) Locations of Grand Cayman and Cayman Brac relative to the Mid-Cayman Rise, the Cayman Trench, the Swan Hills Transform Fault, and the Oriente Transform Fault (modified from Jones, 1994, and based on maps from Perfit and Heezen, 1978, and MacDonald and Holcombe, 1978).

1.2. Tectonic Setting

Each of the Cayman Islands is located on uplifted fault blocks on the Cayman Ridge (Fig. 1B), which is a submarine mountain range that marks the southern margin of the North American Plate. The Cayman Ridge, which is oriented at 070°, extends westward from the Sierra Maestra of Cuba, through the Cayman Islands, to Belize. The crest of the Cayman Ridge varies in depth from 0 m - 3000 m below sea level (bsl) and is, on average, 65 km wide (Iturralde-Vinent and MacPhee, 1999). Deformation of the Cayman Ridge was initiated during the late Mesozoic and extended through the Early Cenozoic (Iturralde-Vinent, 2006; Boschman et al. 2014). Left lateral strike slip motion of the Caribbean Plate relative to the North American Plate takes place along two transform faults that are oriented parallel to the Cayman Ridge (Rojas-Agramonte et al. 2005; Pindell and Keenan, 2009). The Mid-Cayman Rise (Fig. 1B) is a spreading center with east-west extension that offsets the Oriente Transform Fault (east) from the Swan Islands Transform Fault (west). The Mid-Cayman Rise is 1200 km long, 100 km wide, and is bounded by the Cayman Ridge to the north and the Nicaraguan Plateau to the south (Macdonald and Holcombe, 1978; Hayman et al. 2011). Spreading in the Mid-Cayman Rise was initiated during the Eocene (Perfit and Heezen, 1978) and the Caribbean Plate has been displaced 190 km relative to the North American Plate (Leroy et al. 1996). Global positioning system (GPS) measurements indicate a relative plate movement of 20 mm/yr for the Caribbean Plate in a direction of 070° (Dixon et al. 1998). The Cayman Trench is the deepest part of the Caribbean Sea, reaching depths in excess of 7 km (Fig. 1B). Oceanic crustal thickness along the Cayman Trench varies from 2 km - 3 km near the Mid-Cayman Rise to 7 km - 8 km at the far ends of the trench (ten Brink et al. 2002). This region is still tectonically active, as a 6.8 magnitude earthquake was recorded along the Oriente Transform Fault (18°96', 81°41') on December 14, 2004, and a 7.5 magnitude earthquake was recorded along the Swan Islands Transform Fault (17°48', 83°52') on January 10, 2018 (USGS).

Since the early Miocene (Aquitanian - Burdigalian), local subsidence and extensional faulting, oriented perpendicular to the Oriente and Swan Islands transform faults, has segmented the Cayman Ridge into a series of fault blocks (Perfit and Heezen, 1978; Stoddart, 1980; Iturralde-Vinent and MacPhee, 1999; Iturralde-Vinent, 2006; Hayman et al. 2011). Accordingly, each of the Cayman Islands is situated atop separate fault blocks that have undergone independent tectonic histories. Cayman Brac for example, was uplifted between the late Pliocene and ~125 ka, producing a bedrock succession that dips at 0.5° to the southwest (Zhao and Jones, 2012a). In contrast, there is no evidence that Grand Cayman has been tilted in the same manner. Although there are no regionally correlatable marker beds on Grand Cayman, the bedrock succession appears to be horizontal (Jones and Hunter, 1989; Jones and Hunter, 1994b; Liang and Jones, 2014).

1.3. Study Area

The area examined in this study is located on western and central Grand Cayman (Fig. 2A; 2C) and is bounded by the northern, western, and southern coastlines of the island. The 22 wells (Fig. 2A; 2C; Appendix - 1) evaluated in this study were selected because they: (1) cover western and central Grand Cayman with uniform spacing, (2) yielded core with high recovery, (3) reach depths sufficient to characterize the Brac Formation (Lower Oligocene) as defined by Jones and Luth (2003a), (4) include both the upper 'caprock' and lower 'porous unit' of the Cayman

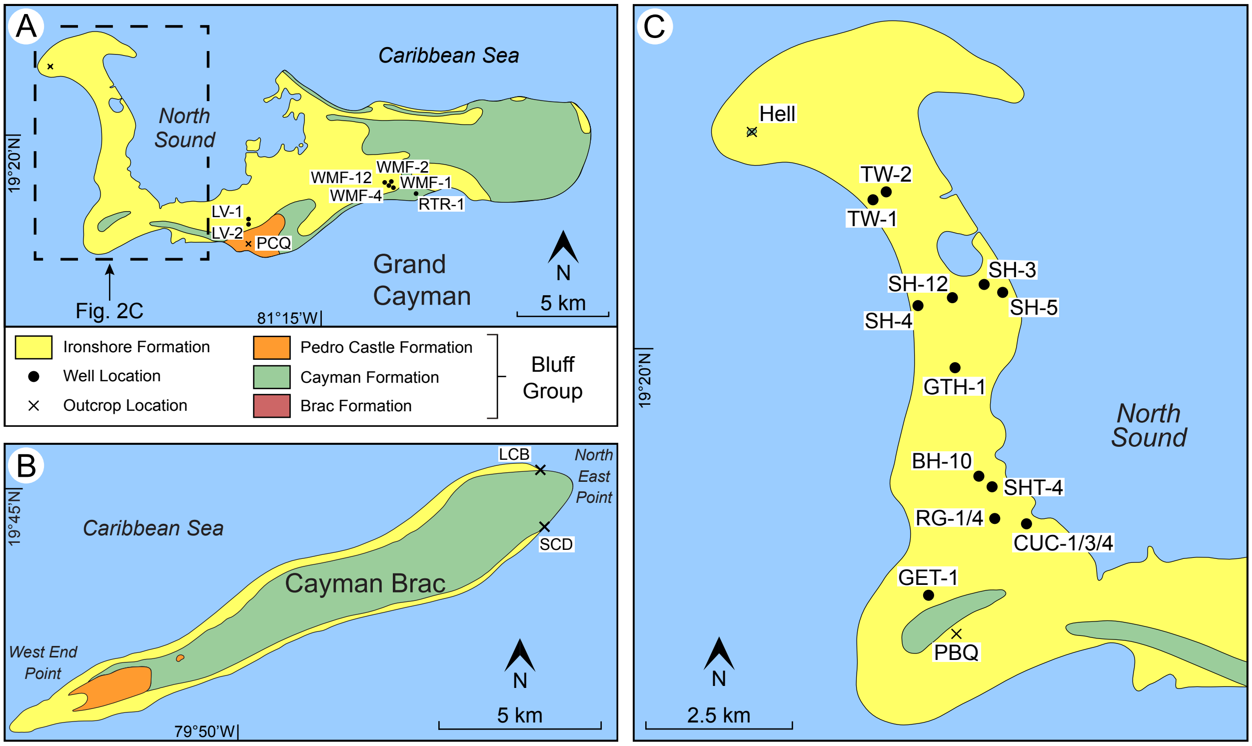

Fig. 2. (A) Geological map of Grand Cayman showing the location of wells and surface exposures; (B) Geological map of Cayman Brac showing key outcrop locations; (C) Detailed geological map of western Grand Cayman showing the location of wells and surface exposures (Modifed from Jones et al., 1994a).

Formation (Middle Miocene) as defined by Jones and Luth (2002), and (5) possess the maximum supplementary data (e.g., thin-sections, porosity/permeability, isotope data, x-ray diffraction, crystal size). Due to the inaccessibility of the heavily vegetated interior of eastern Grand Cayman, most of these wells were drilled on the perimeter of the island. Mechanical limitations of the drilling equipment controlled the depths to which these wells were drilled. The 22 wells used in this study (Appendix - 1) vary in depth from 12 m - 155 m bsl (77 m average). Six wells yielded samples from continuously cored intervals (up to 50 m depth), 4 wells yielded samples from cuttings collected over ~0.76 m intervals while drilling (up to 139 m depth), and 12 wells yielded samples from non-continuous core with cuttings collected between cored intervals (up to 155 m depth). This study expands on previous studies which documented wells LV-2, SHT-4, and CUC-1/3 (Jones and Luth, 2002, 2003a), as well as RTR-1 (Der, 2012; Ren and Jones, 2017).

1.4. Stratigraphic Framework

Matley (1924, 1926) defined the outcropping carbonate succession in the central parts of each of the Cayman Islands as the Bluff Limestone (Tertiary), and those around the islands' peripheries as the Ironshore Formation (Quaternary). The use of the term Bluff Limestone, however, is misleading as the rocks have been pervasively dolomitized (Jones and Hunter, 1989). Accordingly, substantial revisions have been made to the stratigraphic framework (Fig. 3):

(1) Jones and Hunter (1989) renamed the Bluff Limestone as the Bluff Formation, which included the Cayman Member and Pedro Castle Member, the type section being in Pedro Castle Quarry (PCQ) on Grand Cayman (Fig. 2A).

(2) Jones et al. (1994a) formally identified the Brac Formation, which stratigraphically underlies the Bluff Formation, the type section being in outcrop LCB on the northeast coast of Cayman Brac (Fig. 2B).

(3) Jones et al. (1994b) elevated the Bluff Formation to group status, elevated the Cayman Member and Pedro Castle Member to formation status, and included the Brac Formation in the Bluff Group.

As a result, the formal stratigraphic framework for the Cayman Islands (Fig. 3) comprises unconformity-bounded, lithostratigraphic units that can be correlated from island to island (Jones, 1994). The Bluff Group includes the unconformity-bounded Brac Formation (Lower Oligocene), Cayman Formation (Middle Miocene), and Pedro Castle Formation (Pliocene) (Jones et al. 1994b). The Bluff Group is onlapped and overlain by the Ironshore Formation (late Pleistocene). Although later studies proposed informal divisions for the Brac Formation (Uzelman, 2009; Zhao and Jones, 2012b) and the Cayman Formation (Jones and Luth, 2002; Der, 2012; Ren and Jones, 2017), they have not been formally defined. Due to the inherent difficulty of correlating lithologies in carbonate sedimentary successions, ancillary data, such as biostratigraphy and $^{87}Sr/^{86}Sr$ ages have been used to further constrain the stratigraphic framework.

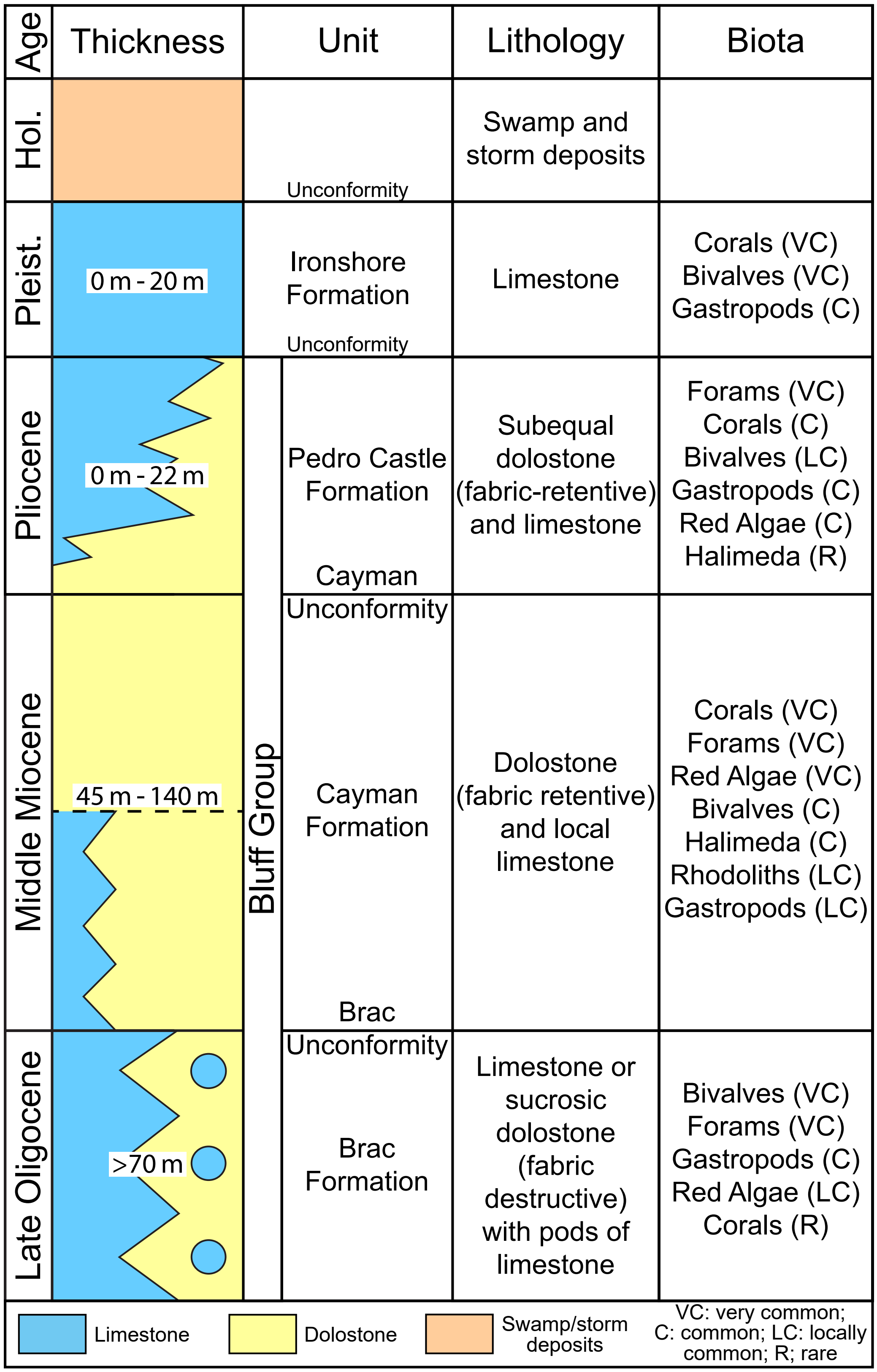

Fig. 3. Stratigraphic succession of the Cayman Islands (modified from Jones, 1994) showing the lithology and dominant biota of each unit.

1.4.1. Bluff Group - Brac Formation

The Brac Formation (Lower Oligocene) outcrops in the vertical cliff faces on the northeast end of Cayman Brac and has been tentatively identified in the subsurface of Cayman Brac and Grand Cayman (Jones et al. 1994a; Jones and Luth, 2003a; Uzelman, 2009; Zhao and Jones, 2012b). The type section for the Brac Formation (outcrop LCB - Fig. 2B), located on the north-east coast of Cayman Brac, consists of *Lepidocyclina*-rich limestone (Jones et al. 1994a). The reference section (outcrop SCD - Fig. 2B), however, located on the southeast coast of Cayman Brac, consists of sucrosic dolostone with isolated pods of *Lepidocyclina*-rich limestone (Jones et al. 1994a). This marked contrast in lithology, which occurs over a distance of 1200 m, complicates the correlation of the Brac Formation between these outcrops and in the subsurface of Cayman Brac and Grand Cayman, where the formation is dolomitic limestone and finely crystalline dolostone, respectively (Jones and Luth, 2003a; Zhao and Jones, 2012b).

The total thickness of the Brac Formation is unknown because the basal contact is not exposed in outcrop and has not been identified in wells drilled on Cayman Brac or Grand Cayman (Jones and Luth, 2003a; Uzelman, 2009; Zhao and Jones, 2012b). The minimum thickness of the Brac Formation on Cayman Brac is 33 m, which was determined from the vertical cliff face beneath the lighthouse at North East Point (Fig. 2B) (Jones et al. 1994a).

The type section for the Brac Formation at locality LCB consists of *Lepidocyclina*-rich limestone (wackestone and packstone) with lesser numbers of other foraminifera (rotalids and miliolids), coralline red algae fragments, molluscs, and echinoid plates (Jones et al. 1994a; Uzelman, 2009). Corals are rare, apart from scattered *Porites* fragments restricted to the uppermost parts of the formation (Jones, 1994). The reference section for the Brac Formation consists of sucrosic dolostone (euhedral crystals, averaging ~1.0 mm in length) with isolated pods of *Lepidocyclina*-rich limestone and dolomitic limestone (Jones et al. 1994a). Foraminifera biostratigraphy (Vaughan, 1926; Matley 1926) and $^{87}Sr/^{86}Sr$ isotope ratios from constituent limestone (average = 0.708189, corresponding to ~28 Ma; Wang et al. 2019, their Fig. 2), that indicate an early Oligocene (Rupelian) age for the Brac Formation (Jones et al. 1994a; Jones and Luth, 2003a). Dolostone sampled from the Brac Formation yield average $^{87}Sr/^{86}Sr$ isotope ratios of 0.708939 (Cayman Brac) and 0.708965 (Grand Cayman), indicating that dolomitization took place during the late Miocene (Tortonian - Messinian) (Jones et al. 1994a; Jones and Luth, 2003a).

1.4.2. Bluff Group - Cayman Formation

The Cayman Formation (Middle Miocene), which is formed largely of fabric-retentive, microcrystalline (euhedral crystals, average 15 μm - 30 μm long) dolostone, is found in surface outcrops and the subsurface of Grand Cayman and Cayman Brac (Jones et al. 1994a, 1994b). The Cayman Formation unconformably overlies the Brac Formation and is up to 140 m thick on Grand Cayman (Jones, 1994; Liang and Jones, 2014; Ren and Jones, 2017). The type section in PCQ on Grand Cayman (Fig. 2A), however, includes only the upper 5.5 m of the Cayman Formation. The biota in the Cayman Formation, which is more diverse than that in the upper part of the Brac Formation, is dominated by corals (domal, branching, platy, free-living), bivalves, foraminifera, coralline red algae, *Halimeda*, and gastropods, with fewer echinoids and rhodoliths (Jones and Hunter, 1989, 1994a; Wignall, 1995; Montpetit, 1998; Willson, 1998; Der, 2012). *Amphistegina* is the most abundant foraminifera in the Cayman Formation, whereas *Lepidocyclina*, which is common in the type section of the Brac Formation, has not been found in the Cayman Formation (Jones et al. 1994a; Jones and Hunter, 1994a).

The age of the Cayman Formation is difficult to establish because of the lack of biostratigraphic index fossils and $^{87}Sr/^{86}Sr$ isotope ratios that have been reset by dolomitization (Pleydell et al. 1990; Jones and Luth, 2003a). Based on the stratigraphic relationship with the overlying and underlying formations, however, it has been suggested that the Cayman Formation is Lower to Middle Miocene (Jones and Hunter, 1994a; Jones and Luth, 2003a). $^{87}Sr/^{86}Sr$ isotope ratios from limestone of the Cayman Formation on the east end of Grand Cayman, which yield a wide range of values (0.70902 - 0.70915), are inconclusive because the constituent carbonate minerals show clear evidence of recrystallization (Der, 2012; Ren and Jones, 2017). $^{87}Sr/^{86}Sr$ isotope ratios from Cayman Formation dolostone indicate that they formed during two phases of dolomitization (late Miocene - early Pliocene and late Pliocene - early Pleistocene) (Jones and Luth, 2003a; Zhao and Jones, 2012a; Ren and Jones, 2017; Wang et al. 2019).

Originally, the Cayman Formation was defined as formed entirely of fabric-retentive, microcrystalline dolostone (Jones and Hunter, 1989; Jones et al. 1994b). This definition was verified in over 100 wells drilled on Grand Cayman and Cayman Brac during the 1990's and early 2000's. At that time, the central part of the east end of Grand Cayman was largely inaccessible and little drilling had been done there. In 2005, however, drilling of wells NSC-1/2/3 in the east-central part of the island revealed a thick succession that included limestone to a depth of ~60 m and dolomitic limestone between 60 m and 122 m. With the aid of additional wells, Der (2012) showed that the central part of the eastern half of Grand Cayman is formed largely of limestone. There is no evidence of structural deformation, such as folding or faulting, which could account for the juxtaposition of this dolostone and limestone (Jones, 1994). Furthermore, the drilling of closely spaced wells on the eastern Grand Cayman has shown that the dolostone found at the island's periphery grade laterally into the interior limestone (Ren and Jones, 2017). Accordingly, the definition of the Cayman Formation has been informally amended to acknowledge that it is formed of limestone and dolostone (Der, 2012, Ren and Jones, 2017).

1.4.3 Bluff Group - Pedro Castle Formation

The Pedro Castle Formation (Pliocene), which unconformably overlies the Cayman Formation, is found in scattered surface outcrops and in the subsurface of Grand Cayman, Cayman Brac, and Little Cayman (Jones, 1994; Jones et al. 1994b; Wignall, 1995; Arts, 2000; MacNeil and Jones, 2003; Etherington, 2004; Jones, 2019). The Pedro Castle Formation is formed of limestone, dolomitic limestone, and dolostone (Jones et al. 1994b; MacNeil and Jones, 2003). Dolomitization of the Pedro Castle Formation varies both laterally and vertically and is commonly fabric-retentive but non-mimetic (MacNeil and Jones, 2003).

On Cayman Brac, the Pedro Castle Formation is restricted to the west end of the island where it is 6 m - 10 m thick (Jones and Hunter, 1994a; MacNeil and Jones, 2003). On western

Grand Cayman, however, the thickness of the Pedro Castle Formation varies considerably. In the type section at Pedro Castle quarry (PCQ - Fig. 2A), the formation 2.5 m thick, whereas in the reference section (well SH-3 - Fig. 2C), it is 21.7 m thick (Jones et al. 1994b).

In the type section, the Pedro Castle Formation consists of off-white dolostone that contains numerous foraminifera (*Amphistegina*), and large, free-living corals (*Trachyphyllia*, *Teleiophyllia*, *Thysanus*), and lesser numbers of coralline red algae fragments, *Halimeda* plates, bivalves, branching corals (*Stylophora*, *Porites*), and echinoid fragments (Jones and Hunter, 1994a; Jones et al. 1994b; Arts, 2000). The reference section for the Pedro Castle Formation on Grand Cayman is formed of limestone, dolomitic limestone, and minor amounts of dolostone that contains a biota similar to that in the type section (Jones et al. 1994b; Wignall, 1995). Based on coral biostratigraphy (*Stylophora*) and $^{87}Sr/^{86}Sr$ isotope ratios from the limestone, the Pedro Castle Formation is Pliocene (Jones et al. 1994b).

1.4.4 Ironshore Formation

The Ironshore Formation (late Pleistocene), which onlaps and overlies the Bluff Group, is evident largely as a coastal platform around the periphery of each of the Cayman Islands (Matley, 1926; Pemberton and Jones, 1988; Jones, 1994). Corals, bivalves, and gastropods are common in the Ironshore Formation (Jones, 1994) along with foraminifera, Halimeda and a diverse suite of well-preserved ichnofossils (Pemberton and Jones, 1988). Aragonitic allochems in the Ironshore Formation are typically well-preserved (Jones et al. 1994b; Jones, 1994).

Although present in the subsurface of the islands, the poorly consolidated, soft, friable nature of the limestone means that core recovery is typically very poor (Jones et al. 1994b; Liang and Jones, 2014). Wells drilled on northeast Grand Cayman (Vezina et al. 1999), and in George Town Harbour (Coyne et al. 2007), however, yielded enough core to determine the internal architecture of the Ironshore Formation. Accordingly, strata in the Ironshore Formation have been formally divided into six (A - F) unconformity-bounded units (Vezina et al. 1999; Coyne et al. 2007). Th/U dates from aragonitic corals indicate that units A - F were deposited from >400 ka to 84 ka (Vezina et al. 1999; Coyne et al. 2007). The Ironshore Formation is typically less than 10 m thick and reaches a maximum thickness of 19 m on the northeast coast of Grand Cayman (Vézina et al. 1999). Unconformities at the tops of each unit are highlighted by terra rossa and/or calcrete (Li and Jones, 2013). Minor amounts of dolomite have been identified in the Unit A of the Ironshore Formation (Li and Jones, 2013). A formal type section/well for the Ironshore Formation has not been proposed.

1.4.5. Formational Boundaries

Delineation of the stratigraphic architecture of the Cayman Islands relies largely on the unconformities found at the top of each formation. These unconformities are karst surfaces that developed when the previously deposited carbonate sequences were subaerially exposed (Jones and Hunter, 1994b; Liang and Jones, 2014). Although these unconformities are discernable in the field, they can be difficult to recognize in the subsurface based on well cuttings and/or non-continuous core. Thus, supplementary data such as biostratigraphy and $^{87}Sr/^{86}Sr$ isotope ratios have been used to establish hiatuses in successions where no obvious unconformity is evident.

Unconformities on the Cayman Islands have typically been named according to the formation which they cap (Jones and Hunter, 1994b; Jones et al. 1994b; Jones, 2016). For example, the Cayman Unconformity denotes the upper boundary of the Cayman Formation. This convention provides no implication regarding the formation that overlies the unconformity. Liang and Jones (2014) proposed an alternate method in which unconformities are named according to the formations below and above the unconformity. For example, the Cayman - Pedro Castle Unconformity separates the Cayman Formation from the overlying Pedro Castle Formation, whereas the Cayman - Ironshore Unconformity is used if the Ironshore Formation directly overlies the Cayman Formation. Although this naming convention is advantageous for specific cases, it has not been widely adopted as it obfuscates the correlation of unconformities overlain by different formations and is inadequate for naming unconformities that form the present-day erosional surface. Herein, the Brac Unconformity denotes the upper boundary of the Brac Formation, the

Cayman Unconformity denotes the upper boundary of the Cayman Formation, and the Pedro Castle Unconformity denotes the upper boundary of the Pedro Castle Formation. In regions where the Pedro Castle Formation or the Cayman Formation are exposed at surface, the modern erosional surface forms their upper boundary. The modern erosional surface typically forms the upper boundary of the Ironshore Formation (Vezina et al. 1999; Coyne et al. 2007). In low lying areas the Ironshore Formation is overlain by mangrove swamp and storm deposits (Woodroffe et al. 1980; Woodroffe, 1981).

1.5. Objectives

The stratigraphy, sedimentology, and diagenesis of the carbonate succession on the Cayman Islands have been meticulously studied and documented (Jones and Hunter, 1989; Pleydell et al. 1990; Jones and Hunter, 1994a, 1994b; Jones et al. 1994a, 1994b; Jones and Luth, 2002, 2003a, 2003b; Uzelman, 2009; Der, 2012; Zhao and Jones, 2012a, 2012b; Liang and Jones, 2014, 2015a, 2015b; Ren and Jones, 2016, 2017, 2018; Jones, 2019). Previous work however, has focused largely on clusters of wells and outcrops in small areas (~10 km^2). Accordingly, the regional geologic controls on the stratigraphy of the Cayman Islands remain poorly constrained. The primary objective of this study, which focuses on western and central Grand Cayman (~120 km^2), is to decouple the impacts of eustacy and tectonism on the development of the Paleogene - Neogene succession on the Cayman Islands. To resolve this, it is first necessary to:

(1) Provide a detailed stratigraphic framework for the Paleogene - Neogene succession on western and central Grand Cayman.

(2) Delineate the Brac Unconformity in the subsurface of Grand Cayman and investigate the influence of antecedent topography on the overlying Cayman Formation.

(3) Constrain the informal division of the upper 'caprock' and the lower 'porous unit' of the Cayman Formation (Jones and Luth, 2002) and investigate the correlation with the diagenetic units proposed by Ren and Jones (2017) on eastern Grand Cayman.

(4) Correlate the stratigraphic framework defined for Grand Cayman to Cayman Brac, which has

experienced uniform eustatic changes in sea level but an independent tectonic history, in order to determine the impact that eustasy and tectonism had on the development of the stratigraphic architecture of the islands.

1.6. Methods

This study is based on samples from surface outcrops and subsurface drill core/cuttings from 22 wells (up to 155 m bsl) on western and central Grand Cayman (Fig. 2A; 2C; Appendix - 1). During the past 35 years, a comprehensive database for the Cenozoic succession on the Cayman Islands has been established through fieldwork and subsurface drilling by Dr. Brian Jones and his graduate students (initiated in 1991). Data from these wells include the well locations, drilling details, thin-sections (140 samples), mineralogy (from x-ray diffraction; 636 samples), $^{87}Sr/^{86}Sr$ isotope ratios (223 samples), and whole rock porosity and permeability (137 samples). Although not the primary focus of this study, dolomite crystal size (measured from SEM), groundwater geochemistry, and $\delta^{18}O$ and $\delta^{13}C$ isotopes are also available. The majority of this dataset was available from samples collected and analysed during past research. Although much of this database was collected prior to this study (e.g. drilling of wells, sampling or core/cuttings data, preparation of thin-section and geochemical data) the observations and interpretations of this data were produced by the author of this thesis. Furthermore, the geochemical data for wells TW-2 and GET-1 (15 XRD samples per well, 15 $^{87}Sr/^{86}Sr$ isotope ratios per well), as well as 15 thin-sections from well SHT-4, are new analyses that are unique to this thesis.

Basic petrography was established by standard thin-section techniques from a total of 140 thin-sections (from 10 wells). Large (7 cm x 5 cm) and small (4.5 cm x 2.5 cm) thin-sections were prepared from samples impregnated with blue epoxy in the Thin-Section Laboratory (University of Alberta). Thin-sections were then stained with Alizarin Red S solution in order to distinguish calcite from dolomite. Mineral compositions of 636 rock samples (1.0 g, powdered) from 12 wells were analyzed using the peak-fitting x-ray diffraction (PF - XRD) method of Jones et al. (2001). In addition to bulk mineralogy, this method allows for the determination of the mol%

$CaCO_3$ (referred to as %Ca) of the constituent dolomites which, following Jones et al. (2001), are separated into low-Ca calcian dolomite (LCD: 50%Ca - 55%Ca) and high-Ca calcian dolomite (HCD: 55%Ca - 62%Ca). This method allows for the determination of the %Ca of dolomite to ±0.5% accuracy, and the weight percentages of each population to ±10% accuracy (Jones et al. 2001). Given the small crystal size of dolomites in the Cayman Formation and the Brac Formation, all XRD and geochemical analyses were based on whole-rock samples. For each well, core samples or drill cuttings formed almost entirely of matrix dolostone or limestone, avoiding large fossils and/or cements, were selected and ground into a fine powder using an agate mortar and pestle. Quartz was then added to each sample as a standard. The powdered samples were scanned using a Rigaku Geigerflex 2173 XRD system with Co Kα radiation from 29° to 38° 2θ at 40 kV and 35 mA following the protocol of Jones et al. (2001). XRD analyses were conducted by the X-Ray Diffraction Laboratory (University of Alberta). $^{87}Sr/^{86}Sr$ isotope ratios were determined for 223 samples (1.0 g, powdered) from 10 wells, following the procedure of MacNeil and Jones (2003) and Jones and Luth (2003a). Mineral compositions (from XRD) have been previously analyzed for those samples prior to $^{87}Sr/^{86}Sr$ analysis. $^{87}Sr/^{86}Sr$ analyses were carried out by the Radiogenic Isotope Laboratory (University of Alberta). Results were normalized to a standard value (0.1194) for $^{86}Sr/^{88}Sr$ and normalized to SRM 987 standard (0.710245). This procedure corrects for the isotopic fractionations between ^{84}Sr, ^{86}Sr, ^{87}Sr and ^{88}Sr that occur during measurement and removes any natural fractionation (McArthur et al. 2012). The 2 standard error of the mean, or 95% confidence interval, for these analyses is ± 0.00002 (McArthur et al. 2012). Porosity and permeability (K_{max}, K_{90}, K_{vert}) measurements were obtained for 137 whole-core samples from 11 wells by Core Laboratories (Calgary, AB). Permeability to air was measured in the horizontal (K_{max}, K_{90}) and vertical (K_{vert}) directions and porosity was determined by the Boyle's Law Technique using helium as the gaseous medium.

Chapter 2: Unconformities in the Paleogene - Neogene Succession on Grand Cayman

The Brac Unconformity, Cayman Unconformity, and Pedro Castle Unconformity are critical elements in defining the stratigraphic framework of the Cayman Islands. These unconformities, however, are a challenge to identify in the subsurface because they may not be immediately discernable in well cuttings and/or non-continuous core. This is particularly true for the Brac Unconformity, given that it is seen only in outcrop on the northeast end of Cayman Brac and little is known about it in the subsurface of Grand Cayman (Jones et al. 1994a; Jones and Luth, 2003a; Uzelman, 2009; Zhao and Jones, 2012b). In part, this is because many of the wells were terminated before the Brac Unconformity was reached. Thus, in order to develop a reliable stratigraphic framework for western and central Grand Cayman, it is first necessary to develop a criterion by which each of these unconformities is identified.

2.1. Brac Unconformity

As originally defined on the northeast end of Cayman Brac, the Brac Unconformity denotes the upper boundary of the Brac Formation (Fig. 4B) (Jones et al. 1994a). The Brac Unconformity formed as a result of subaerial exposure and karst development during the late Oligocene (Chattian) and possibly extended into the early Miocene (Jones et al. 1994a; Liang and Jones, 2014). On Cayman Brac, the Brac Unconformity has an estimated regional dip of 0.5° - 2.0° to the southwest (Jones et al. 1994a; Zhao and Jones, 2012b). Inactive springs that emerged from the Brac Unconformity, which are evident from flowstone deposits on the outcropping cliff faces on the northeast end of Cayman Brac, indicate a permeability contrast between the Brac Formation and the overlying Cayman Formation (Jones et al. 1994a; Uzelman, 2009). Furthermore, the Brac Unconformity commonly forms the roofs of caves in the upper part of the Brac Formation (Jones et al. 1994a). Due to the presence of caymanite (*sensu* Jones, 1992) in solution cavities below the Brac Unconformity, and up to 25 m of topographic relief on the unconformity on the northeast end of Cayman Brac, Jones et al. (1994a) suggested that the Brac Formation underwent subaerial exposure, lithification, and erosion prior to the deposition of the sediments that now comprise the

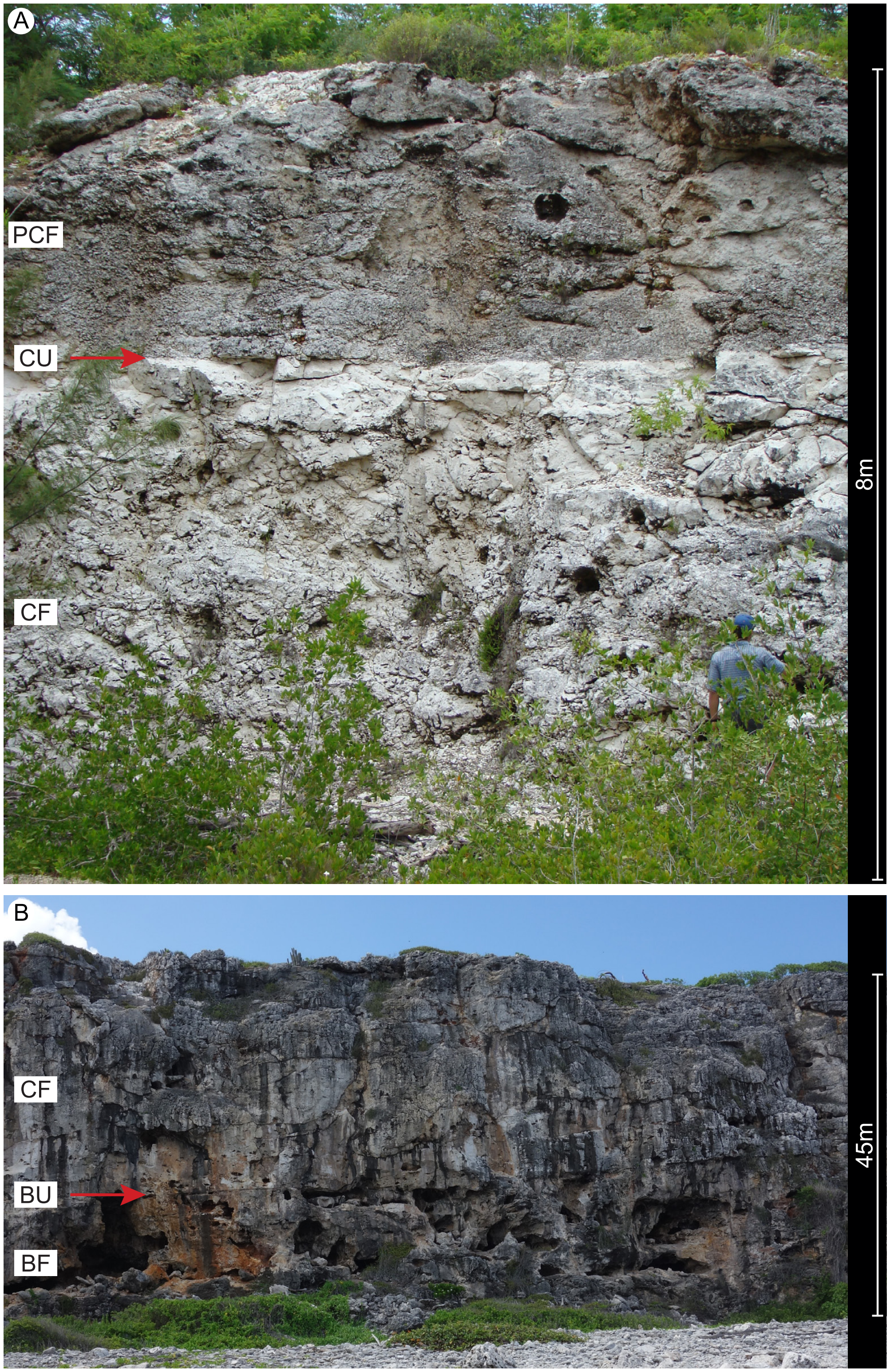

Fig. 4. (A) Surface exposure of the Pedro Castle Formation (PCF), Cayman Unconformity (CU), and Cayman Formation (CF) at Pedro Castle Quarry (PCQ), Grand Cayman; (B) Surface exposure of the Cayman Formation (CF), Brac Unconformity (BU), and Brac Formation (BF) at North East Point, Cayman Brac (see Fig. 2A, 2B for locations). Photographs provided by Dr. B. Jones.

Cayman Formation. Available information suggests that the Brac Unconformity developed over a 12 - 15 million year period during the late Oligocene to early Miocene (Jones and Luth, 2003a; Zhao and Jones, 2012b; Liang and Jones, 2014).

Although the Brac Formation has tentatively been identified in a few wells drilled on Grand Cayman (Jones and Luth, 2003a; Der, 2012; Ren and Jones, 2017), the Brac Unconformity is not visually discernable in the core and/or well-cuttings that were used in those studies. Non-continuous core from well LV-2 (Jones and Luth, 2003a) did not include the Brac Unconformity and it was not identifiable from the well cuttings from RTR-1 (Der, 2012; Ren and Jones, 2017). As a result, other criteria, such as the $^{87}Sr/^{86}Sr$ isotope ratios, were used to locate the position of the Brac Unconformity in those wells (Jones and Luth, 2003a; Der, 2012; Ren and Jones, 2017). SHT-4, which is the deepest well (146 m bsl) drilled on western Grand Cayman, yielded an extensive set of samples that includes non-continuous core, well cuttings, and an extensive petrographic and geochemical database. Furthermore, the Brac Unconformity is only visually discernable in the core from SHT-4 (located at 77 m bsl), where it is a sharp, erosive, subaerial unconformity that is covered and highlighted by a thin (1.0 cm) layer of terra rossa (Fig. 5A; 5B). Accordingly, SHT-4 is herein used as a reference section to establish the criteria by which the Brac Unconformity is identified and correlated in the subsurface of western and central Grand Cayman.

2.1.1. $^{87}Sr/^{86}Sr$ Isotope Ratio Characterization of the Brac Unconformity

In the context of a single subsurface well, with samples obtained from non-continuous core and/or cuttings, the Brac Unconformity is a paraconformity that separates apparently conformable strata. It is, therefore, necessary to establish an integrated approach to the characterization of the Brac Unconformity and develop criteria by which the unconformity can be correlated in wells where data is limited.

Marked breaks in the profile of depth vs. $^{87}Sr/^{86}Sr$ isotope ratio in carbonate strata can be used to establish the position of unconformities in carbonate sedimentary successions (Jones and Luth, 2003a; Liang and Jones, 2014). Marine carbonate sediments preserve the $^{87}Sr/^{86}Sr$ isotope

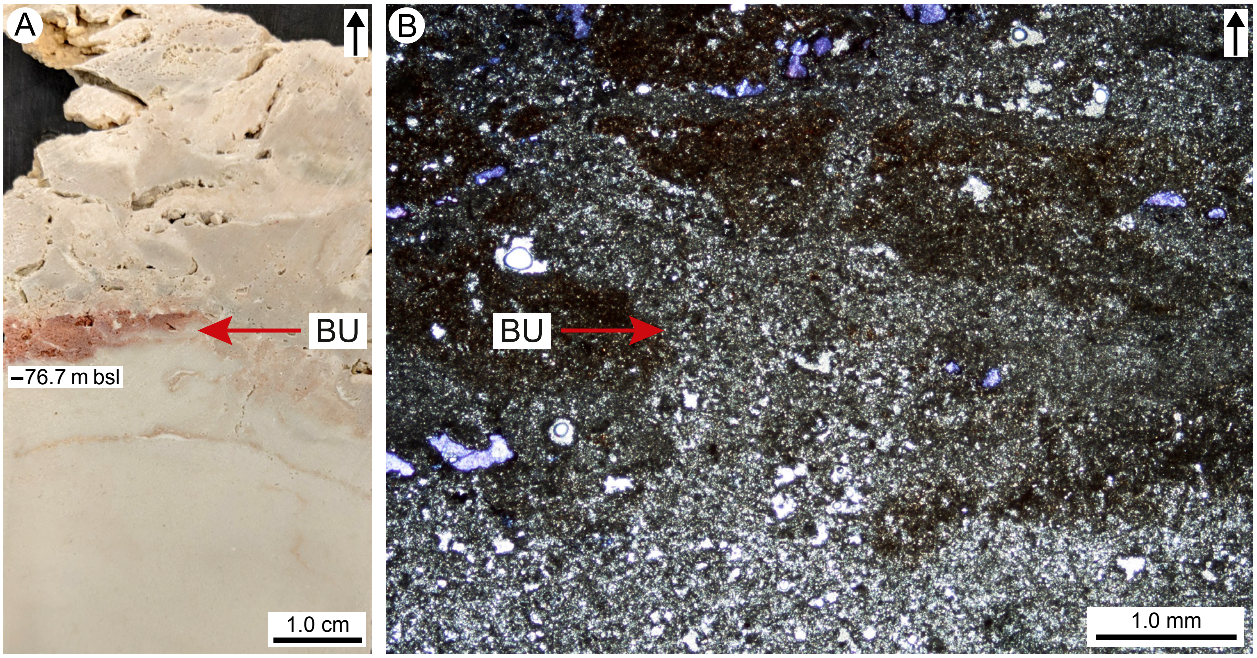

Fig. 5. (A) Core photograph of the Brac Unconformity (BU) in SHT-4, 76.7 m bsl, Grand Cayman; (B) Thin section photomicrograph of the Brac Unconformity (BU) in SHT-4, 76.7 m bsl, plane polarized light (PPL).

ratio of seawater, which has progressively increased since ~40 Ma, at their time of formation (MacArthur et al. 2012; Kuznetsov et al. 2018; Wang et al. 2019). Accordingly, numerous data sets have been assembled to produce curves (e.g., Hodell et al. 1991, their Fig. 1; McArthur et al. 2001, their Fig. 1; MacArthur et al. 2012, their Fig. 7.2; Wang et al. 2019, their Fig. 2) that show how $^{87}Sr/^{86}Sr$ isotope ratios have varied with time. Determining the absolute age from a given $^{87}Sr/^{86}Sr$ isotope ratio, however, must be treated with some caution as $^{87}Sr/^{86}Sr$ isotope ratios are largely overprinted by dolomitization (Swart et al. 1987; Vahrenkamp et al. 1988). Using $^{87}Sr/^{86}Sr$ isotope ratios for the dating of dolostone is valid only if dolomitization was mediated by seawater (Swart et al. 1987; Budd 1997). The $^{87}Sr/^{86}Sr$ isotope ratios of dolostone in the succession can provide the oldest possible age of dolomitization and the youngest possible age of deposition (Vahrenkamp et al. 1988; Vahrenkamp et al. 1991). Furthermore, the age from a given $^{87}Sr/^{86}Sr$ isotope ratio also depends on the $^{87}Sr/^{86}Sr$ age curve that is used, which vary due to analytical uncertainty, the number/type of samples used, and if those samples were free from diagenetic alteration (Hodell et al. 1991; McArthur et al. 2001, 2012; Swart et al. 2001; Wang et al. 2019).

The reported average $^{87}Sr/^{86}Sr$ values of dolostone from the upper part of the Brac Formation is 0.708939 (n = 10) on Cayman Brac (Jones et al. 1994a) and 0.708965 (n = 12) on Grand Cayman (Jones and Luth, 2003a). In contrast, dolostone from the Cayman Formation have an average $^{87}Sr/^{86}Sr$ value of 0.708992 (n = 4) on Cayman Brac (Jones et al. 1994a) and 0.709023 (n = 123) on Grand Cayman (Jones and Luth, 2003a). There is, therefore, a $^{87}Sr/^{86}Sr$ isotope ratio offset of 0.00005 (Cayman Brac) and 0.00006 (Grand Cayman) between the dolostone of the Cayman Formation and the dolostone of the Brac Formation. Limestone and dolomitic limestone samples (n = 19) from the Cayman Formation have an average $^{87}Sr/^{86}Sr$ value of 0.709045 (Ren and Jones, 2017), indicating that this offset cannot be attributed to dolomitization. The 2 standard error of the mean, or 95% confidence interval, for these analyses is ± 0.00002 (McArthur et al. 2012). Following Jones et al. (2003a), the position of the Brac Unconformity is herein established by utilizing marked breaks in the profile of depth vs. $^{87}Sr/^{86}Sr$ isotope ratio in each well (Appendix - 3; Fig. 6).

In SHT-4, $^{87}Sr/^{86}Sr$ isotope ratios from dolostone in the upper part of the Brac Formation have an average value of 0.70895 (n = 3), whereas the $^{87}Sr/^{86}Sr$ isotope ratios from the basal dolostone of the overlying Cayman Formation have an average value of 0.70903 (n = 3). There is, therefore, an offset of 0.00008 in the profile of depth vs. $^{87}Sr/^{86}Sr$ isotope ratio across the Brac Unconformity in SHT-4 (Fig. 7A). This offset is evident in all the wells on western Grand Cayman that intersected the Brac Unconformity and is therefore used to correlate this boundary from well to well. The $^{87}Sr/^{86}Sr$ isotope ratio offset across the Brac Unconformity in wells drilled on western Grand Cayman ranges from 0.00006 in CUC-4, to 0.00009 in GET-1 and GTH-1 (Fig. 7A). On central Grand Cayman, the Brac Unconformity has a $^{87}Sr/^{86}Sr$ isotope ratio offset that ranges from 0.00008 in RTR-1 to 0.00011 in LV-2 (Fig. 7B).

In addition to the offset in the profile of depth vs. $^{87}Sr/^{86}Sr$ isotope ratio, the pattern of the profile of depth vs. $^{87}Sr/^{86}Sr$ isotope ratio itself is indicative of the position of the Brac Unconformity. In wells CUC-3, RG-1, and CUC-4 for example (Fig. 6), the profile of depth vs. $^{87}Sr/^{86}Sr$ isotope ratio of the Cayman Formation follows a smooth trend line that ranges from ~0.708975 in the basal part of the Cayman Formation to ~0.709050 in the upper part of the Cayman Formation. In the

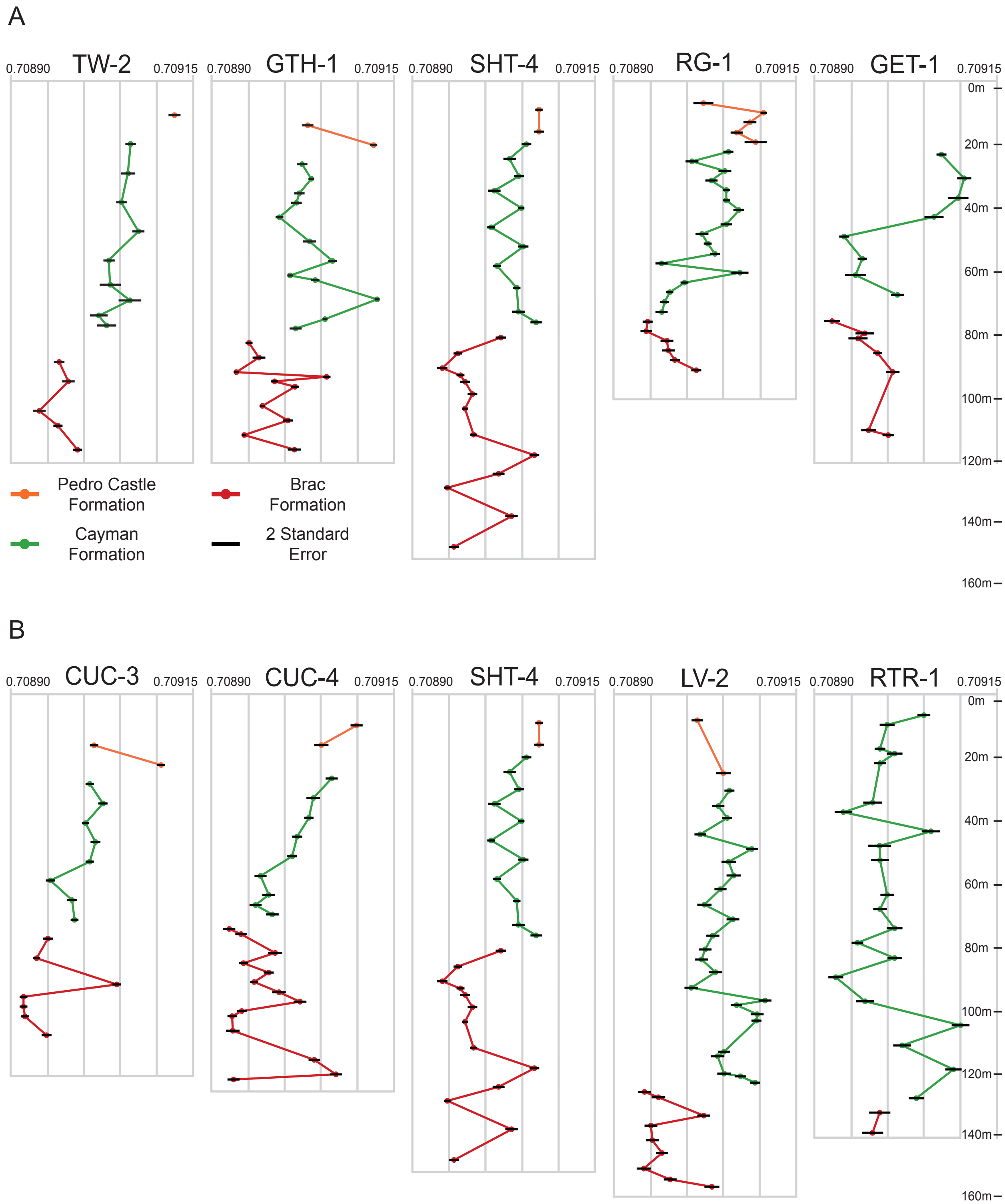

Fig. 6: $^{87}Sr/^{86}Sr$ isotope ratio vs. depth profile for wells on western and central Grand Cayman. Horizontal bars indicate 2 standard error of the mean, or 95% confidence interval, for each $^{87}Sr/^{86}Sr$ isotope ratio (see Fig. 2A, 2C for locations). Depth is below modern sea level.

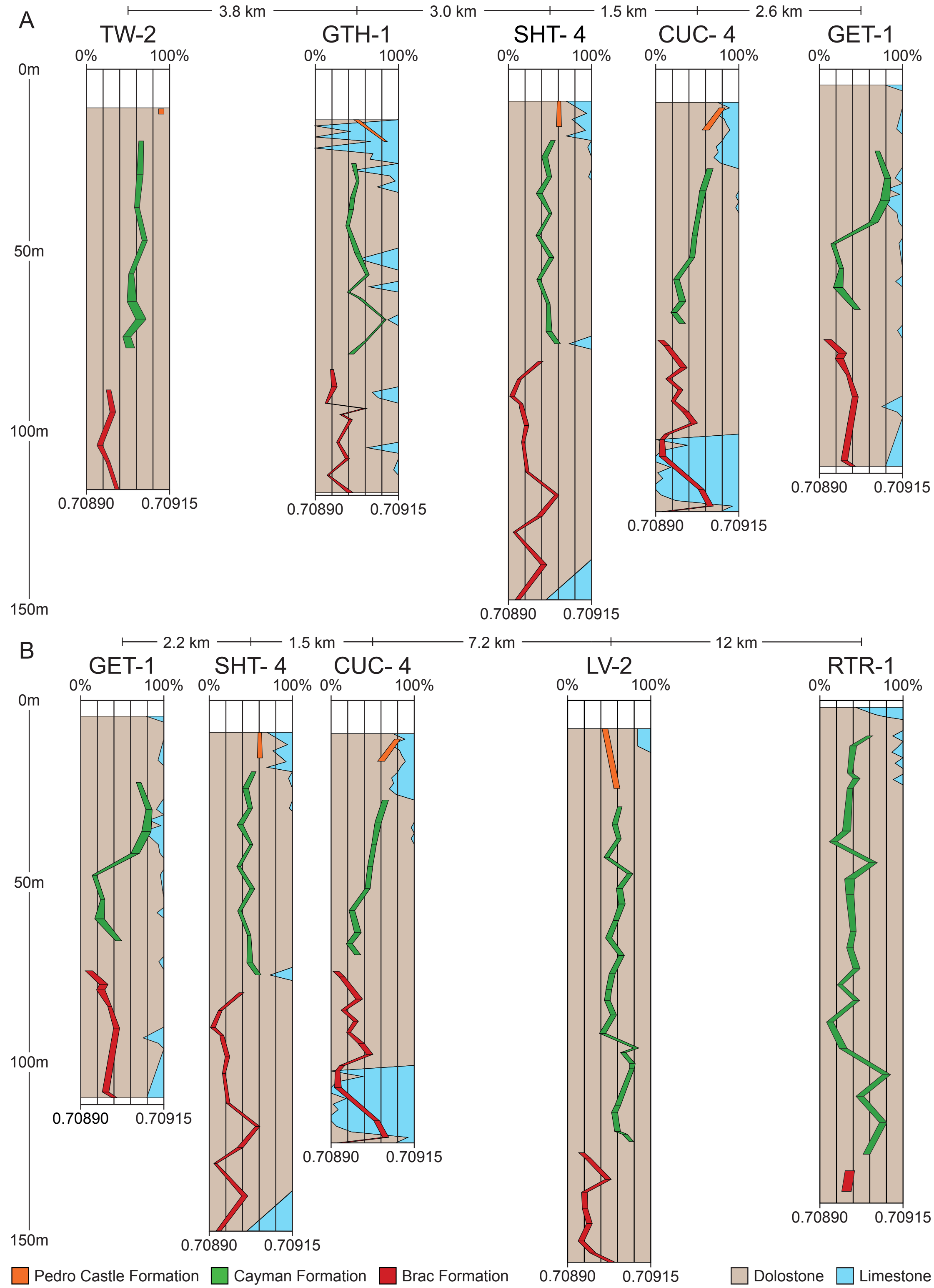

Fig. 7: (A) North to South cross section showing the mineralogy and the $^{87}Sr/^{86}Sr$ isotope ratios of wells on western Grand Cayman; (B) West to East cross section showing the mineralogy and the $^{87}Sr/^{86}Sr$ isotope ratios of wells on western and central Grand Cayman (see Fig. 2A; 2C for well locations). Width of the $^{87}Sr/^{86}Sr$ isotope ratio plot indicates the 2 standard error of the mean for each sample. Depth is below modern sea level.

Brac Formation however, the pattern of the profile of depth vs. $^{87}Sr/^{86}Sr$ isotope ratio is irregular and commonly includes an increase in the $^{87}Sr/^{86}Sr$ isotope ratios towards the base of the well. This may reflect changing lithologies as dolostone in the upper part of the Brac Formation grades downwards into calcareous dolostone and dolomitic limestone (Fig. 7A; Fig. 7B). The offset in the profile of depth vs. $^{87}Sr/^{86}Sr$ isotope ratio, which indicates a period of non-deposition and/or erosion, identifies an interval that includes the Brac Unconformity. The thickness of this interval is dictated by the spacing between successive $^{87}Sr/^{86}Sr$ isotope ratios. There is a marked decrease in the drilling rate from the basal part of the Cayman Formation (soft, friable, dolostone) to the upper part of the Brac Formation (hard, tightly cemented dolostone). Accordingly, the accurate placement of the Brac Unconformity within the interval between successive $^{87}Sr/^{86}Sr$ isotope ratios is based on: (1) the rate of drilling, and (2) lithological differences evident in the well cuttings.

2.1.2. Position of the Brac Unconformity on Grand Cayman

In the subsurface of western Grand Cayman, the Brac Unconformity dips gently to the north and forms a subdued plateau that is located at a relatively consistent depth of ~78 m bsl. In the southwest part of Grand Cayman, the Brac Unconformity is at 72 m bsl in CUC-4 and 73 m bsl in GET-1. Towards the west-central part of the island, the Brac Unconformity dips gently to 77 m bsl in SHT-4 and 79 m bsl in GTH-1. The Brac Unconformity reaches a depth of 83 m bsl in TW-2 towards the northwest part of Grand Cayman (Fig. 7A). The position of the Brac Unconformity is notably more variable in a west-to-east orientation across Grand Cayman relative to its position on the western part of the island. In LV-2, for example, the unconformity is 123 m bsl, 46 m lower than in SHT-4. In the east-central part of the island, the unconformity flattens out at a maximum depth of 129 m bsl in well RTR-1 (Fig. 7B), 57 m lower than in CUC-4. There is, therefore, at least 11 m of relief on the Brac Unconformity in the subsurface of western Grand Cayman and at least 57 m of relief on the Brac Unconformity in the subsurface of the entire western and central parts of the island.

2.2. Cayman Unconformity

The Cayman Unconformity has been the focus of comprehensive previous research and has been well described in previous studies (Jones and Hunter, 1994b; Jones et al. 1994b; Wignall, 1995; Der, 2012; Liang and Jones, 2014; Liang and Jones, 2015a; Liang and Jones, 2015b; Jones, 2016). As originally defined in the quarry at Pedro Castle, the Cayman Unconformity denotes the upper boundary of the Cayman Formation and its separation from the overlying Pedro Castle Formation (Fig. 4A) (Jones and Hunter, 1989). Subaerial exposure and weathering during the late Miocene (Tortonian - Messinian) produced up to 62 m of relief on the Cayman Unconformity (Jones and Hunter, 1994b; Liang and Jones, 2014, 2015a). The Cayman Unconformity has an extensive suite of paleokarst features, and numerous worm, bivalve (*Lithophaga*), and sponge borings (Jones and Hunter, 1994b; Jones, 2016). Cavities in strata beneath the Cayman Unconformity are typically lined with limpid dolomite cement (Jones and Hunter, 1994b). Late Miocene weathering formed an elevated 'peripheral rim' around the coast of Grand Cayman and a central depression on the western part of the island (Jones and Hunter, 1994b). The peripheral rim typically reaches elevations up to 13.5 m above sea level (asl), whereas the depression reaches depths of at least 30 m bsl under North Sound (Jones and Hunter, 1994b; Liang and Jones, 2015a). Relative to present day sea level, the maximum positive feature on the Cayman Unconformity is the Mountain (22 m asl) located on east-central Grand Cayman, whereas the maximum negative feature is a sinkhole located on the northeast corner of the island (39 m bsl). Jones and Hunter (1994b) suggested that the Cayman Formation underwent subaerial exposure, lithification, and erosion prior to the deposition of the Pedro Castle Formation. Available information suggests that the Cayman Unconformity developed over an ~2 to 6 million year period during the Messinian (Jones and Hunter, 1994b; Liang and Jones, 2015a; Jones, 2016).

2.3. Pedro Castle Unconformity

The Pedro Castle Unconformity has been the focus of comprehensive previous research and has been well described in previous studies (Jones and Hunter, 1989; Jones et al. 1994b;

Wignall, 1995; Arts, 2000; MacNeil and Jones, 2003; Etherington, 2004; Liang and Jones, 2014; Jones, 2019). The Pedro Castle Unconformity, which developed due to subaerial exposure and weathering during the late Pliocene to early Pleistocene, denotes the upper boundary of the Pedro Castle Formation (Jones and Hunter, 1989; Jones et al. 1994b; Liang and Jones, 2014; Jones, 2019). The Pedro Castle Unconformity is commonly overlain by the soft, friable limestone of the Ironshore Formation (Jones, 1994; Liang and Jones, 2014). Outcrop exposures including the Pedro Castle Unconformity are rare and, due to the poor core recovery of the overlying Ironshore Formation, detailed observations of the Pedro Castle Unconformity are limited (Jones et al. 1994b; Liang and Jones, 2014; Jones, 2019). Instead, in wells from regions in which the soft limestone of the Ironshore Formation overlie the hard dolomitic limestone of the Pedro Castle Formation, the Pedro Castle Unconformity typically coincides with a significant decrease in drilling rate and increased core recovery (Wignall, 1995; Arts, 2000; MacNeil and Jones, 2003; Etherington, 2004; Liang and Jones, 2014). The Pedro Castle Unconformity is typically highlighted by a thin layer of calcrete (Li and Jones, 2013). The maximum relief on the Pedro Castle Unconformity is ~8 m on Grand Cayman (Jones et al. 1997; Liang and Jones, 2014).

Chapter 3: Facies in the Paleogene - Neogene Succession on Grand Cayman

The Paleogene - Neogene carbonate succession on Grand Cayman includes the Brac Formation (Lower Oligocene), Cayman Formation (Middle Miocene), and the Pedro Castle Formation (Pliocene). Samples and data from the Brac Formation are limited, as many of the wells were terminated before it was reached or yielded non-continuous core/well cuttings that produced limited supplementary data. Well SHT-4 (Fig. 8) is herein used as a reference section to establish the criteria by which facies on western Grand Cayman are identified and correlated because it includes the most extensive database of core, thin-sections, and geochemical data.

In the core from SHT-4, the Brac Formation is divided into six facies that are assigned to facies associations FA1 and FA2, and the Cayman Formation is divided into five facies that are assigned to facies associations FA3 and FA4. Facies associations are defined by their color, biota, and texture. Facies in the Pedro Castle Formation are well described in previous studies (Jones and Hunter, 1994a; Wignall, 1995; Arts, 2000; MacNeil and Jones, 2003; Etherington, 2004). On west-central Grand Cayman, three additional facies are recognized and assigned to FA3 of the Cayman Formation, whereas one additional facies is recognized and assigned to FA4.

Allochems found in the Brac Formation and the Cayman Formation are bimodal in size and are therefore characterized using a two-fold method where macroscopic allochems (> 2 mm) are described separately from microscopic allochems (< 2 mm). Matrices are named according to Embry and Klovan's (1971) modifications to Dunham's (1962) classification scheme.

3.1. Facies in the Brac Formation

In the core from SHT-4, the Brac Formation is characterized by brown to cream, wackestone and mud-dominated packstone that have been replaced by finely crystalline dolomite. Macroscopic allochems in the Brac Formation were derived primarily from branching corals (predominantly *Porites*) and bivalves. Microscopic allochems include coralline red algae fragments, small benthic foraminifera (thin-walled, diminutive tests, < 0.5 mm in diameter), and large benthic foraminifera (thick-walled, robust tests, > 0.5 mm in diameter). Less abundant macroscopic allochems include

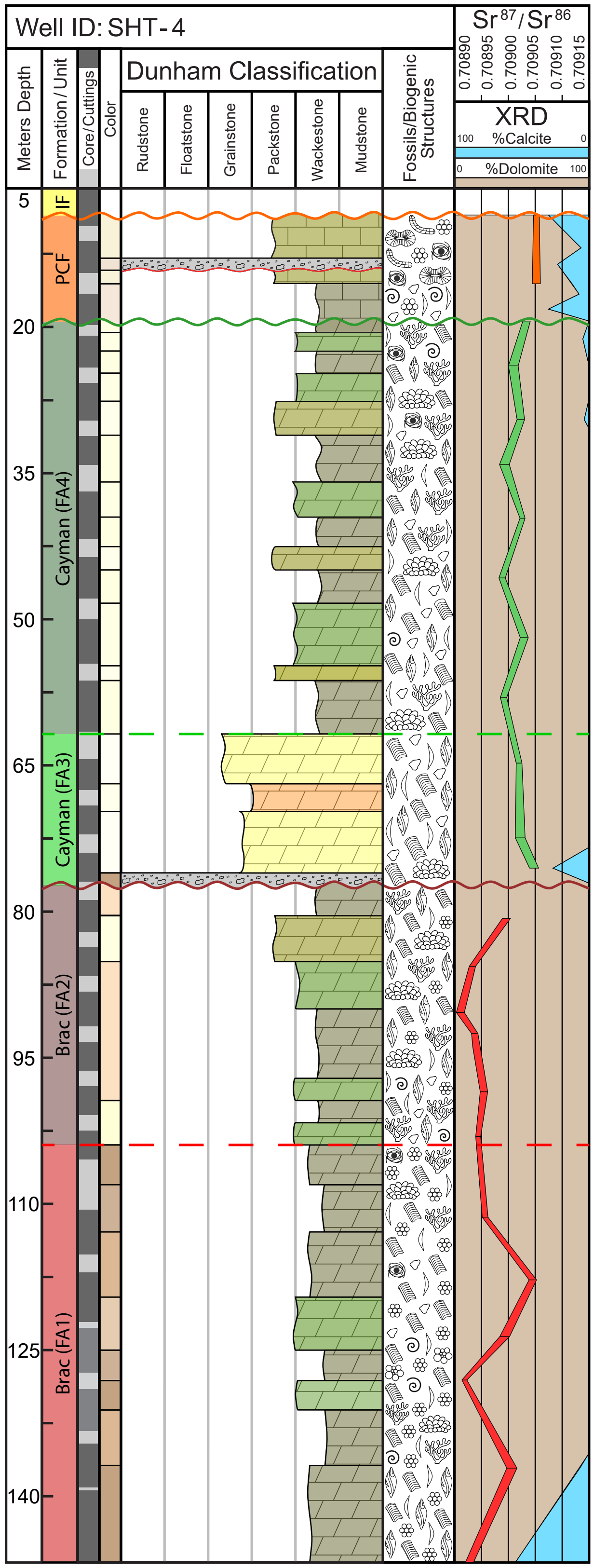

Fig. 8: SHT-4 litholog showing the formations, unconformities, facies associations (FA), biota and Dunham textures that comprise the succession. XRD mineralogy and $^{87}Sr/^{86}Sr$ isotope ratios shown for reference.

green algae plates (e.g., *Halimeda*), gastropods, domal (e.g., *Siderastrea*, *Astrocoenia*), platy (e.g., *Leptoseris*), and other branching (e.g., *Stylophora*) corals. Fossil moldic porosity is minor in the Brac Formation as most of the aragonitic allochems were replaced by finely crystalline dolomite.

In the core from SHT-4, facies in the Brac Formation are assigned to facies associations FA1 and FA2, which are defined by their color, biota, and texture (Fig. 8; Table - 1). FA1 forms the lower part of the Brac Formation, whereas FA2 forms the upper part. The basal contact of FA1 is unknown, as it was not reached during drilling (total = 146 m bsl). The contact between FA1 and FA2 is at 104 m bsl, and the Brac Unconformity (77 m bsl) forms the upper boundary of FA2 (Appendix - 2). In SHT-4, FA1 is at least 42 m thick, whereas FA2 is 27 m thick.

3.1.1. Brac Formation - Facies Association 1 (FA1)

FA1 consists of a succession of brown wackestone that contains numerous small benthic foraminifera and scattered branching corals (predominantly *Porites*). FA1 is comprised of dolostone with minor calcareous dolostone and dolomitic limestone in the basal part. In the core from SHT-4, FA1 encompasses facies 1A, 1B, and 1C (Table - 1).

- Facies 1A (Fig. 9A; 9B; 9C) consists of dolomitized, large-diameter (8 mm - 18 mm) branching corals in growth position with scattered bivalves, green algae plates, and gastropods that are held in a medium brown wackestone matrix formed of red algae fragments, small benthic foraminifera, and dolomitized micrite with fewer, finely abraded (0.1 mm - 0.2 mm) mollusc and echinoid fragments. Locally, packstone fills the spaces between the branching corals.
- Facies 1B (Fig. 10A; 10B; 10C) consists of small-diameter (4 mm - 8 mm) branching coral fragments, rhodoliths (6 mm - 8 mm), and bivalves that are held in a dark brown wackestone matrix formed of red algae fragments and large benthic foraminifera (0.4 mm - 0.8 mm). Scattered gastropods, small benthic foraminifera (0.2 mm - 0.4 mm), and dolomitized micrite are present. Coral fragments, which form the nuclei of rhodoliths, are now leached.
- Facies 1C consists of bivalves, gastropods, and green algae plates (4 mm - 8 mm) that are held in a medium brown wacke- to packstone matrix that is formed of red algae fragments, small

Facies		Color	Macroscopic Allochems		Microscopic Allochems		Dunham Classification
			Major	Minor	Major	Minor	
Facies Association 1 (FA1)	1A	Medium Brown	Branching Coral	Bivalve + Gastropod	Red Algae + Small Benthic Foram	Mollusc Fragments + Echinoid Fragments	Wackestone (Packstone fill between corals)
	1B	Dark Brown	Branching Coral + Rhodolith + Bivalve	Gastropod	Red Algae + Large Benthic Foram	Mollusc Fragments + Small Benthic Foram	Wackestone
	1C	Medium Brown	Bivalve + *Halimeda*	Gastropod	Red Algae + Small Benthic Foram	Mollusc Fragments + Large Benthic Foram	Wacke - to Packstone
Facies Association 2 (FA2)	2A	Light Brown	Laminar Coral + Bivalve + *Halimeda*	Massive + Branching Coral + Gastropod	Red Algae + Large Benthic Foram	Small Benthic Foram	Wacke - to Packstone
	2B	Off - White to Cream	Branching Coral	Massive Coral + Bivalve + *Halimeda*	Large Benthic Foram + Red Algae	Echinoid Fragments + Small Benthic Foram	Packstone
	2C	Off - White to Cream	Bivalve	*Halimeda* + Gastropod	Red Algae	Large + Small Benthic Foram	Wacke - to Packstone

Table 1: Facies in the Brac Formation, including the descriptions of color, biota, and Dunham classification.

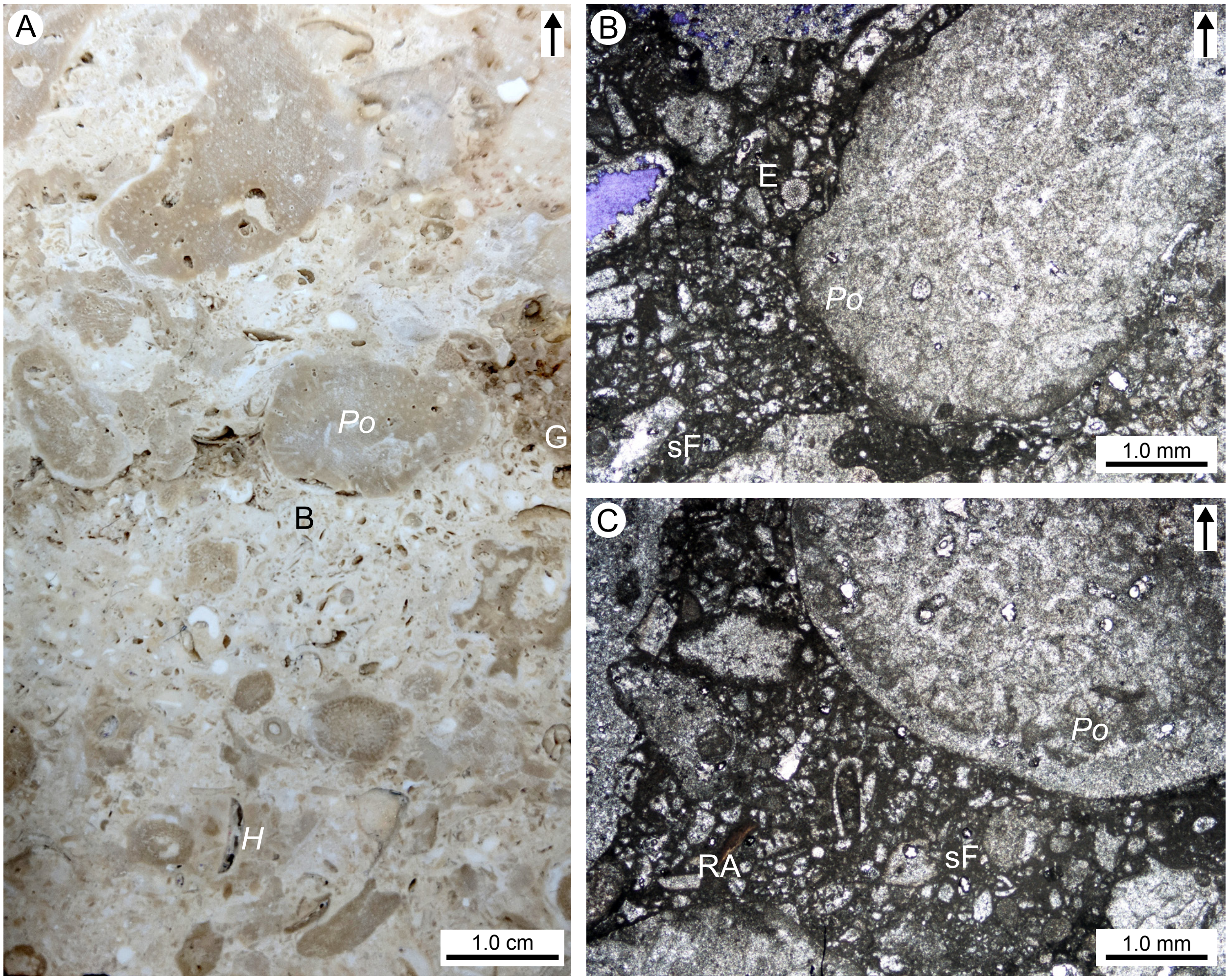

Fig. 9: A) Facies 1A core photograph from SHT-4: 105.3 m bsl; B) Facies 1A thin section photomicrograph from SHT-4: 105.3 m bsl, PPL; C) Facies 1A thin section photomicrograph from SHT-4: 105.3 m bsl, PPL. *Po* = *Porites*; *H* = *Halimeda*; B = Bivalve; G = Gastropod; sF = Small benthic foraminifera; E = Echinoid; RA = Red algae.

benthic foraminifera, scattered mollusc fragments, and large benthic foraminifera with lesser quantities of dolomitized micrite. Corals are rare.

3.1.2. Brac Formation - Facies Association 2 (FA2)

FA2 consists of a succession of off-white to cream packstone that contains numerous large benthic foraminifera and a more robust, diverse, and abundant suite of corals (domal, platy, branching) relative to FA1. FA2 is entirely formed of dolostone. In the core from SHT-4, FA2 encompasses facies 2A, 2B, and 2C (Table - 1).

- Facies 2A (Fig. 11A; 11B; 11C) consists of bivalves, platy corals in growth position, and

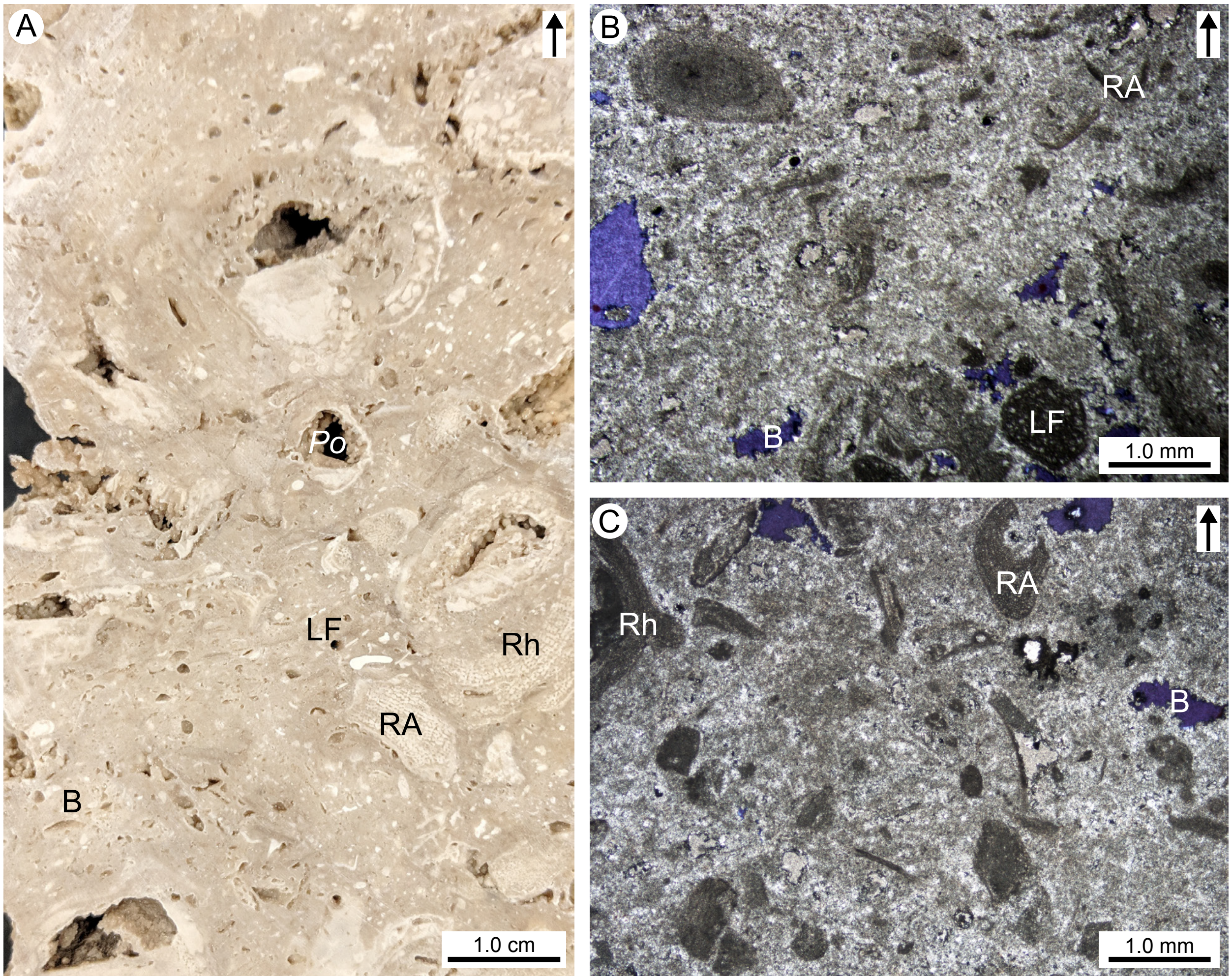

Fig. 10: A) Facies 1B core photograph from SHT-4: 127.5 m bsl; B) Facies 1B thin section photomicrograph from SHT-4: 127.5 m bsl, PPL; C) Facies 1B thin section photomicrograph from SHT-4: 127.5 m bsl, PPL. *Po* = *Porites*; LF = Large benthic foraminifera; Rh = Rhodolith; B = Bivalve; RA = Red algae.

green algae plates (6 mm - 10 mm) that are held in a light brown wacke- to packstone matrix formed of red algae fragments and large benthic foraminifera (0.4 mm - 1.6 mm) with fewer small benthic foraminifera and dolomitized micrite. Scattered gastropods, domal corals, and branching corals are also present.

- Facies 2B (Fig. 12A; 12B; 12C) consists of a framework of large-diameter (8 mm - 16 mm) branching corals in growth position that are held in a coarse (0.6 mm - 1.8 mm), off-white to cream packstone matrix that is formed of large benthic foraminifera and red algae fragments. Dolomitized micrite is rare to absent. Scattered bivalves, green algae plates, and domal corals are present, along with fewer echinoid fragments and small benthic foraminifera.

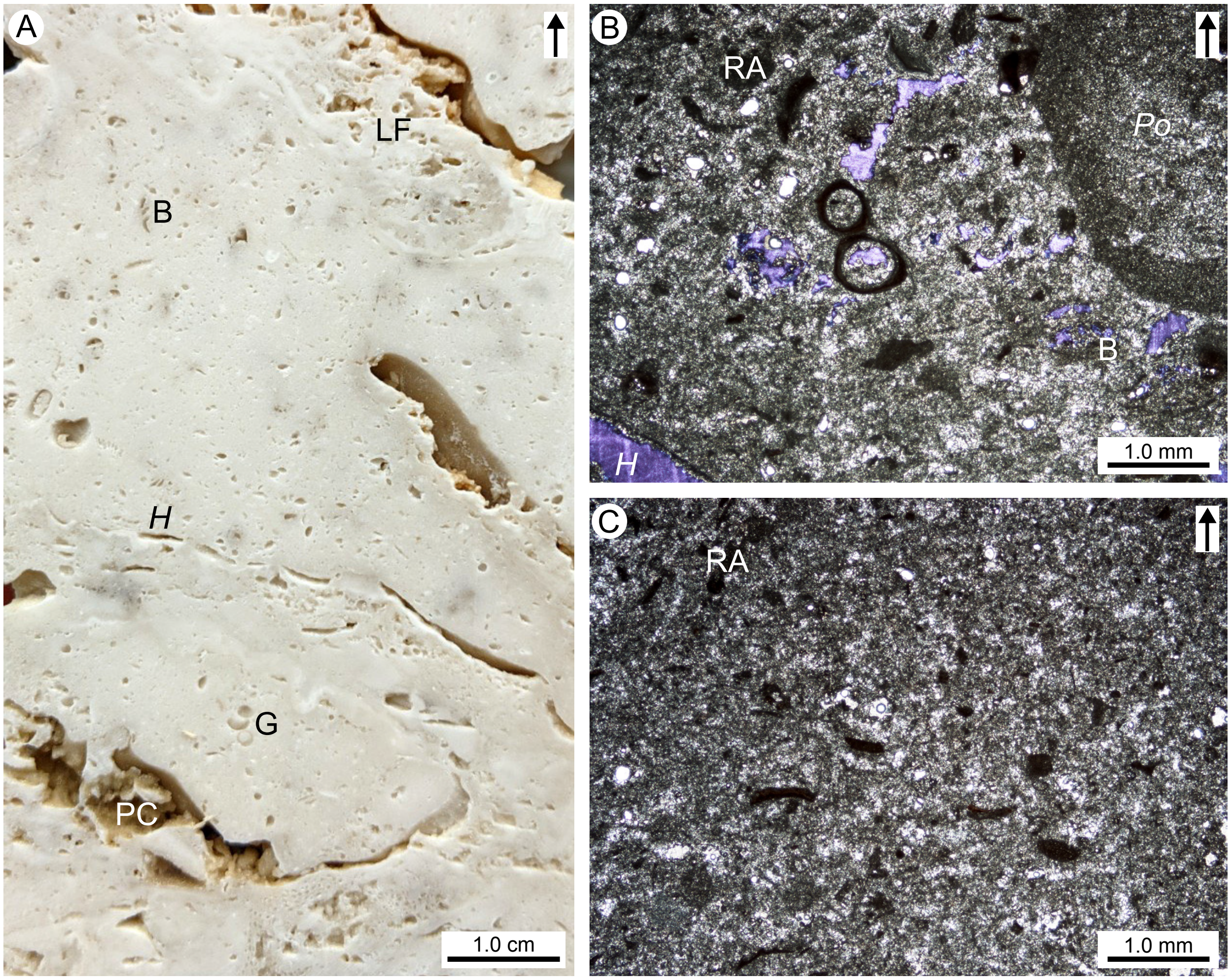

Fig. 11: A) Facies 2A core photograph from SHT-4: 82.3 m bsl; B) Facies 2A thin section photomicrograph from SHT-4: 82.3 m bsl, PPL; C) Facies 2A thin section photomicrograph from SHT-4: 82.3 m bsl, PPL. LF = Large bethic foraminifera; B = Bivalve; *H* = *Halimeda*; G = Gastropod; PC = Platy coral.

- Facies 2C consists of bivalve fragments, green algae plates, and gastropods (4 mm - 8 mm) that are held in an off-white to cream wacke- to packstone matrix formed of red algae fragments and fewer large benthic (0.4 mm - 1.2 mm) and small benthic foraminifera (0.2 mm - 0.6 mm), as well as dolomitized micrite. Corals are rare to absent.

3.2. Cayman Formation

In the core from SHT-4, the Cayman Formation consists of a succession of off-white to cream, fabric-retentive, microcrystalline dolostone. Macroscopic allochems in the Cayman Formation were derived primarily from domal corals (e.g., *Porites*, *Montastrea*), branching corals

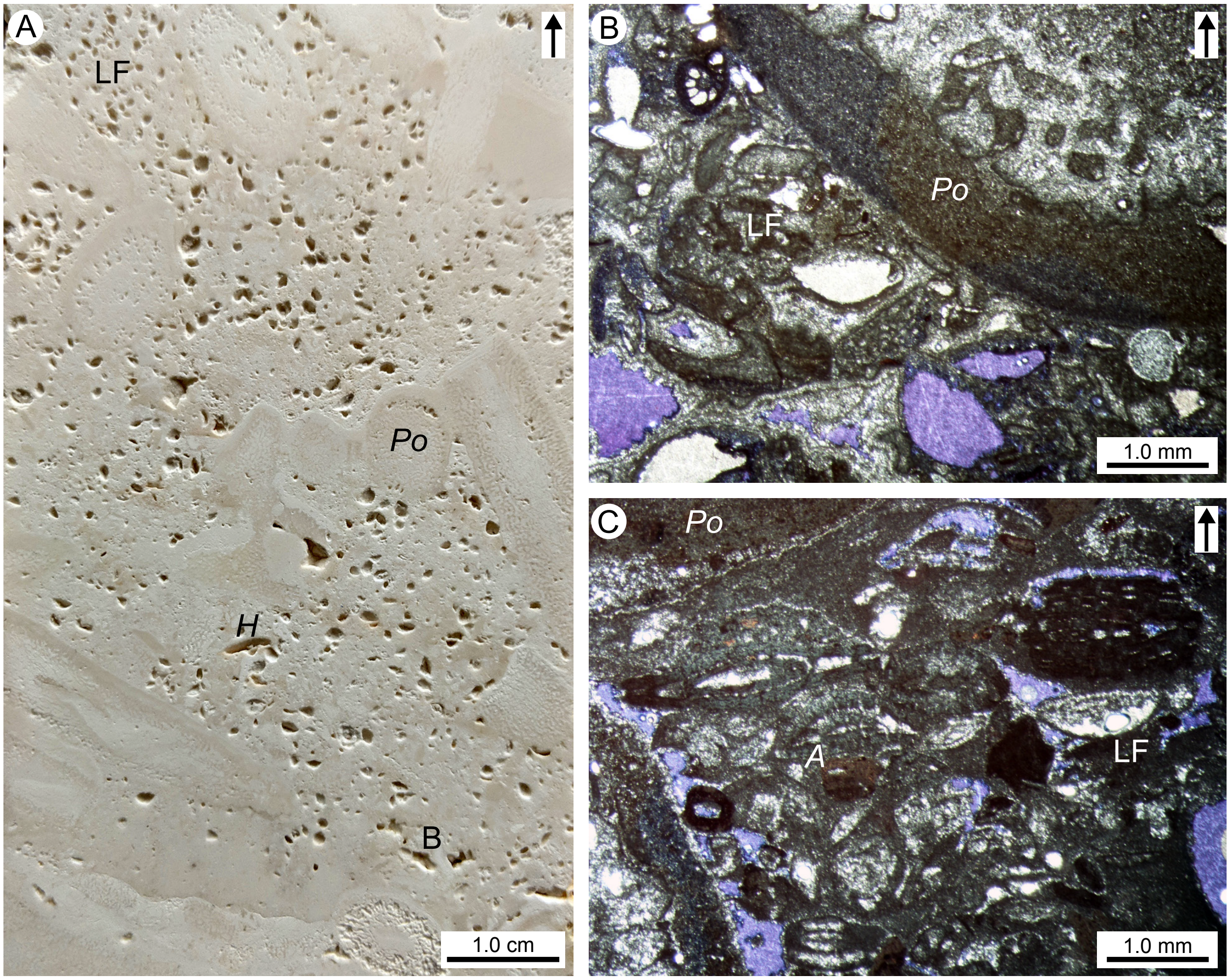

Fig. 12: A) Facies 2B core photograph from SHT-4: 87.4 m bsl; B) Facies 2B thin section photomicrograph from SHT-4: 87.4 m bsl, PPL; C) Facies 2B thin section photomicrograph from SHT-4: 87.4 m bsl, PPL. *Po* = *Porites*; LF = Large benthic foraminifera; *A* = *Amphistegina*; B = Bivalve; *H* = *Halimeda*.

(predominantly *Stylophora*, fewer *Porites*), bivalves, and green algae plates (e.g., *Halimeda*) with fewer rhodoliths, platy corals (e.g., *Leptoseris*), and gastropods. Microscopic allochems were derived primarily from large benthic foraminifera (predominantly *Amphistegina*), and coralline red algae fragments with fewer echinoid fragments. Aragonitic allochems, such as corals, molluscs, and green algae plates, have been leached and are now represented by internal and/or external molds. Accordingly, fossil-moldic porosity is ubiquitous in the Cayman Formation, as most of the aragonitic allochems have been leached. Foraminifera, red algae, and rhodoliths, which were originally low-magnesium calcite, have been replaced by dolomite.

Facies in the Cayman Formation are assigned to facies associations FA3 and FA4, which are defined by their color, biota, and texture (Fig. 8; Table - 2). FA3 forms the lower part of the Cayman Formation, whereas FA4 forms the upper part. FA3 unconformably overlies the Brac Unconformity, which is at 77 m bsl in SHT-4. The gradational contact between FA3 and FA4 is at 62 m bsl, and the Cayman Unconformity (19 m bsl) forms the upper boundary of FA4 (Appendix - 2). In SHT-4, FA3 is 15 m thick, whereas FA4 is 43 m thick.

3.2.1. Cayman Formation - Facies Association 3 (FA3)

FA3 consists of a succession of friable, porous grainstone that contains numerous large benthic foraminifera (predominantly *Amphistegina*), red algae fragments, bivalves, and fragments of domal corals with fewer green algae plates, encrusting foraminifera, and rhodoliths. In the core from SHT-4, FA3 encompasses facies 3A and 3B (Table - 2):

- Facies 3A (Fig. 13A; 13B; 13C) consists of cream to off-white grainstone that contains large benthic foraminifera, finely abraded red algae fragments (0.2 mm - 0.6 mm), and encrusting foraminifera that are loosely cemented by microcrystalline dolomite. Rare macroscopic allochems include bivalve fragments, green algae plates, and fragmented domal corals.
- Facies 3B consists of cream packstone that contains large grains derived from bivalves and green algae plates (4 mm - 12 mm) in a matrix formed of large benthic foraminifera with fewer red algae fragments (0.2 mm - 1.6 mm) and dolomitized micrite. Scattered domal corals, rhodoliths, and gastropods are also present. Microcrystalline dolomite cement is locally common. Facies 3B is also present in LV-2 (Fig. 14A; 14B; 14C).

On western Grand Cayman, FA3 encompasses one additional facies (3C) in the core from TW-2, whereas on central Grand Cayman, FA3 encompasses two additional facies (3D, 3E) in the core from LV-2 (Table - 2).

- Facies 3C consists of cream to off-white packstone that contains large disarticulated bivalves (8 mm - 20 mm), gastropod fragments, and green algae plates that are held in a matrix formed of large benthic foraminifera, red algae fragments (0.2 mm - 0.4 mm), peloids and dolomitized micrite. Domal corals are present, as well as fewer branching and platy coral fragments.

Facies		Color	Macroscopic Allochems		Microscopic Allochems		Dunham Classification
			Major	Minor	Major	Minor	
Facies Association 3 (FA3)	3A	Cream to Off-White	None	Bivalve + *Halimeda* + *Porites*	Red Algae	Encrusting + Large Benthic Foram	Grainstone
	3B	Cream	Bivalve + *Halimeda*	*Porites* + Rhodolith + Gastropod	Large Benthic Foram	Red Algae	Packstone
	3C	Cream to Off-White	Bivalve + Gastropod + *Halimeda*	*Porites* + *Leptoseris* + *Stylophora*	Large Benthic Foram + Red Algae	Peloids	Packstone
	3D	Off-White	*Amphistegina* + Bivalve	*Porites* + Rhodolith	Red Algae + Large Benthic Foram	Encrusting Foram + Echinoid	Grain- to Rudstone
	3E	Chalky White	*Porites* + Bivalve + *Montastrea*	Rhodolith + *Halimeda* + *Stylophora*	Encrusting + Large Benthic Foram	Red Algae + Echinoid Fragments	Rudstone
Facies Association 4 (FA4)	4A	Tan to Light Brown	Bivalve + *Halimeda*	Rhodolith + *Stylophora* + *Porites* + Gastropod	Red Algae + *Amphistegina*	Small + Large Benthic Foram	Pack- to Wackstone
	4B	Tan	*Stylophora* + *Porites*	Bivalve + *Leptoseris* + Rhodolith + *Halimeda*	Red Algae + Peloids	Small Benthic Foram	Floatstone (Wackestone matrix)
	4C	Tan to Light Brown	Rhodolith + Bivalve + *Stylophora* + *Porites*	*Halimeda* + *Leptoseris* + *Montastrea*	*Amphistegina* + Red Algae	Small + Large Benthic Foram + Peloids	Floatstone (Wackestone matrix)
	4D	Cream to Tan	Bivalve + Rhodolith	*Stylophora* + *Porites* + *Halimeda*	Red Algae + Peloids + *Amphistegina*	Small Benthic Foram	Floatstone (Wackestone matrix)

Table 2: Facies in the Cayman Formation, including the descriptions of color, biota, and Dunham classification.

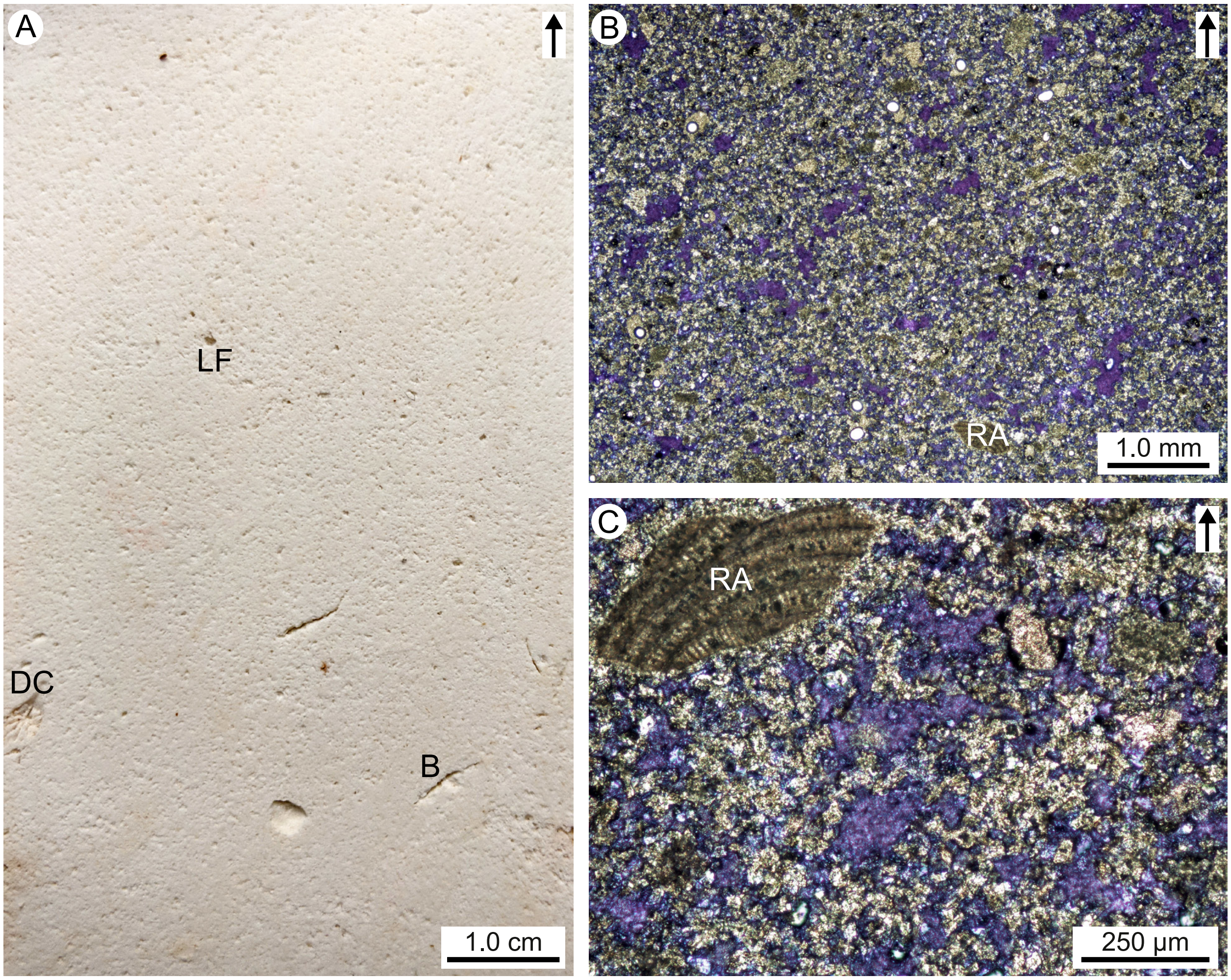

Fig. 13: A) Facies 3A core photograph from SHT-4: 73.2 m bsl; B) Facies 3A thin section photomicrograph from SHT-4: 72.0 m bsl, PPL; C) Facies 3A thin section photomicrograph from SHT-4: 72.0 m bsl, PPL. LF = Large benthic foraminifera; DC = Domal coral; B = Bivalve; RA = Red algae.

- Facies 3D (Fig. 15A; 15B; 15C) consists of off-white grainstone and rudstone that contains large grains (0.6 mm - 4 mm) derived from large benthic foraminifera, red algae fragments, encrusting foraminifera, and bivalves that are loosely cemented by microcrystalline dolomite. Scattered fragments of domal corals, rhodoliths, and echinoid fragments are present.
- Facies 3E (Fig. 16A; 16B; 16C; 16D) consists of chalky white rudstone that contains large (8 mm - 22 mm) fragments of domal corals and bivalves that are held in a coarse matrix (1.2 mm - 1.8 mm) formed of large benthic foraminifera, red algae fragments, encrusting foraminifera, and echinoid fragments. Scattered rhodoliths, green algae, and large diameter (8 mm - 32 mm) branching coral fragments are also present.

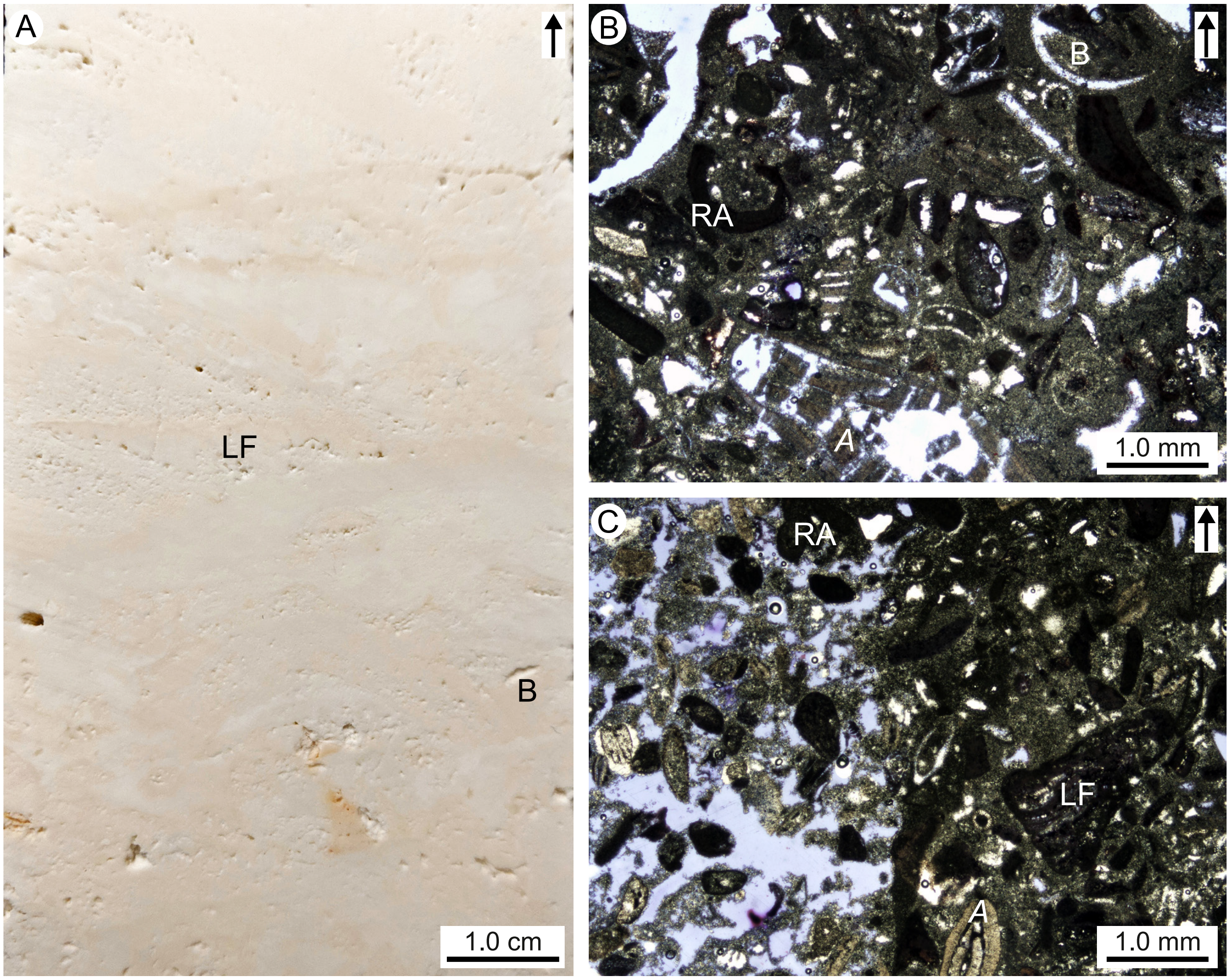

Fig. 14: A) Facies 3B core photograph from LV-2: 96.9 m bsl; B) Facies 3B thin section photomicrograph from LV-2: 96.9 m bsl, PPL; C) Facies 3B thin section photomicrograph from LV-2: 96.9 m bsl, PPL. LF = Large benthic foraminifera; *A* = *Amphistegina*; B = Bivalve; RA = Red algae.

3.2.2. Cayman Formation - Facies Association 4 (FA4)

FA4 consists of a succession of hard, tightly cemented wackestone and floatstone that contains numerous branching corals (predominantly *Stylophora*, fewer *Porites*) in growth position, rhodoliths, and bivalves with fewer red algae fragments, green algae plates, small benthic foraminifera, and large benthic foraminifera. In the core from SHT-4, FA4 encompasses facies 4A, 4B, and 4C (Table - 2).

- Facies 4A (Fig. 17A; 17B) consists of tan to light brown wackestone and packstone that contains bivalve fragments (4 mm - 16 mm) and green algae plates that are held in a matrix formed of red algae fragments and large benthic (0.2 mm - 0.4 mm) and small benthic foraminifera (0.05

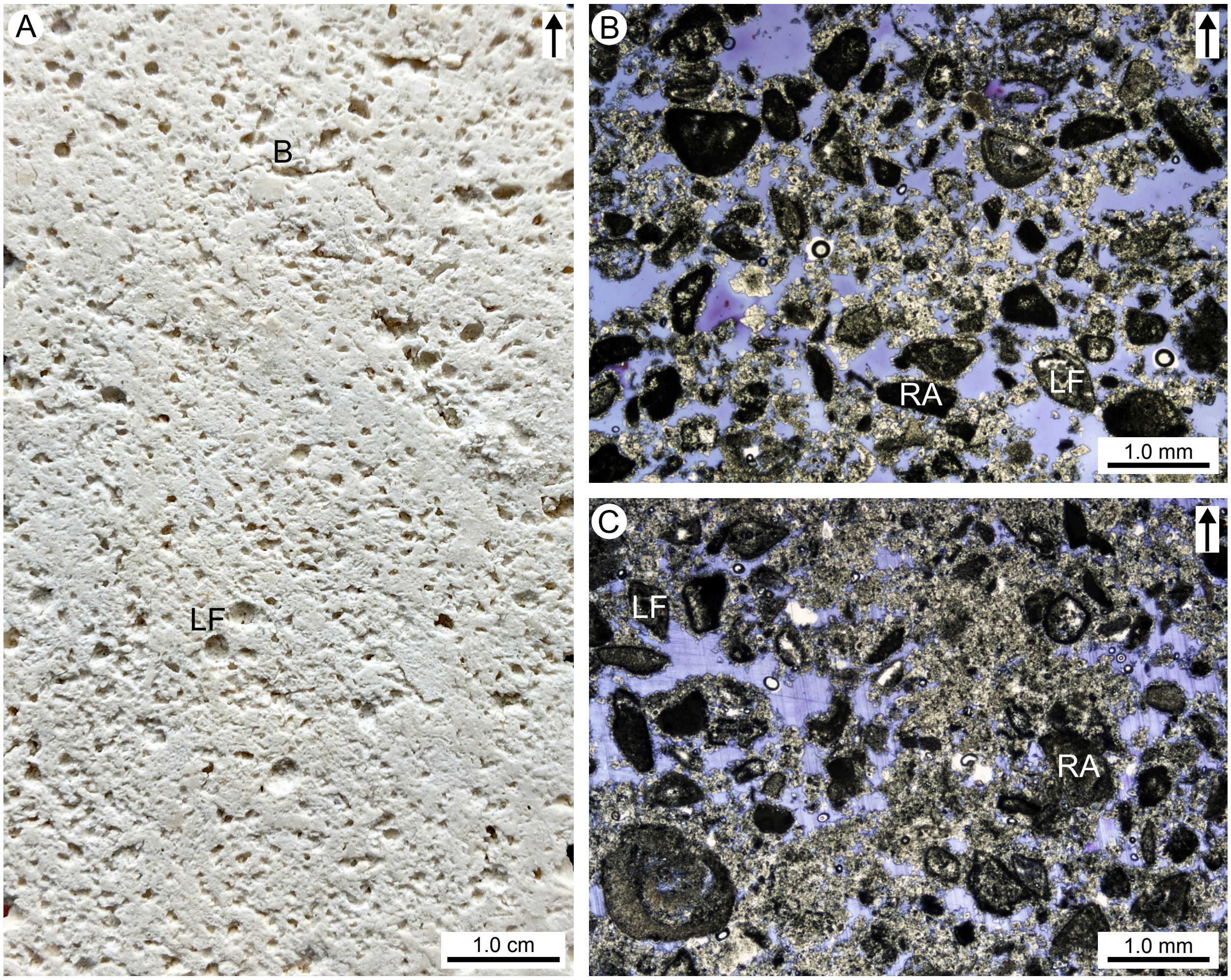

Fig. 15: A) Facies 3D core photograph from LV-2: 120.1 m bsl; B) Facies 3D thin section photomicrograph from LV-2: 120.1 m bsl, PPL; C) Facies 3D thin section photomicrograph from LV-2: 119.3 m bsl, PPL. LF = Large benthic foraminifera; B = Bivalve; RA = Red algae.

mm - 0.2 mm). Scattered rhodoliths, branching corals, and gastropods are present. Dolomitized micrite is rare, whereas dolomite cement and fractures are pervasive.

- Facies 4B (Fig. 18A; 18B; 18C) consists of tan floatstone that contains large-diameter (6 mm - 22 mm) branching corals in growth position that are held in a wackestone matrix formed of red algae fragments with fewer peloids, small benthic foraminifera (0.01 mm - 0.05 mm), and dolomitized micrite. Scattered bivalves, platy corals, rhodoliths, and green algae plates are present. Facies 4B is also present in LV-2 and WMF-1 (Fig. 19A; 19B; 19C; 19D).
- Facies 4C (Fig. 20A; 20B) consists of tan to light brown floatstone that contains rhodoliths (4 mm - 28 mm) with fewer bivalve fragments and small-diameter (2 mm - 12 mm) branching

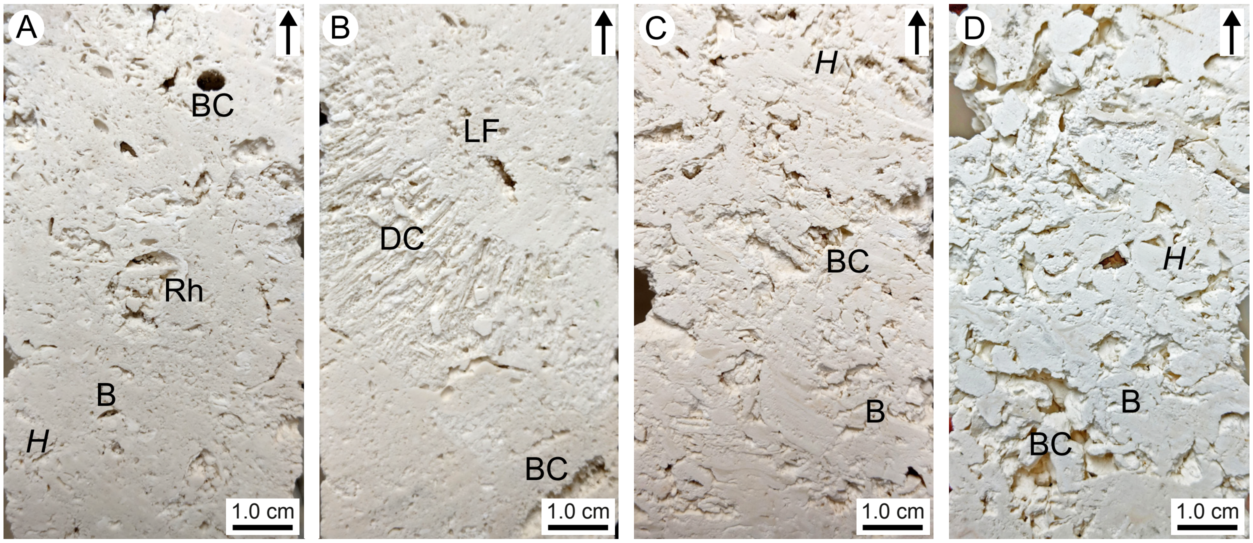

Fig. 16: A) Facies 3E core photograph from LV-2: 51.9 m bsl; B) Facies 3E core photograph from LV-2: 53.2 m bsl; C) Facies 3E core photograph from LV-2: 55.0 m bsl; D) Facies 3E core photograph from LV-2: 56.3 m bsl. BC = Branching coral; DC = Domal coral; Rh = Rhodolith; LF = Large benthic foraminifera; B = Bivalve; *H* = *Halimeda*.

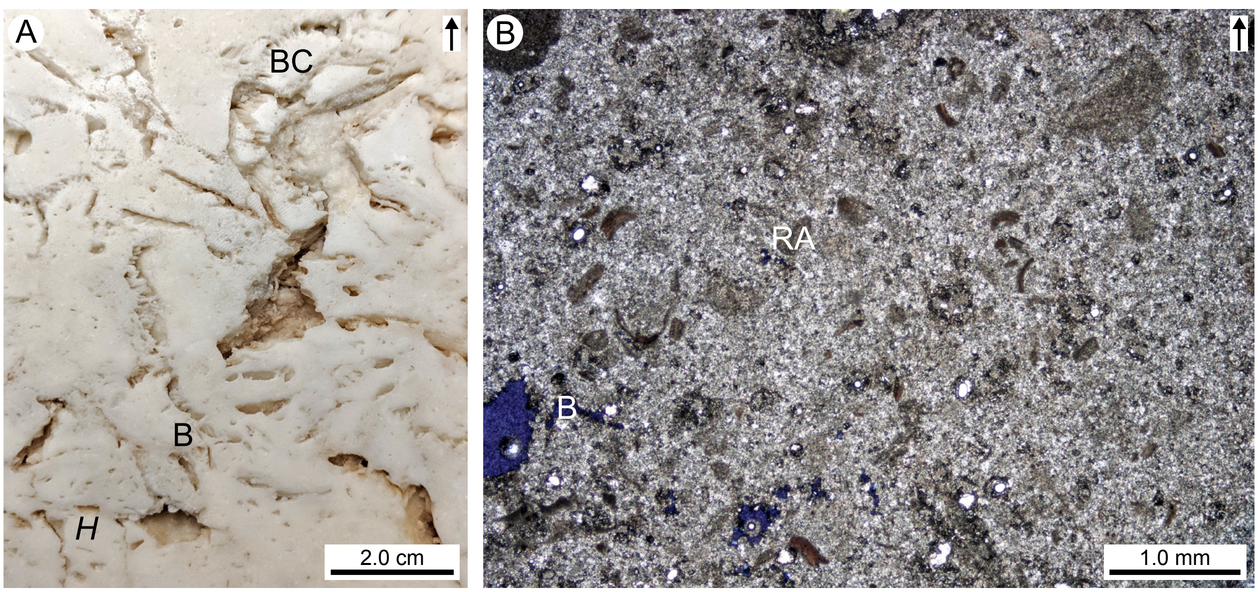

Fig. 17: A) Facies 4A core photograph from SHT-4: 43.3 m bsl; B) Facies 4A thin section photomicrograph from SHT-4: 48.5 m bsl, PPL. BC = Branching coral; B = Bivalve; *H* = *Halimeda*; RA = Red algae.

coral fragments that are held in a wackestone matrix formed of red algae fragments (0.1 mm - 0.4 mm), large benthic foraminifera (0.6 mm - 1.2 mm), small benthic foraminifera (0.1 mm - 0.4 mm), peloids, and dolomitized micrite. Scattered green algae plates, domal corals, and platy coral fragments are present. Coral fragments, which form the nuclei of rhodoliths, are now leached. Facies 4C is also present in LV-2 (Fig. 21A; 21B).

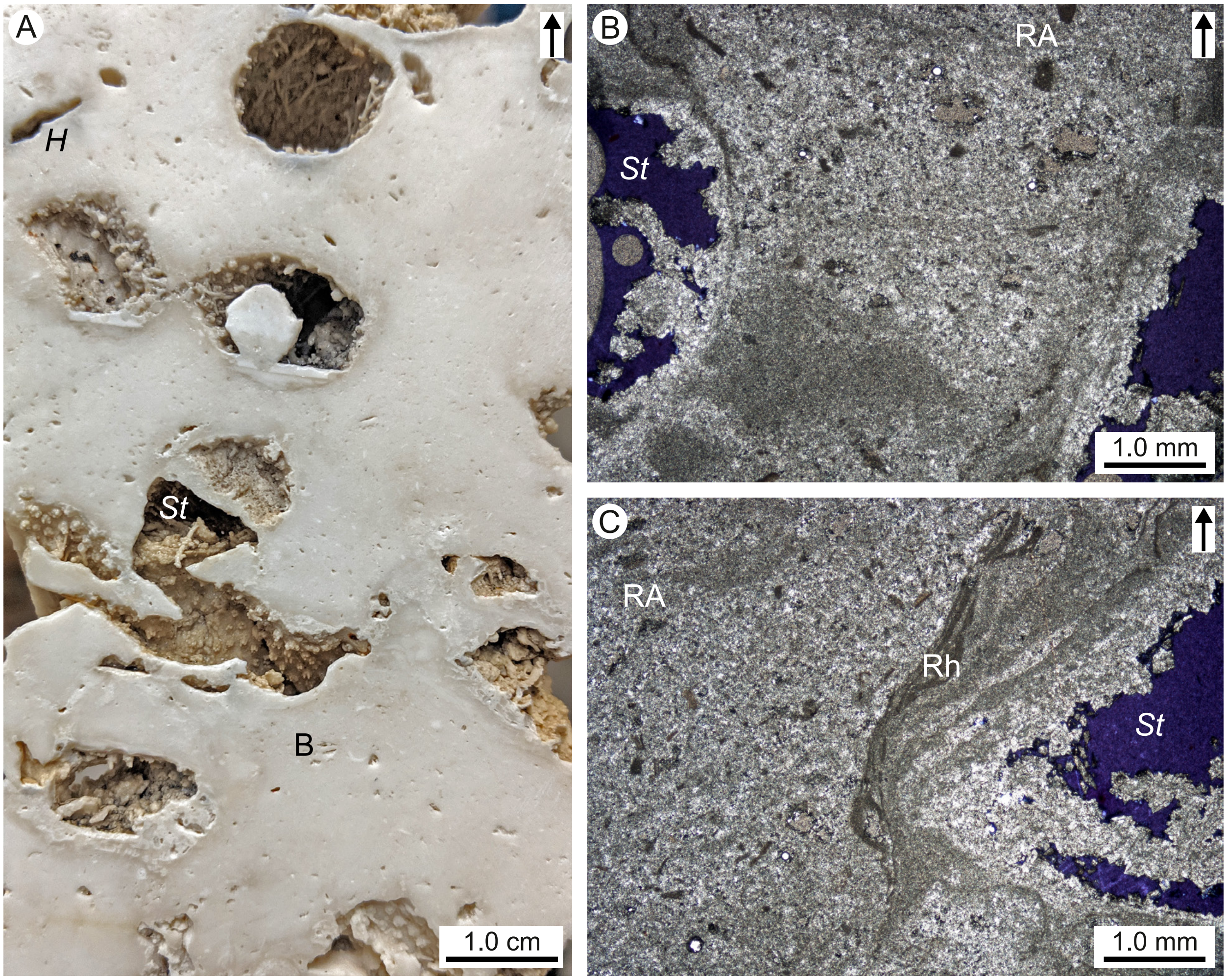

Fig. 18: A) Facies 4B core photograph from SHT-4: 35.1 m bsl; B) Facies 4B thin section photomicrograph from SHT-4: 33.7 m bsl, PPL; C) Facies 4B thin section photomicrograph from SHT-4: 33.7 m bsl, PPL. *St* = *Stylophora*; B = Bivalve; *H* = *Halimeda*; RA = Red algae; Rh = Rhodolith.

On western Grand Cayman, FA4 encompasses one additional facies (4D) in the core from TW-1. The facies defined on western Grand Cayman are typically representative of FA4 on the central parts of the island (Table - 2).

- Facies 4D consists of cream to tan floatstone that contains large disarticulated bivalves (12 mm - 28 mm) and rhodoliths, with fewer small-diameter (2 mm - 8 mm) branching corals in growth position, and green algae plates that are held in a wackestone matrix formed of finely abraded (0.2 mm - 0.4 mm) red algae fragments, peloids, and dolomitized micrite. Small benthic foraminifera are common. The number of branching corals increases upwards, whereas the number of bivalves decreases upwards.

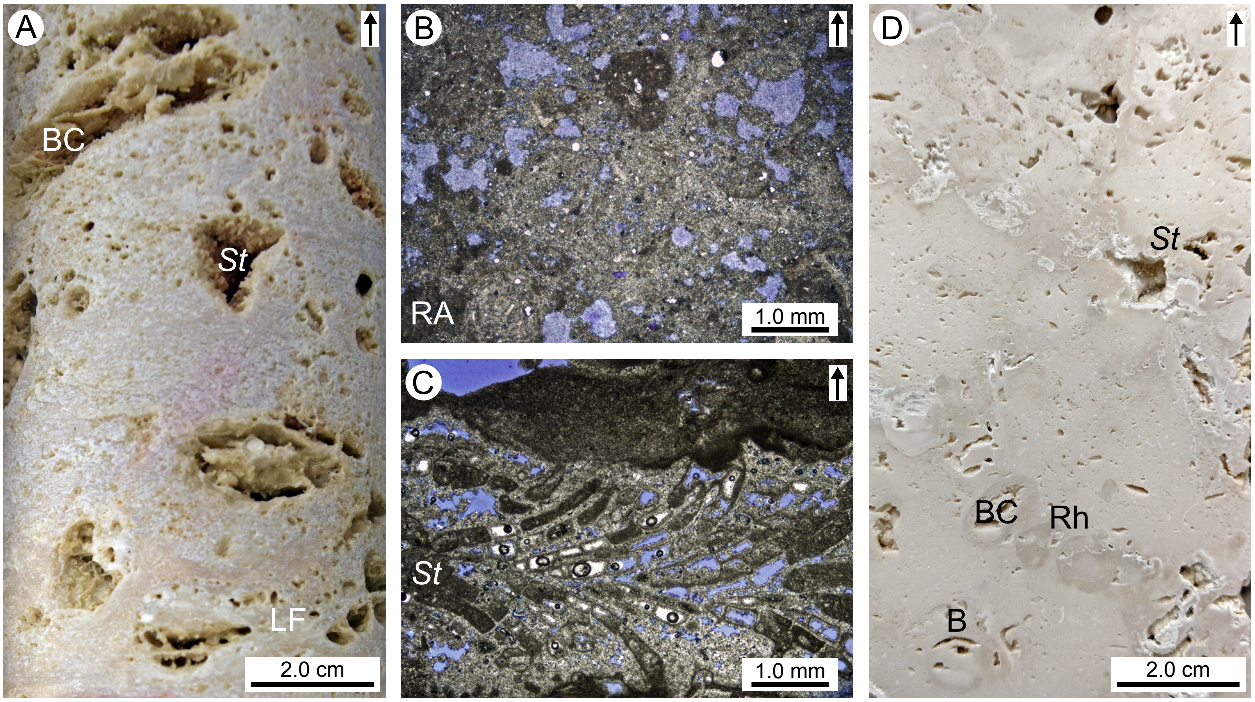

Fig. 19: A) Facies 4D core photograph from WMF-1: 18.3 m bsl; B) Facies 4D thin section photomicrograph from WMF-1: 27.4 m bsl, PPL; C) Facies 4D thin section photomicrograph from LV-2: 39.0 m bsl, PPL; D) Facies 4D core photograph from LV-2: 39.0 m bsl. BC = Branching coral; *St* = *Stylophora*; LF = Large benthic foraminifera; B = Bivalve; Rh = Rhodolith; RA = Red algae.

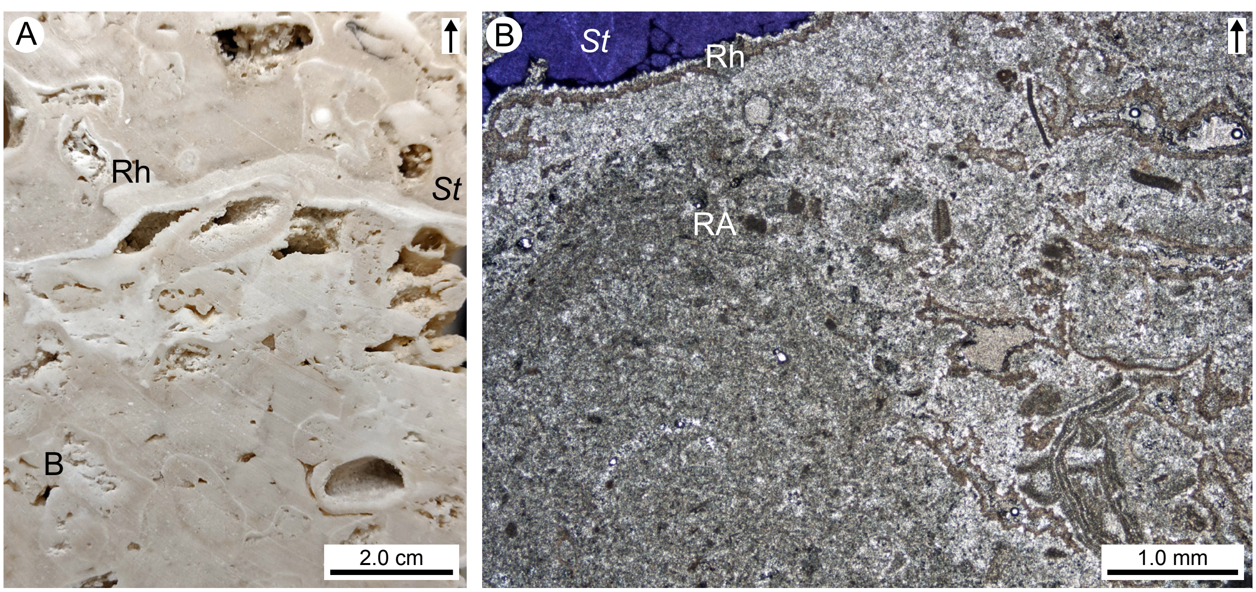

Fig. 20: A) Facies 4C core photograph from SHT-4: 20.1 m bsl; B) Facies 4C thin section photomicrograph from SHT-4: 20.1 m bsl, PPL. *St* = *Stylophora*; B = Bivalve; Rh = Rhodolith; RA = Red algae.

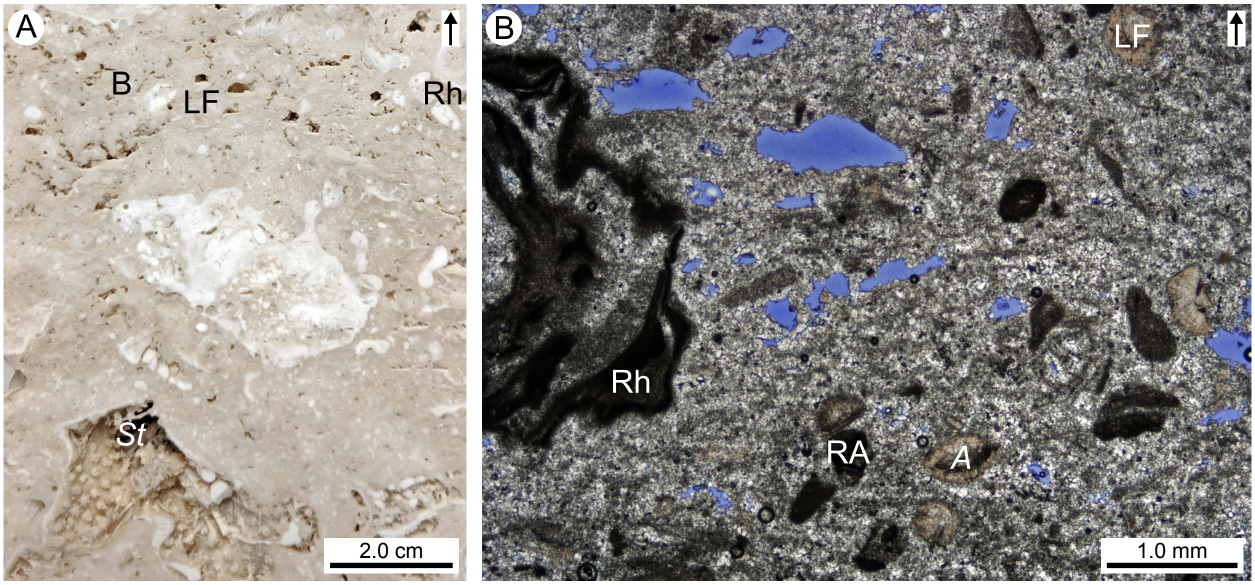

Fig. 21: A) Facies 4C core photo from LV-2: 25.0 m bsl; B) Facies 4C thin section photomicrograph from LV-2: 25.0 m bsl, PPL. *St* = *Stylophora*; B = Bivalve; LF = Large benthic foraminifera; Rh = Rhodolith; *A* = *Amphistegina*; RA = Red algae.

3.3. Pedro Castle Formation in SHT-4

Facies in the Pedro Castle Formation have been well described by previous authors (Jones and Hunter, 1994a; Wignall, 1995; Arts, 2000; MacNeil and Jones, 2003; Etherington, 2004). The Pedro Castle Formation, which is 9 m thick in SHT-4, is characterized by a succession of light brown to off-white calcareous dolostone (Fig. 8). The Pedro Castle Formation unconformably overlies the Cayman Formation (19 m bsl in SHT-4), whereas its upper boundary is formed by the Pedro Castle Unconformity (10 m bsl in SHT-4). Macroscopic allochems in the Pedro Castle Formation were derived primarily from free-living corals (e.g., *Trachyphyllia*, *Teleiophyllia*, *Thysanus*), rhodoliths, and bivalves with fewer green algae plates (e.g., *Halimeda*) and gastropods. Scattered branching corals (e.g., *Stylophora*, *Porites*) are present. Microscopic allochems were derived from large benthic foraminifera (e.g., *Amphistegina*), and coralline red algae fragments with fewer small benthic foraminifera and echinoid fragments.

Chapter 4: Facies Architecture and Reservoir Quality on Grand Cayman

On Grand Cayman, many of the wells were terminated at shallow depths (commonly < 50 m bsl; Appendix - 1). Accordingly, samples and data from the Pedro Castle Formation (Pliocene) and the Cayman Formation (Middle Miocene) are abundant, whereas samples and data from the Brac Formation (Lower Oligocene) are limited. On western and central Grand Cayman, the Brac Formation includes facies associations FA1 and FA2, whereas the Cayman Formation includes facies associations FA3 and FA4. On western and central Grand Cayman, the Brac Formation is at least 69 m thick, the Cayman Formation is 45 m - 129 m thick, and the Pedro Castle Formation is 0 m - 22 m thick.

4.1. Facies Architecture - Western and Central Grand Cayman

In the subsurface of western Grand Cayman (Fig. 2C), the facies architecture described here in the Brac Formation is based primarily on the core from SHT-4, and limited samples from TW-2, GTH-1, GET-1, and CUC-1 (Fig. 2C; 22; Appendix - 2). In the subsurface of central Grand Cayman (Fig. 2A), however, data from the Brac Formation in LV-2 and RTR-1 are limited to samples collected from well-cuttings. In contrast, the facies architectures in the Cayman Formation and in the Pedro Castle Formation are based on samples from 22 wells that were selected for this study from western and central Grand Cayman (Fig. 2A; 2C; 22; 23; Appendix - 2).

4.1.1. Formational Boundaries and Thicknesses

In the subsurface of western Grand Cayman, the basal contact of the Brac Formation either has not been recognized or has not been reached from drilling, whereas the Brac Unconformity forms the upper contact. The Brac Unconformity is between 72 m - 83 m bsl and dips gently northwest at ~0.05° (Fig. 22). The maximum depth reached from drilling is 146 m bsl in SHT-4, where the Brac Unconformity is at 77 m bsl. The Brac Formation is, therefore, at least 69 m thick. On western Grand Cayman, the Cayman Unconformity is located between 28 m bsl and 5 m asl. On western Grand Cayman, the relief on the Brac Unconformity, which is up to 11 m, is

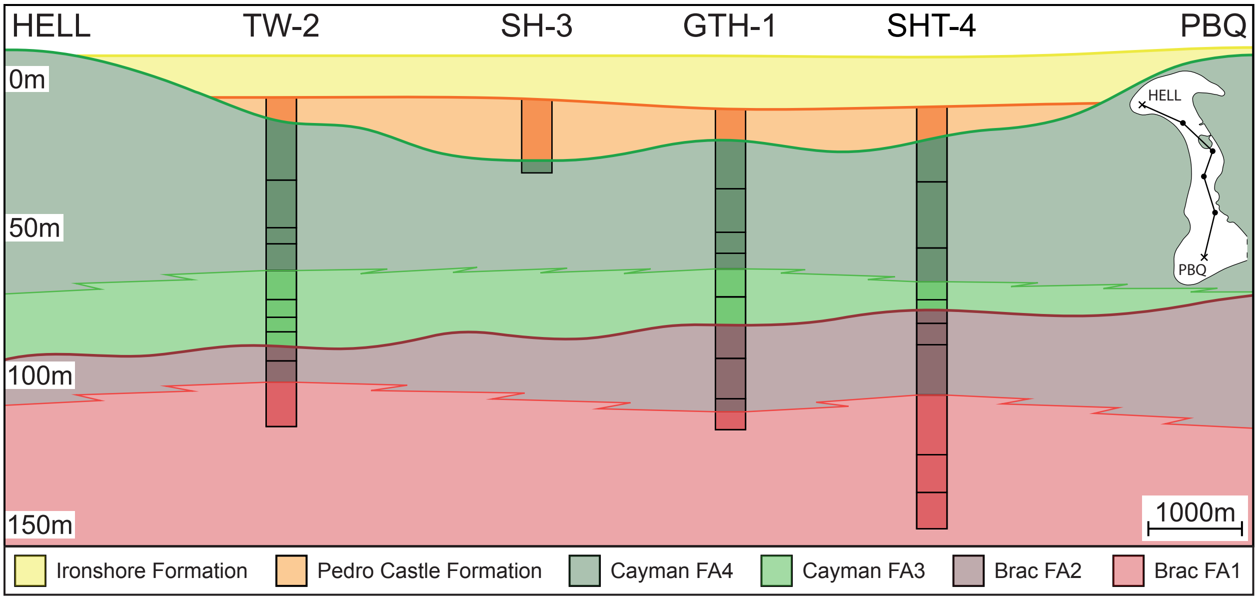

Fig. 22: 12 km N - S cross section, from Hell to Paul Bodden's Quarry (PBQ), showing the stratigraphy and facies architecture of western Grand Cayman. FA = Facies association. Depth is below modern sea level.

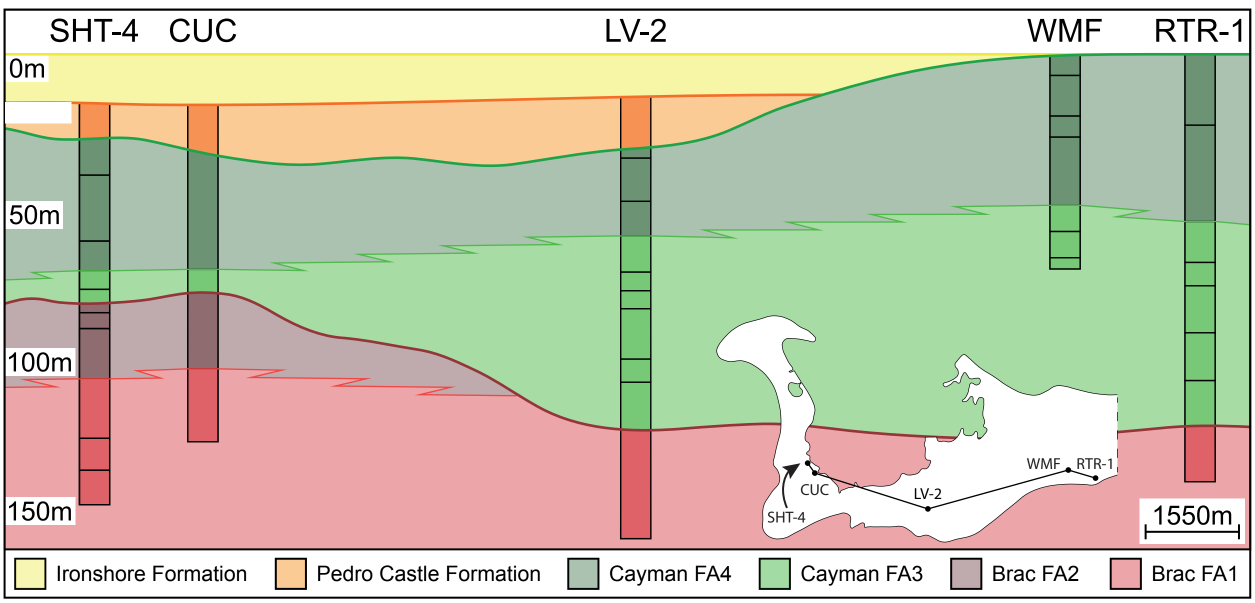

Fig. 23: 20 km W - E cross section, from SHT-4 to RTR-1, showing the stratigraphy and facies architecture of western and central Grand Cayman. FA = Facies association. Depth is below modern sea level.

relatively subdued in contrast to the relief on the Cayman Unconformity, which is up to 33 m. Accordingly, the thickness of the Cayman Formation, which ranges from 45 m - 70 m thick, is controlled largely by the erosional relief on the overlying Cayman Unconformity (Fig. 22). During the Pliocene, the antecedent topography on the Cayman Unconformity was characterized by a dish-shaped depression centered under North Sound. Deposition of the sediments that now form the Pedro Castle Formation, which ranges from 0 m - 22 m thick, filled paleo-topographic lows on the underlying Cayman Unconformity (Fig. 22).

In the subsurface of central Grand Cayman, the Brac Unconformity is between 72 m - 129 m bsl and dips east at ~0.2° (Fig. 23). The maximum depth reached from drilling is 155 m bsl in LV-2, where the Brac Unconformity is at 123 m bsl. The Brac Formation is, therefore, at least 32 m thick on central Grand Cayman. Deposition of the sediments that now form the Cayman Formation, which ranges 98 m - 129 m thick on central Grand Cayman, filled paleo-topographic lows on the underlying Brac Unconformity. The Cayman Unconformity is typically between 15 m asl - 25 m bsl and dips west at ~0.15°. The Pedro Castle Formation, which varies in thickness from 0 m - 16 m on the central parts of the island, has been fully eroded on east-central Grand Cayman where the Cayman Unconformity is exposed at surface (Fig. 23).

4.1.2. Facies Architecture in the Brac Formation

Facies evident in the core from SHT-4 are discernable in the limited core that is available from TW-2, GTH-1, GET-1, and CUC-1. Samples and data from these wells reveal the following information regarding the facies architecture in the Brac Formation on western Grand Cayman.

(1) The lower part of the Brac Formation in TW-2 and GTH-1 is assigned to FA1. FA1 is at least 11 m thick in GTH-1 and at least 13 m thick in TW-2 (Appendix - 2).
(2) The upper part of the Brac Formation in TW-2, GTH-1, and GET-1 is assigned to FA2. FA2 ranges from 12 m (TW-2) to 27 m thick (GTH-1). The basal contact of FA2 is not discernable in GET-1 (Appendix - 2).
(3) In GTH-1, the contact between FA1 and FA2 is at 106 m bsl, whereas in TW-2, it is in a 9 m thick gap between cored intervals (95 m bsl - 104 m bsl).

In the subsurface of western Grand Cayman, the Brac Formation is largely finely crystalline dolostone with lesser calcareous dolostone. Towards the southern end of North Sound however, the basal part of the Brac Formation in CUC-1, CUC-3, and CUC-4 is dolomitic limestone (Fig. 24).

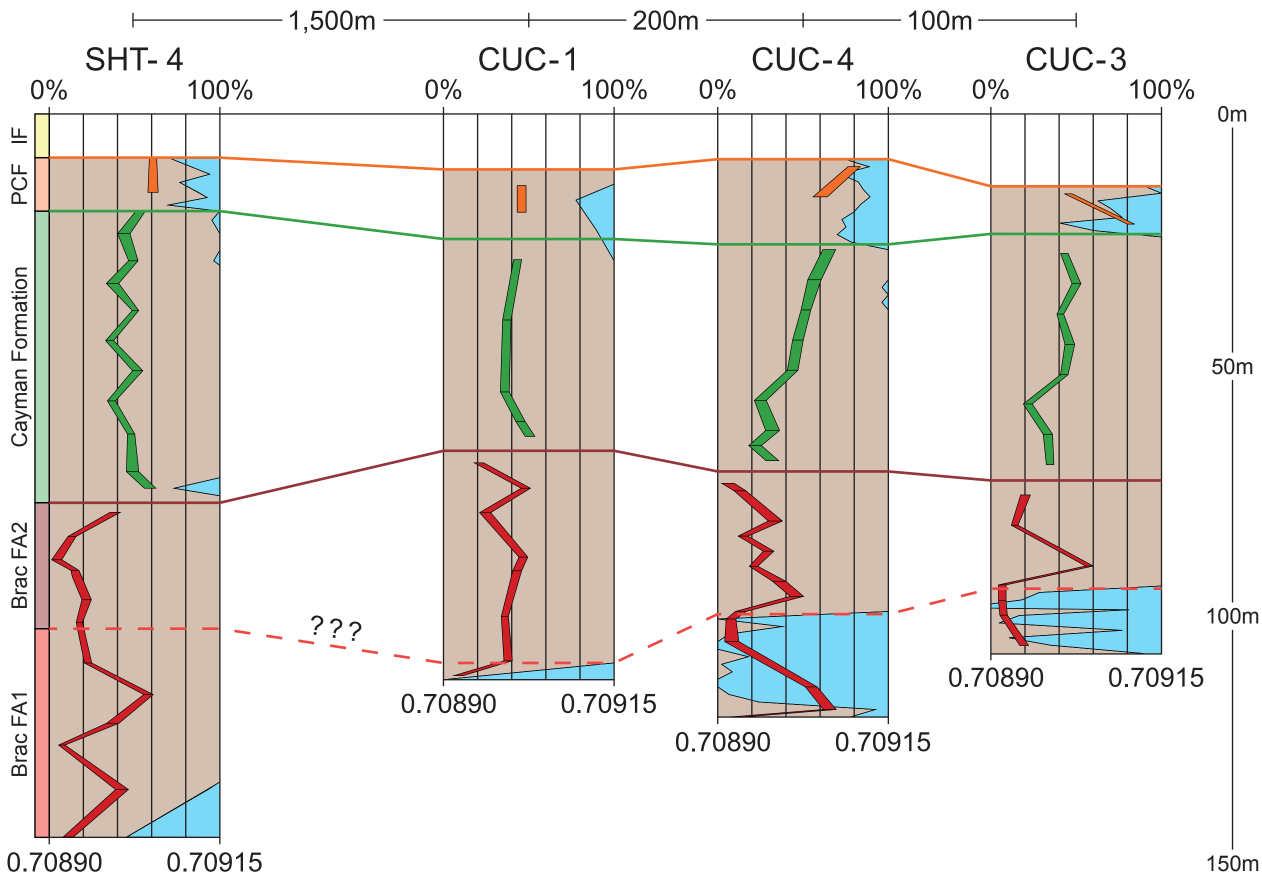

Fig. 24: Cross section from SHT-4 to the wells from the Cayman Utilities Company area (CUC) showing the mineralogy and $^{87}Sr/^{86}Sr$ isotope ratios of the wells on western Grand Cayman (see Fig. 2C for locations). Facies associations (FA) in the Brac Formation shown for reference. Width of the $^{87}Sr/^{86}Sr$ isotope ratio plot indicates the 2 standard error of the mean for each sample. Depth is below modern sea level.

Core samples from the Brac Formation in these wells, however, are limited to 0.8 m from CUC-1. Accordingly, the samples collected from well-cuttings in these wells, which appear to be relatively homogenous, have typically been characterized geochemically (Jones and Luth, 2003a; Wang et al. 2019). Based on these samples, the boundary between dolostone and dolomitic limestone is at a depth of 96 m bsl in CUC-3, 101 m bsl in CUC-4, and 110 m bsl in CUC-1 (Fig. 24). In the core from CUC-1, the upper part of the Brac Formation is assigned to FA2. Core sampling from 113 m - 114 m bsl, however, yielded 0.15 m of poorly lithified dolomitic limestone. The position of the boundary between dolostone and dolomitic limestone is not discernable in the samples from well cuttings. The mineralogical boundary between dolostone and dolomitic limestone in the CUC area roughly corresponds to the boundary between FA1 and FA2 in the core from SHT-4, which is located at 104 m bsl (Fig. 24).

Data from the Brac Formation on central Grand Cayman are limited to samples collected from well-cuttings from LV-2 and RTR-1. Facies in the Brac Formation, however, are well established in the core from SHT-4, which is located 8 km from LV-2. Accordingly, the correlation of facies in the Brac Formation is largely restricted to western Grand Cayman. In the subsurface of central Grand Cayman, the Brac Formation is entirely finely crystalline dolostone.

4.1.3. Facies Architecture in the Cayman Formation

FA3 of the Cayman Formation, which consists of large benthic foraminifera, red algae, bivalve, and domal coral grainstone and rudstone, is 12 m (GET-1) to 24 m (TW-2) thick on western Grand Cayman (Fig. 22; Appendix 2). The thickness of FA3 is controlled largely by the antecedent topography on the underlying Brac Unconformity, as the upper contact with FA4 is flat (56 m - 60 m bsl). Facies evident in the core from SHT-4 are representative of FA3 in the subsurface of western Grand Cayman. Facies 3A is present in SHT-4, GTH-1, and TW-2, but absent in GET-1, whereas facies 3B is present in SHT-4, GET-1, and TW-2, but absent in GTH-1.

On central Grand Cayman, FA3 of the Cayman Formation is up to 73 m thick in LV-2 (Fig. 23; Appendix - 2). The thickness of FA3 is controlled largely by antecedent topography on the Brac Unconformity, as the upper contact with FA4 is relatively flat (35 m - 60 m bsl). Furthermore, the geographic distribution of facies in FA3, which onlap the Brac Unconformity towards western Grand Cayman, is also controlled by antecedent topography (Fig. 23). Facies evident in the cores from western Grand Cayman are representative of the upper parts of FA3 on the central parts of the island, which are found at similar depths. Facies found in the lower parts of FA3, the deposition of which filled paleo-topographic lows on the Brac Unconformity, are unique to central Grand Cayman. Facies 3A is present in LV-2, WMF-1, and RTR-1, whereas facies 3B is present in LV-2 and RTR-1 but absent in WMF-1. Facies 3C has not been recognized on central Grand Cayman. Facies 3D is present in the lower parts of all the wells on eastern Grand Cayman but has not been recognized on the western parts of the island. Facies 3E is unique to LV-2.

FA4 of the Cayman Formation, which consists of branching corals in growth position, green algae, and rhodolith wackestone and floatstone, is 38 m (GET-1) to 47 m (TW-2) thick on western Grand Cayman (Fig. 22). The thickness of FA4 is controlled largely by erosional relief on the overlying Cayman Unconformity, as the basal contact with FA3 is relatively flat (56 m - 60 m bsl). Facies evident in the core from SHT-4 are representative of FA4 in the subsurface of western Grand Cayman. Facies 4A is evident in all wells that reach sufficient depths to intersect its gradational basal contact with FA3 (GET-1, SHT-4, GTH-1, TW-2). Facies 4B and 4C are evident in all wells on western Grand Cayman, whereas facies 4D is unique to TW-1.

On central Grand Cayman, FA4 of the Cayman Formation ranges from 26 m - 47 m thick (Fig. 23). The thickness of FA4 is controlled largely by erosional relief on the overlying Cayman Unconformity, as the basal contact with FA3 is relatively flat (35 m - 60 m bsl). Facies evident in the cores from western Grand Cayman are representative of FA4 on the central parts of the island. Facies 4A is present in LV-2, WMF-1, and RTR-1, whereas facies 4B is present in LV-2 and WMF-1 but absent in RTR-1. Facies 4C is present in LV-2, WMF-1, and RTR-1. Facies 4D has not been recognized on central Grand Cayman.

4.1.4. Facies Architecture in the Pedro Castle Formation

The facies architecture in the Pedro Castle Formation for western Grand Cayman has been well described in previous studies (Jones and Hunter, 1989; Jones and Hunter, 1994a; Wignall, 1995; Etherington, 2004). The Pedro Castle Formation consists of a transgressive succession of packstone, wackestone, and floatstone that are formed of calcareous dolostone and dolomitic limestone (Wignall, 1995; Etherington, 2004). The basal part of the Pedro Castle Formation consists of packstone that contains numerous rhodoliths and foraminifera (e.g., *Amphistegina*) with fewer free-living corals (e.g., *Trachyphyllia*, *Teleiophyllia*, *Thysanus*). The middle part of the succession consists of packstone and wackestone that contains numerous molluscs, green algae plates (e.g., *Halimeda*), and free-living corals with fewer foraminifera, and rhodoliths. The upper part of the Pedro Castle Formation consists of wackestone and floatstone that contains numerous free-living and branching (e.g., *Stylophora*) corals in growth position with fewer foraminifera, molluscs, and rhodoliths (Jones and Hunter, 1994a; Wignall, 1995; Etherington, 2004). The dolomite content in the Pedro Castle Formation generally decreases upwards (MacNeil and Jones, 2003; Etherington, 2004).

Facies evident in the Pedro Castle Formation on central Grand Cayman are analogous to those described on the western parts of the island, where the formation consists of a transgressive succession of packstone, wackestone, and floatstone (Jones and Hunter, 1994a; Wignall, 1995; Arts, 2000; Etherington, 2004). On central Grand Cayman, however, the Pedro Castle Formation is entirely dolostone (Jones and Hunter, 1994a; Arts, 2000).

4.2. Reservoir Quality - Western and Central Grand Cayman

In the cores from SHT-4 and LV-2 (Fig. 25), the wackestone and packstone that form the Pedro Castle Formation have an average porosity of 8.9% (n = 3). The wackestone and floatstone that form facies association 4 (FA4) of the Cayman Formation have an average porosity of 10.1% (n = 14), whereas the grainstone and rudstone that form facies association 3 (FA3) of the Cayman Formation have an average porosity of 38.6% (n = 18). In the core from SHT-4, the packstone that forms facies association 2 (FA2) of the Brac Formation have an average porosity of 13.2% (n = 7), whereas the wackestone that forms facies association 1 (FA1) of the Brac Formation have an average porosity of 5.3% (n = 4).

The complexity of pore types in carbonate sedimentary successions typically produce non-linear relationships between porosity and permeability. Accordingly, porosity is a weak proxy for flow properties in carbonate strata and it is necessary to understand the distribution of pore types in the succession and their relationship with permeability (Lucia, 1999; Hollis et al. 2010; Van der Land, 2013). There is a distinct contrast in pore types, which are named according to Choquette and Pray's (1970) classification scheme, in each stratigraphic interval defined in this study. Primary pores in FA1 of the Brac Formation are occluded largely by dolomitized micrite, whereas primary pores in FA2 have been occluded by finely crystalline dolomite cement. Secondary pores in FA1 are

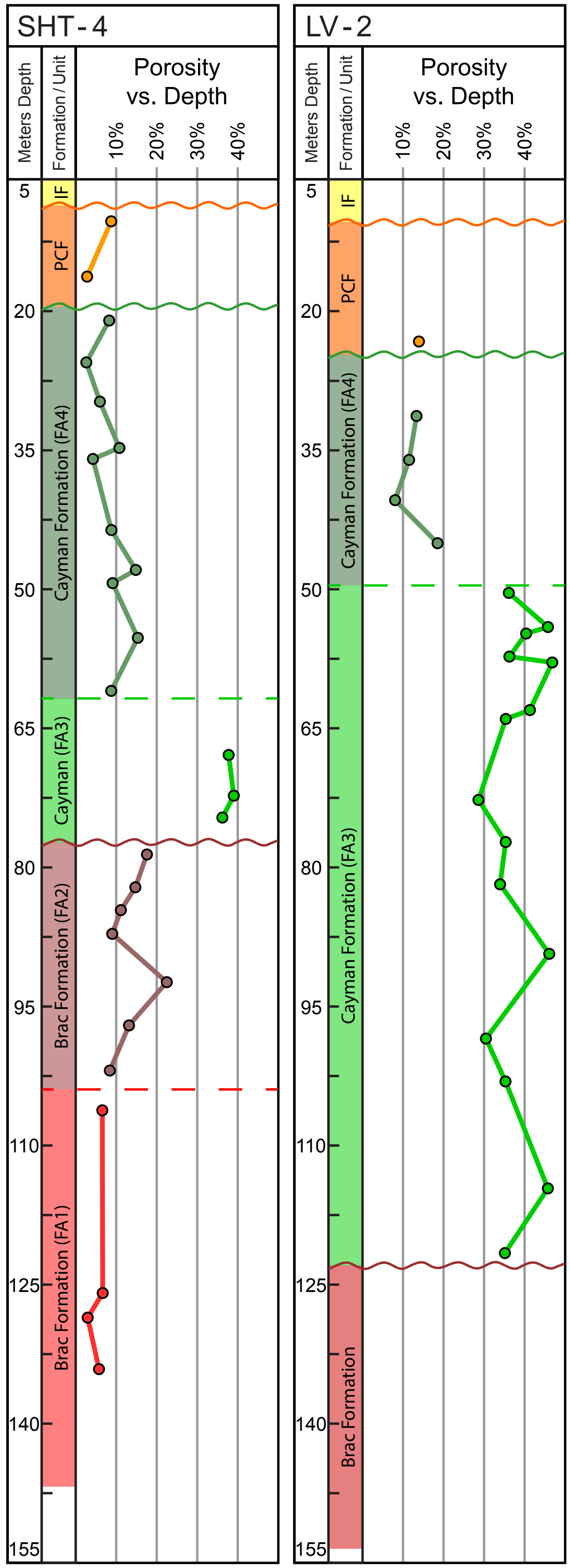

Fig. 25: Porosity vs. depth profile showing the stratigraphy and facies associations in SHT-4 and LV-2.

rare, whereas FA2 contains fabric-non-selective (e.g., vugs, fractures) and fewer fabric-selective (e.g., fossil-moldic, intercrystal) secondary pores. FA3 of the Cayman Formation is dominated by well-preserved primary porosity (predominantly interparticle), whereas primary pores in FA4 have been occluded by microcrystalline dolomite cement. FA3 contains scattered fabric-selective secondary pores, whereas FA4 contains both fabric-selective (predominantly fossil-moldic) and fabric-non-selective secondary pores (predominantly vugs). The morphologies of fabric-selective pores typically mimic the morphologies of the biota that are now leached. Descriptions of pore types are representative of the size of the samples available for this study, which is based primarily on core samples and thin-section data. Accordingly, pores larger than the core diameter, which is typically 5.0 cm, may not be discernable (e.g., large fossil-moldic, large vugs, channels, fractures, caverns).

There is a clear correlation between pore types (primary vs. secondary; fabric-selective vs. fabric-non-selective) and the relationship between porosity, maximum horizontal permeability (K_{max}), and vertical permeability (K_{vert}). Facies associations that have well-preserved primary pores (e.g., FA3) have a narrow range of K_{max} values, a wide range of porosity values, and a near-linear relationship between K_{vert} and K_{max}. In contrast, facies associations that have primary pores that are occluded (e.g., FA1, FA2, FA4), either through the presence of dolomite cement or dolomitized micrite, have a narrow range of porosity values and a wide range of K_{max} values that are considerably larger than K_{vert}.

4.2.1. Porosity and Permeability in the Brac Formation

On western and central Grand Cayman, the Brac Formation is comprised by a succession of low porosity, moderate permeability dolostone (Fig. 26A; 26B; 26C; 26D). The Brac Formation has small interparticle pores (< 50 μm) that are largely occluded by dolomitized micrite. Fabric-selective secondary pores are minor in the Brac Formation, as most of the allochems have been replaced by finely crystalline dolomite.

The wackestone that forms FA1 of the Brac Formation have an average porosity of 5.7%,

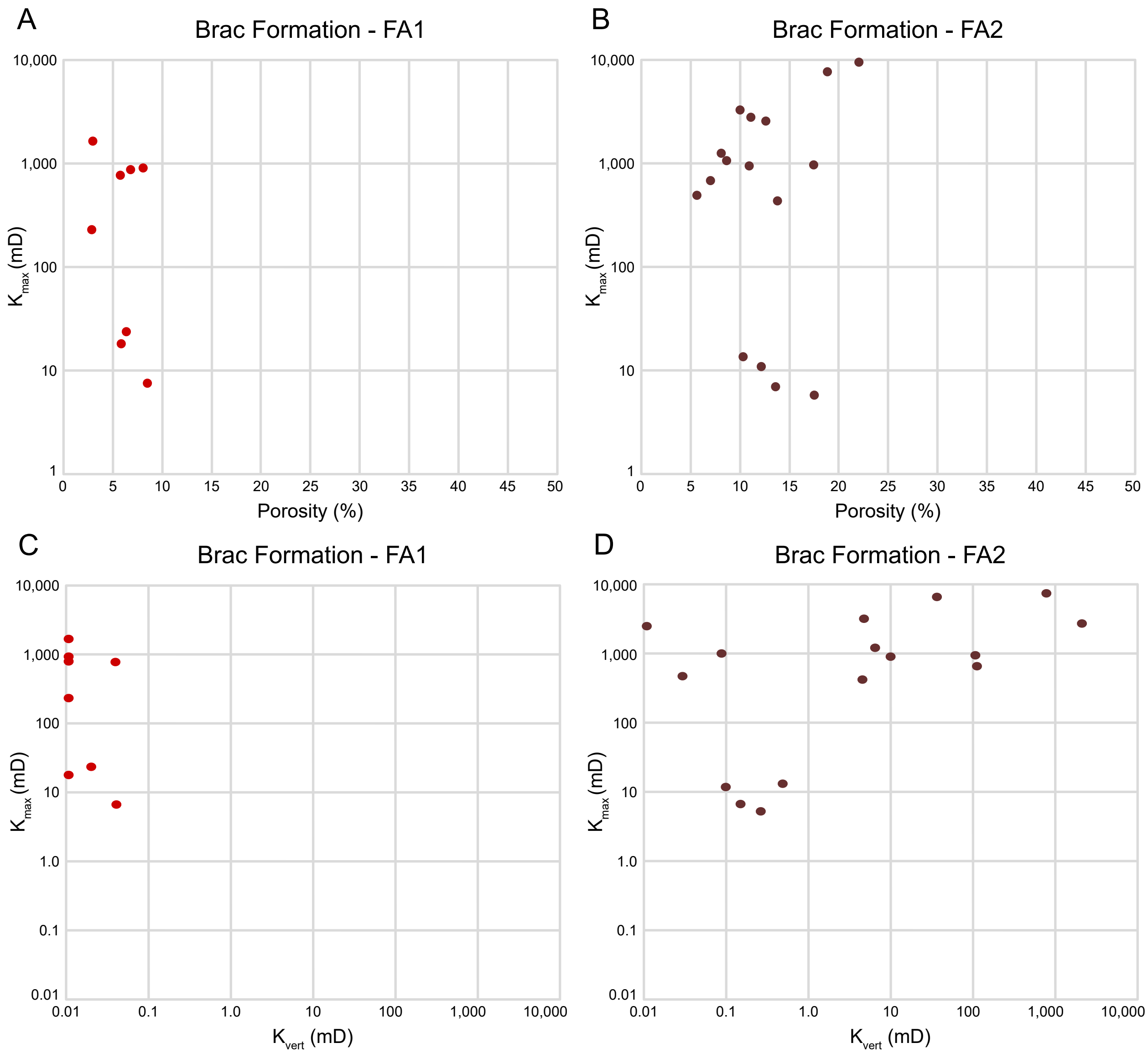

Fig. 26: (A) Facies association 1 permeability (Kmax) vs. porosity plot; (B) Facies association 2 permeability (Kmax) vs. porosity plot; (C) Facies association 1 vertical permeability (Kvert) vs. maximum permeability (Kmax) plot; (D) Facies association 2 vertical permeability (Kvert) vs. maximum permeability (Kmax) plot. Plots include all data from western and central Grand Cayman.

an average K_{max} of 576.1 mD, and an average K_{vert} of 0.02 mD (n = 8). In the core from SHT-4, the porosity in FA1 is largely derived from primary pores with fewer fabric-selective secondary pores. Fabric-non-selective secondary pores are rare. Allochems in FA1 have typically been mimetically replaced by finely crystalline dolomite. Dolomite cement is minor, whereas dolomitized micrite is common in the matrix of FA1 and occludes pore throats between the allochems (Fig. 9B; 9C). Accordingly, porosity in FA1 narrowly ranges from 3 % - 8%, whereas K_{max} varies widely from 20 mD - 800 mD (Fig. 26A). FA1 has an average K_{max} that is ~30,000 times greater than the average K_{vert}, which is typically < 0.1 mD (Fig. 26C).

The packstone that forms FA2 of the Brac Formation have an average porosity of 12.3%, an average K_{max} of 1997 mD, and an average K_{vert} of 204.5 mD (n = 16). In the core from SHT-4, the porosity in FA2 is largely in the form of secondary pores, as primary pores have been occluded by finely crystalline dolomite cement (Fig. 11B; 11C). Accordingly, porosity in FA2 narrowly ranges from 7 % - 17%, whereas K_{max} varies widely from 80 mD - 1,200 mD (Fig. 26B). FA2 has an average K_{max} that is ~10 times greater than the average K_{vert} (Fig. 26D).

4.2.2. Porosity and Permeability in the Cayman Formation

On western and central Grand Cayman, the Cayman Formation is comprised by a succession of dolostone with strikingly disparate reservoir characteristics (Fig. 27A; 27B; 27C; 27D). In fact, the Cayman Formation has been informally divided into the lower "Porous Unit" and the upper "Caprock" (Jones and Luth, 2002, 2003b). This informal division, although based on pore types and magnitudes, is analogous largely to the division of facies associations FA3 and FA4 that is presented in this study. Fabric-selective (e.g., fossil-moldic) secondary pores are widespread in the Cayman Formation, as most of the aragonitic allochems were leached. The magnitude of porosity and permeability, however, depends largely upon the preservation of primary pores (predominantly interparticle).

The grainstone and rudstone that form FA3 of the Cayman Formation have an average porosity of 32.5%, an average K_{max} of 2379 mD, and an average K_{vert} of 1586 mD (n = 36). Porosity in FA3 is largely derived from primary pores (predominantly interparticle) with fewer fabric-selective secondary pores (Fig. 15A). Intracrystalline pores, which are derived from hollow dolomite crystals that are ~25 μm long with walls < 2 μm thick, are common in FA3 (Jones and Luth, 2003b, their Fig. 5D). Jones and Luth (2002; 2003b) suggested that these hollow dolomite crystals resulted from preferential dissolution of the cores of replacive dolomite crystals and/or dolomite cement crystals. Facies that comprise FA3 of the Cayman Formation typically have open

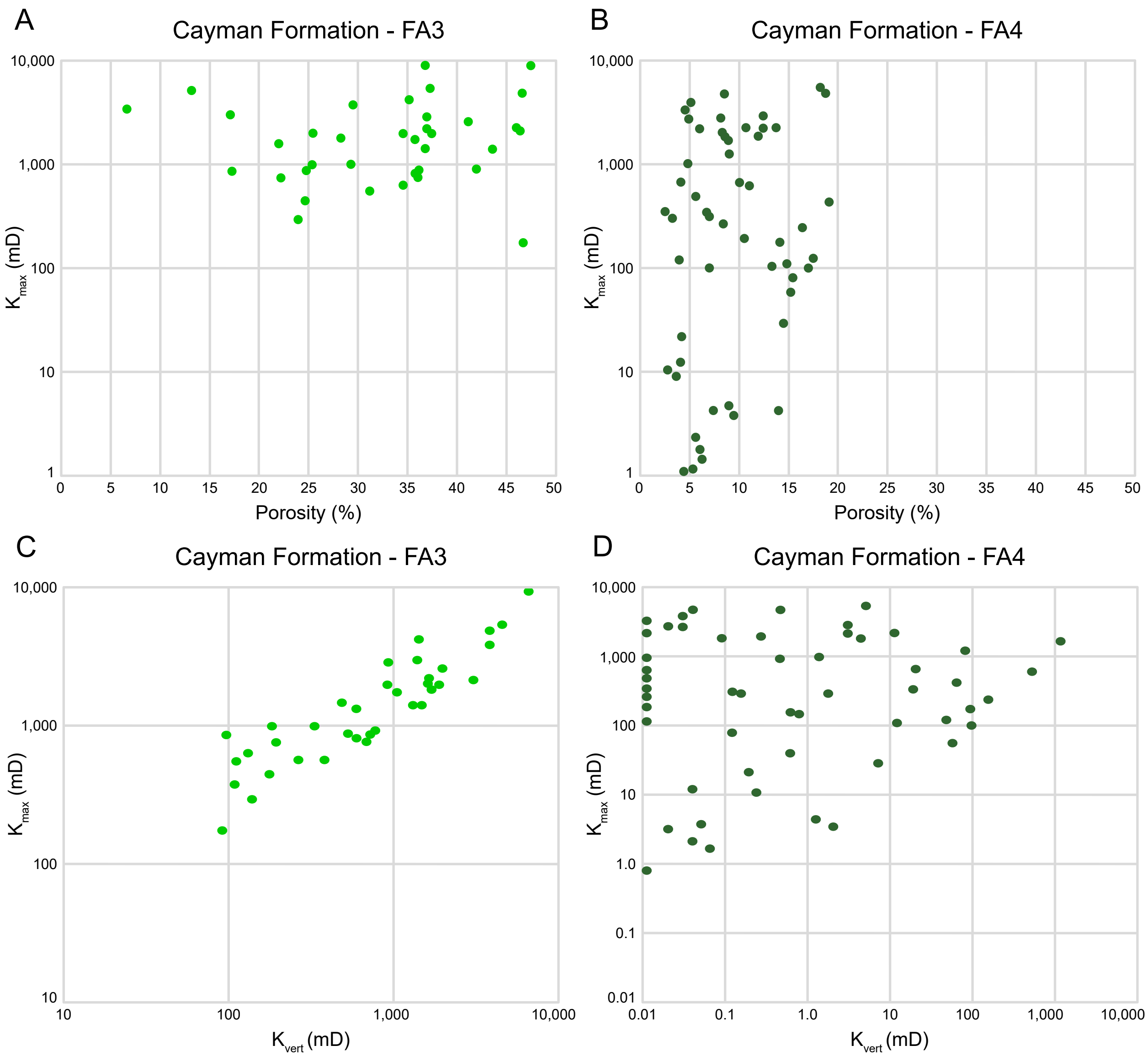

Fig. 27: (A) Facies association 3 permeability (Kmax) vs. porosity plot; (B) Facies association 4 permeability (Kmax) vs. porosity plot; (C) Facies association 3 vertical permeability (Kvert) vs. maximum permeability (Kmax) plot; (D) Facies association 4 vertical permeability (Kvert) vs. maximum permeability (Kmax) plot. Plots include all data from western and central Grand Cayman.

pore throats, because dolomite cement and internal sediments are rare (Fig. 13B; 13C; 15B; 15C). Accordingly, K_{max} in FA3 is consistently greater than 800 mD, whereas porosity varies widely from 25% - 45% (Fig. 27A). FA3 has a near-linear relationship between K_{max} and K_{vert} (Fig. 27C).

The wackestone and floatstone that form FA4 of the Cayman Formation have an average porosity of 9.3%, an average K_{max} of 1044 mD, and an average K_{vert} of 44.2 mD (n = 53). Porosity in FA4 is derived from both fabric-selective (predominantly fossil moldic) and fabric-non-selective secondary pores (predominantly vugs), as primary pores have been largely occluded by microcrystalline dolomite cement (Fig. 18A; 18B; 18C). Interparticle pores in FA4 are lined with, or completely occluded by, interlocking euhedral limpid dolomite crystals that are ~25 μm long (Jones and Luth, 2003b, their Fig. 8B; 8C). Jones and Luth (2003b) suggested that cavities in the upper part of the Cayman Formation contain up to five phases of dolomite cements. The distribution of these isopachous dolomite cements are controlled largely by the textures of the precursor limestone (Jones and Luth, 2002, 2003b). FA4 also contains fabric-non-selective karst features such as terra rossa, flowstones, collapse breccias, and caymanite (a laminated cave-filling deposit) that occlude porosity. Accordingly, porosity in FA4 narrowly ranges from 5 % - 15%, whereas K_{max} varies widely from 80 mD - 1,200 mD (Fig. 27B). FA4 is has an average K_{max} that is ~25 times greater than the average K_{vert} (Fig. 27D).

Chapter 5: Interpretation

The Paleogene-Neogene succession on each of the Cayman Islands is formed primarily of carbonate sediments. Terra rossa, the only siliciclastic deposit found on these islands, is formed largely of wind-borne clays that originated from the Sahara Desert (Merino and Banerjee, 2008; Muhs and Budahn, 2009; Liang and Jones, 2015b). Stratigraphic cyclicity in the carbonate succession was governed primarily by changes in relative sea level, which is the combined effect of eustatic sea level and local tectonism. Sea level highstands led to the deposition of the sediments that now form the succession on the Cayman Islands, whereas subaerial erosion during sea level lowstands gave rise to the development of unconformities that form the boundaries between the formations in the succession (Jones and Hunter, 1994a; Liang and Jones, 2014).

The Paleogene - Neogene succession on Grand Cayman developed on a shallow-water, carbonate bank that has a near-vertical shelf-edge (Fig. 28) (Jones and Hunter, 1994a). Carbonate banks are small, isolated carbonate platforms, that are surrounded by deep water and do not have a complete array of depositional environments (e.g., peritidal, lagoon, reef, slope etc.) (Vecsei, 2004; Bosence, 2005; James and Jones, 2015). Deposition of the sediments that now form this succession was controlled primarily by water depth, whereas antecedent topography on erosional unconformities was a critical secondary control on sedimentation. Antecedent topography influenced the distribution of water depths on the bank during the early part of transgressions and determined if it was open to circulation from the surrounding oceanic water (Fig. 28). Although modern banks are found largely at depths between 0 and 70 m (Vecsei, 2004, his Fig. 2), the highly productive Bahamian banks are covered by waters <10 m in depth, whereas the less productive southern Caribbean banks have water depths of ~40 m (Triffleman et al. 1992; Vecsei, 2004).

5.1. Paleo-environmental Interpretation of Facies Associations

Biota found in carbonate environments are sensitive to conditions such as energy levels, light, substrate conditions, salinity, temperature, and nutrients. Three light-dependent groups of biota are typically recognized, which include euphotic (well-lit, shallow water, wave-agitated

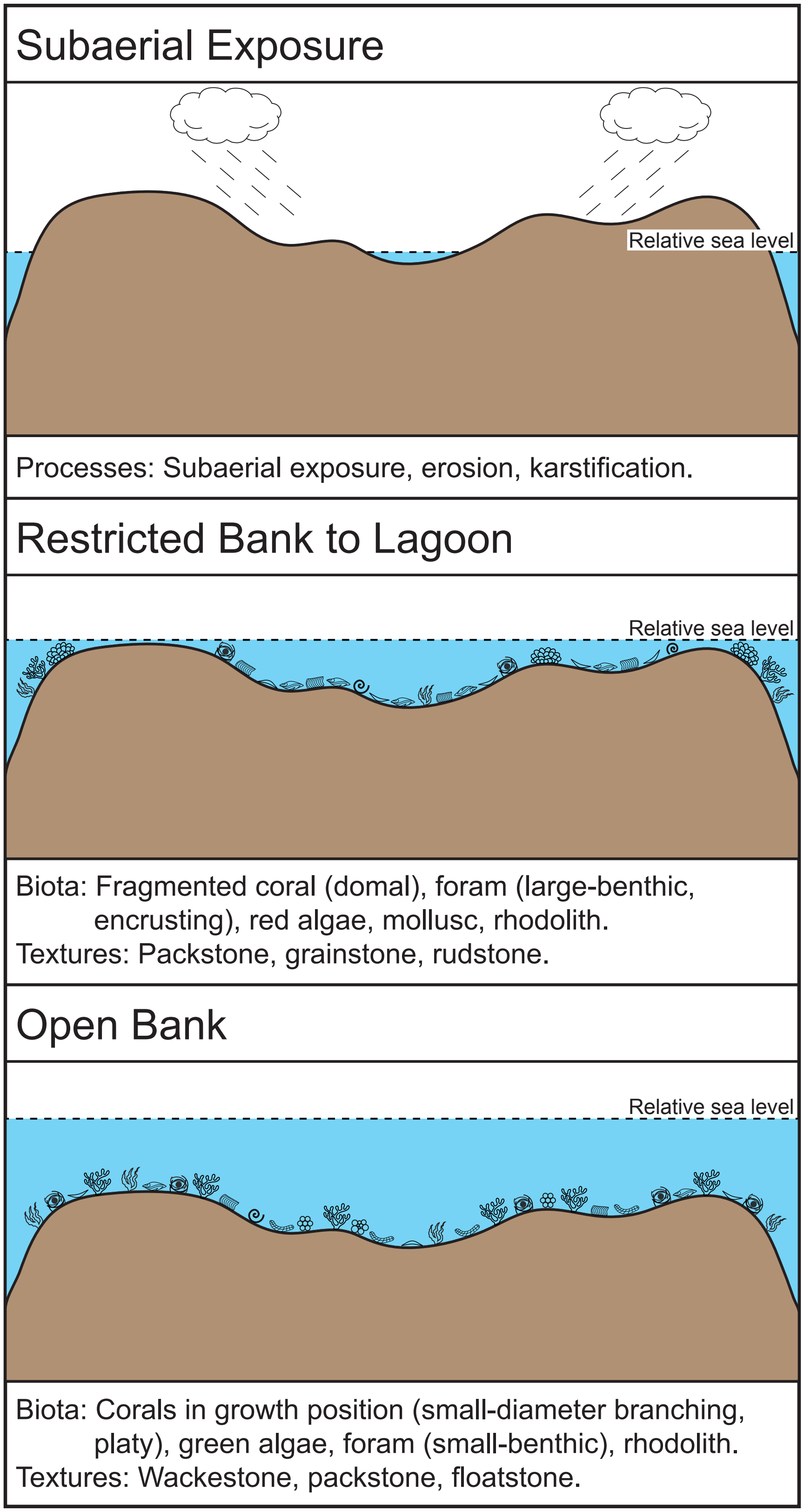

Fig. 28: Idealized carbonate bank depositional environment schematic (modified from Kindler and Hearty, 1996; Hearty and Tormey, 2017).

settings), oligophotic (poorly-lit, deeper water, non-agitated settings), and aphotic (light-independent) assemblages (Pomar, 2001; Pomar and Kendall, 2008). The Paleogene - Neogene succession on Grand Cayman includes a wide array of euphotic, oligophotic, and aphotic biota. The sediments that now form this succession, however, were derived primarily from shallow-water (< 40 m water depth) euphotic settings and instead largely represent fluctuating hydrodynamic conditions. Interpretations of the water depths in which the sediments that now form this succession were deposited are based on: (1) the abundance of biota, (2) their growth forms, and (3) their preservation style. Supporting evidence for the interpretation of energy conditions is based on the textures of the rocks (e.g., Dunham classification, presence/abundance of mud). Shallow-water, high-energy conditions are generally indicated by abundant: (1) rhodoliths, coralline red algae, and large benthic foraminifera, (2) domal and large-diameter branching coral growth forms, and (3) coral fragments (Bosellini and Ginsburg, 1971; Reid and MacIntyre, 1988; Frost et al. 1983; Hallock and Glenn, 1986; Hills and Jones, 2000; Todd, 2008; James and Wood, 2010). In contrast, deeper-water, low-energy conditions are generally indicated by abundant: (1) green algae and small benthic foraminifera, (2) platy and small-diameter branching coral growth forms, and (3) corals in growth position (Hallock and Glenn, 1986; Kooistra et al. 2002; Todd, 2008; Semesi et al. 2009; James and Wood, 2010). Supporting evidence for high-energy conditions are indicated by grain-dominated textures (e.g., rudstone, grainstone), whereas low-energy conditions are indicated by mud-dominated textures (e.g., floatstone, wackestone) (Gischler et al. 2013; Harris et al. 2015).

Six facies that are assigned to FA1 and FA2 have been identified in the Brac Formation, whereas nine facies that are assigned to FA3 and FA4 have been identified in the Cayman Formation on western and central Grand Cayman. Although the constituent facies are locally variable, each of the facies associations is laterally continuous across the island.

5.1.1. Brac Formation - Facies Association 1

Facies Association 1 (FA1), which forms the lower part of the Brac Formation on Grand Cayman, is at least 42 m thick and consists of wackestone that contains numerous oligophotic biota (red algae, small benthic foraminifera, bivalves, gastropods, rhodoliths) with fewer euphotic organisms (branching corals, green algae).

Branching forms of *Porites*, which are typically in growth position, are the predominant coral present in FA1. Isolated thickets of *Porites* baffle the only grain-supported sediments that are now found in FA1. There is no clear evidence, however, of reef development in the Brac Formation. Todd (2008) suggested that branching corals are well adapted to well-lit environments, with moderate water depths and moderate sedimentation rates. Modern branching forms of *Porites* are found in shallow, protected, reef environments (Veron, 2010c), and Hunter (1994) estimated that *Porites* in the overlying Cayman Formation probably grew in water <30 m deep as small, isolated patch reefs or as individual coral thickets. Local facies in the upper parts of FA1 show evidence that coral fragments, which form the nuclei of rhodoliths, have been transported. Although rhodoliths are not uniquely indicative of a specific depositional environment, they are generally associated with shallow water, high-energy, settings (Adey and MacIntyre, 1973; Reid and MacIntyre, 1988). The foraminifera assemblage in FA1 consists of diminutive, sub-spherical benthic forms, with thin-walled tests. Hallock and Glenn (1986) showed that small benthic foraminifera with thin-walled tests are indicative of decreased light levels and more quiescent waters. Micrite, which is now dolomitized, forms a substantial component of the matrix of FA1. Abundant micrite, which is typically found in settings that are not subject to winnowing from waves, tides, and currents, suggests that sediments were deposited in relatively deep, low energy, waters (Gischler et al. 2013; Harris et al. 2015).

The biota and textures in the facies that comprise FA1 indicate a shallowing-upward trend. The abundance of small benthic foraminifera, dolomitized micrite, and corals in growth position decreases upwards, whereas the abundance of coral fragments, rhodoliths, and green algae plates increases upwards. Furthermore, mud-rich wackestone deposits are more common at the base of FA1, whereas allochem-rich wackestone and packstone deposits are more common in the upper parts of the succession. Although the basal contact of FA1 has not been reached from drilling, there is no evidence that antecedent topography restricted circulation from the surrounding oceanic water. FA1, which was deposited in an open bank setting, comprises a shallowing-upward succession of facies that indicate deposition in moderate water depths, probably 20 m - 40 m, with low to moderate sedimentation rates.

5.1.2. Brac Formation - Facies Association 2

Facies Association 2 (FA2), which forms the upper 12 m - 27 m of the Brac Formation on Grand Cayman, consists of packstone that contains numerous euphotic biota (branching corals, platy corals, large benthic foraminifera, green algae) with fewer oligophotic organisms (small benthic foraminifera, red algae, bivalves, gastropods).

The coral fauna in FA2 is both fragmented and in growth position, with no systematic trend in their preservation. The diameter of branching corals, however, increases from an average diameter of 8 mm at the base of the succession to an average diameter of 12 mm in the upper parts of the succession. Todd (2008) suggested that domal corals prefer shallow, well-lit environments with low sedimentation rates, whereas platy corals are better adapted to poorly-lit, moderate depth waters, with low sedimentation rates. Modern domal corals are found in lagoons and upper reef slopes in water <30 m deep (Veron, 2010d), whereas platy corals (e.g., *Leptoseris*) are found on reefs in areas of lower light and decreased water turbulence (Veron, 2010a). Hunter (1994) estimated that domal corals in the overlying Cayman Formation grew in water between 20 m - 30 m deep and platy corals grew in water 10 m - 30 m deep. Accordingly, the diverse suite of corals present in FA2 indicates that deposition occurred in moderate to shallow water with low sedimentation rates. The foraminifera assemblage in FA2 consists of large benthic and encrusting forms (0.5 mm - 2.0 mm in diameter), with robust tests and elongate to flat-sided morphologies. Due to their association with photosynthetic algae, large benthic foraminifera are indicative of shallow water settings (Frost and Langenheim, 1974; Murray, 1991; Wilson, 2004). Hallock and Glenn (1986) showed that benthic foraminifera with flat or lenticular shapes are indicative of decreased light levels and more quiescent waters, whereas forms with robust tests are indicative of shallow water (typically <10 m), high-energy settings. Fine sediment was largely swept off the bank during the deposition of the sediments that now form FA2, implying that this packstone were largely winnowed by waves, tides, and currents.

The biota and textures in the facies that comprise FA2 indicate a shallowing-upward trend. The abundance of domal corals and red algae increases towards the upper part of the succession, whereas the abundance of platy corals and green algae plates decreases upwards. Furthermore, wackestone is more common at the base of FA2, whereas packstone is more common in the upper parts of the succession. Antecedent topography did not restrict circulation from the surrounding oceanic water, because the gradational basal contact with FA1 is sub-horizontal. FA2, which was deposited in an open-bank setting, comprises a shallowing-upward succession of facies that indicate deposition in moderate water depths, probably 10 m - 30 m, with moderate sedimentation rates.

5.1.3. Cayman Formation - Facies Association 3

Facies Association 3 (FA3), which forms the lower part of the Cayman Formation on Grand Cayman, consists of grainstone and rudstone that contains numerous euphotic (large benthic foraminifera, encrusting foraminifera, domal corals, green algae) and oligophotic (red algae, rhodoliths, bivalves, gastropods) biota. Deposition of the sediments that now form FA3 onlapped and filled antecedent topography on the underlying Brac Unconformity (Fig. 29). Accordingly, FA3 is 12 m - 24 m thick on western Grand Cayman, whereas it is up to 73 m thick on the central parts of the island. The facies that comprise FA3 are analogous to the ‘porous unit’ defined by Jones and Luth (2002; 2003b) and, although now dolomitized, are analogous to the ‘interior limestone’ defined by Ren and Jones (2017).

Although not in growth position, domal corals (e.g., *Porites*, *Montastrea*) are common in FA3. Fragments of domal corals, which form the nuclei of rhodoliths, show clear evidence of transportation. Coral fragments found in FA3 were probably transported to shallower waters from lagoonal and upper reef settings in the deep-euphotic zone (waters 10 m - 30 m deep). The paucity of reef-building organisms in growth position suggests that hard substrates for the colonization of corals were rare and that a mobile sedimentary blanket of skeletal fragments may have prevailed across the bank during the deposition of the sediments that now form FA3; a feature that was similarly recognized for the modern sediments of the Florida-Bahamas region (Ball, 1967) and the Pleistocene succession on the Bahamas (Kindler and Hearty, 1996; Hearty and Tormey, 2017). Benthic foraminifera and coralline red algae are the most abundant element of the biota in FA3. Red algae dominate shallow water (<15 m) sheltered settings and are broken down into sand sized particles upon their demise (Aguirre et. al. 2000; Braga et al. 2010). The foraminifera assemblage in FA3 consists of large benthic and encrusting forms (1.0 mm - 4.0 mm in diameter), with thick-walled tests and elongate to flat-sided morphologies. *Amphistegina*, which are the most common benthic foraminifera in FA3, typically live as epibionts on sea grasses (e.g., Thalassia) or hard substrates (Corlett and Jones, 2007). *Amphistegina* are commonly found on shallow water, carbonate bank, and near reef environments (Frost et al. 1983; Li and Jones, 1997). The absence of fine sediment in FA3 suggests it was either: (1) not originally present, or (2) it was winnowed by waves, tides, and currents and was entirely swept off bank. It is not clear if the fine-grained material present in the matrix of packstone deposits, which are rare, is microcrystalline dolomite cement or micrite that has been replaced by microcrystalline dolomite.

The biota and textures in the facies that comprise FA3 indicate a deepening-upward trend. Although the abundance of domal corals is constant, the abundance of large-diameter branching corals and green algae plates increases upwards, whereas the abundance of large benthic and encrusting foraminifera decreases upwards. Furthermore, scattered packstone is found only in the upper parts of FA3, whereas the base of the succession is formed of grainstone and rudstone. Antecedent topography on the underlying Brac Unconformity restricted circulation from the surrounding oceanic water, and largely accounts for the heterogeneous facies distribution across the bank (Fig. 29). FA3, which was deposited in a restricted bank to lagoonal environment, comprises a deepening-upward succession of facies that indicate deposition in very shallow water, probably <10 m, with high sedimentation rates.

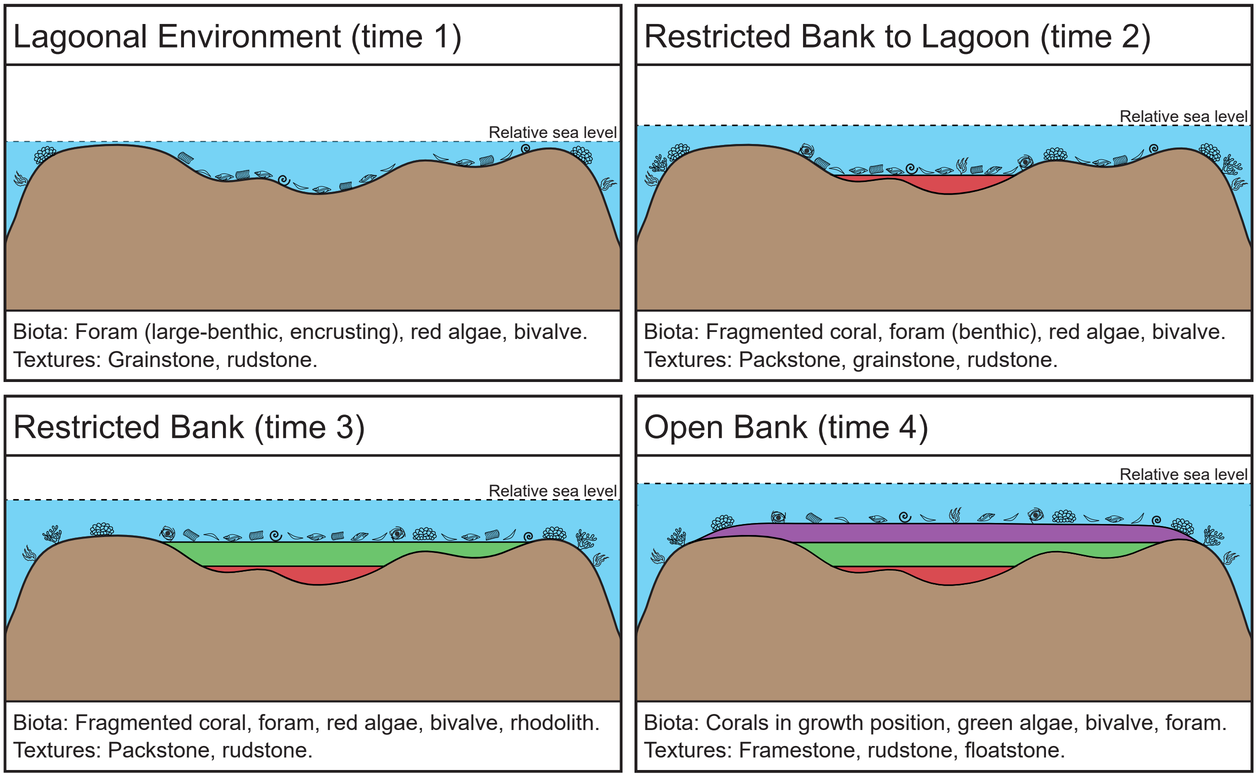

Fig. 29: Idealized diagram showing the distribution of faciers in a restricted bank to lagoonal environment during periods of transgression (modified from Kindler and Hearty, 1996; Hearty and Tormey, 2017).

5.1.4. Cayman Formation - Facies Association 4 (FA4)

Facies Association 4 (FA4), which forms the upper 26 m - 47 m of the Cayman Formation on Grand Cayman, consists of wackestone and floatstone that contains numerous euphotic biota (branching corals, green algae) with fewer oligophotic organisms (rhodoliths, small benthic foraminifera, red algae, bivalves, gastropods). The boundary between FA3 and FA4 may represent a rapid transgressive event that, based on the interpretation of facies, represents a relative sea level rise of 20 m - 30 m. The facies that comprise FA4 are analogous to the 'caprock' defined by Jones and Luth (2002, 2003b) and are analogous to the 'interior dolostone' and 'peripheral dolostone' defined by Ren and Jones (2017).

Branching corals (predominantly *Stylophora*, fewer *Porites*) are common in FA4, with fewer platy and domal corals. The coral fauna is typically in growth position in the lower parts FA4, whereas in the upper parts of the succession, corals are fragmented and commonly form the nuclei of rhodoliths. Branching corals are indicative of well-lit environments with high sedimentation rates in deeper waters, whereas platy corals are well adapted to poorly-lit settings with low sedimentation rates in deeper waters (Todd, 2008; James and Wood, 2010). *Stylophora*, which is a branching coral that became extinct in the Caribbean Sea at the end of the Pliocene, are commonly found in the modern Pacific and Indian oceans in shallow reef environments, sheltered lagoons, or on the mid-lower slope in low to moderate wave energy (Veron, 2010b). Hunter (1994) suggested that *Stylophora* in the Cayman Formation probably grew in waters 15 m - 20 m deep. Although FA4 consists of a wide array of reef-building organisms, there is no evidence of reefs in the Cayman Formation. The foraminifera assemblage in FA4 consists of both diminutive, sub-spherical benthic forms, as well as larger, elongate benthic forms. Carbonate mud is abundant in FA4 and implies that fine sediment was largely baffled by branching corals and green algae and was not winnowed by waves, tides, and currents.

The biota and textures in the facies that comprise FA4 indicate a shallowing-upward trend. Facies at the base of FA4 are formed of wackestone and floatstone, whereas packstone deposits are also present in the upper parts of the succession. The abundance of corals in growth position and small benthic foraminifera decreases towards the upper part of the FA4, whereas the abundance of rhodoliths, fragmented corals, and large benthic foraminifera increases upwards. Antecedent topography did not restrict circulation from the surrounding oceanic water, because the basal contact with FA3 is sub-horizontal. FA4, which was deposited in an open bank setting, comprises a shallowing-upward succession of facies that indicate deposition in moderate water depths, probably 10 m - 30 m, with moderate to high sedimentation rates.

5.1.5. Pedro Castle Formation

The Pedro Castle Formation, which is 0 m - 22 m thick on Grand Cayman, consists of wackestone, packstone, and floatstone that contains numerous euphotic biota (large benthic foraminifera, branching corals, free-living corals, rhodoliths, green algae) with fewer oligophotic organisms (red algae, bivalves, gastropods, small benthic foraminifera). Deposition of the sediments that now form the Pedro Castle Formation onlapped and filled antecedent topography on the underlying Cayman Unconformity (Fig. 29).

Branching (e.g., *Stylophora*, *Porites*) and free-living (e.g., *Trachyphyllia*, *Teleiophyllia*, *Thysanus*) corals, which are typically in growth position, are more common in the Pedro Castle Formation than domal corals. Similar to the underlying Brac Formation and Cayman Formation, the Pedro Castle Formation contains no evidence of reef development apart from scattered branching coral thickets (Jones and Hunter, 1994a). Modern free-living corals are typically found in modern lagoons and inter-reef settings, in waters 10 m - 40 m deep (Veron, 2010e). Hunter (1994) suggested that their distinctive cup shape indicates that these corals were immobile in soft substrates and grew upwards in response to high sedimentation rates. The presence of coexisting branching corals and free-living corals indicate that the sediments that now form the Pedro Castle Formation were deposited in settings with low to moderate wave energy and high sedimentation rates. The foraminifera assemblage in the Pedro Castle Formation consists of both diminutive, sub-spherical benthic forms, as well as larger, elongate benthic forms. Mudstone and wackestone deposits are common in the Pedro Castle Formation and suggests that fine sediment was largely baffled by corals and was not winnowed by waves, tides, and currents.

The biota and textures in the facies that comprise the Pedro Castle Formation indicate a deepening-upward trend (Arts, 2000; Etherington, 2004). The basal parts of the succession consists of packstone and wackestone that contains numerous rhodoliths and benthic foraminifera with fewer free-living corals, whereas the upper parts are formed of wackestone and floatstone that contains numerous free-living and branching corals with fewer foraminifera, rhodoliths, and molluscs (Jones and Hunter, 1994a; Wignall, 1995; Etherington, 2004). Deposition of these sediments, which now form the facies in the Pedro Castle Formation, onlapped and filled antecedent topography on the underlying Cayman Unconformity. (Arts, 2000; Etherington, 2004). The sediments that now form the Pedro Castle Formation, which were deposited in a restricted bank to lagoonal environment (Fig. 29), comprises a deepening-upward succession of facies that indicate deposition in moderate water depths, probably 15 m - 35 m, with high sedimentation rates.

5.2. Evolution of the Paleogene - Neogene Carbonate Bank on Grand Cayman

Due to its isolated position in the Caribbean Sea, the carbonate sedimentary succession on Grand Cayman is ideally suited for assessing changes in relative sea level. Changing water depth is the predominant control on the distribution of facies in the succession and the island can, therefore, be used as an 'oceanic dipstick' that reflects the combined effect of eustacy and tectonism (Wheeler and Aharon, 1991). The Paleogene - Neogene evolution of Grand Cayman was controlled primarily by highstand-lowstand cycles (Fig. 30), whereby relative sea level highstands facilitate deposition and relative sea level lowstands gave rise to subaerial erosion (Jones and Hunter, 1994a, 1994b).

5.2.1. Age Constraints in the Paleogene - Neogene Succession

The early Oligocene (Rupelian) age of the Brac Formation is well-constrained on Cayman Brac due to foraminifera biostratigraphy (Vaughan, 1926; Matley 1926) and limestone $^{87}Sr/^{86}Sr$ isotope ratios (Jones et al. 1994a; Jones and Luth, 2003a; Zhao and Jones, 2012b). The interpretation of the Brac Formation on Grand Cayman hinges largely on the concept that, although now dolomitized, the succession is coeval to the Brac Formation on Cayman Brac. The basal contact of the Brac Formation either has not been recognized or has not been reached from drilling on Grand Cayman or on Cayman Brac, where the formation is at least 69 m thick and at least 33 m thick, respectively. The Brac Unconformity, which forms the upper boundary of the Brac Formation, probably developed over a 12 - 15 million year period during the late Oligocene (Chattian) to early Miocene (Zhao and Jones, 2012b; Liang and Jones, 2014).

The predominant source of uncertainty regarding age constraints in the succession arises largely because of the lack of age diagnostic fossils in the Cayman Formation and the fact that the $^{87}Sr/^{86}Sr$ isotope ratios were reset by dolomitization (Pleydell et al. 1990; Jones et al. 1994b; Jones and Luth, 2003a). Recent investigation of limestone $^{87}Sr/^{86}Sr$ isotope ratios on eastern Grand Cayman are inconclusive, as the constituent carbonate minerals show clear evidence of recrystallization (Der, 2012; Ren and Jones, 2017). $^{87}Sr/^{86}Sr$ isotope ratios from dolostone suggest an late Miocene

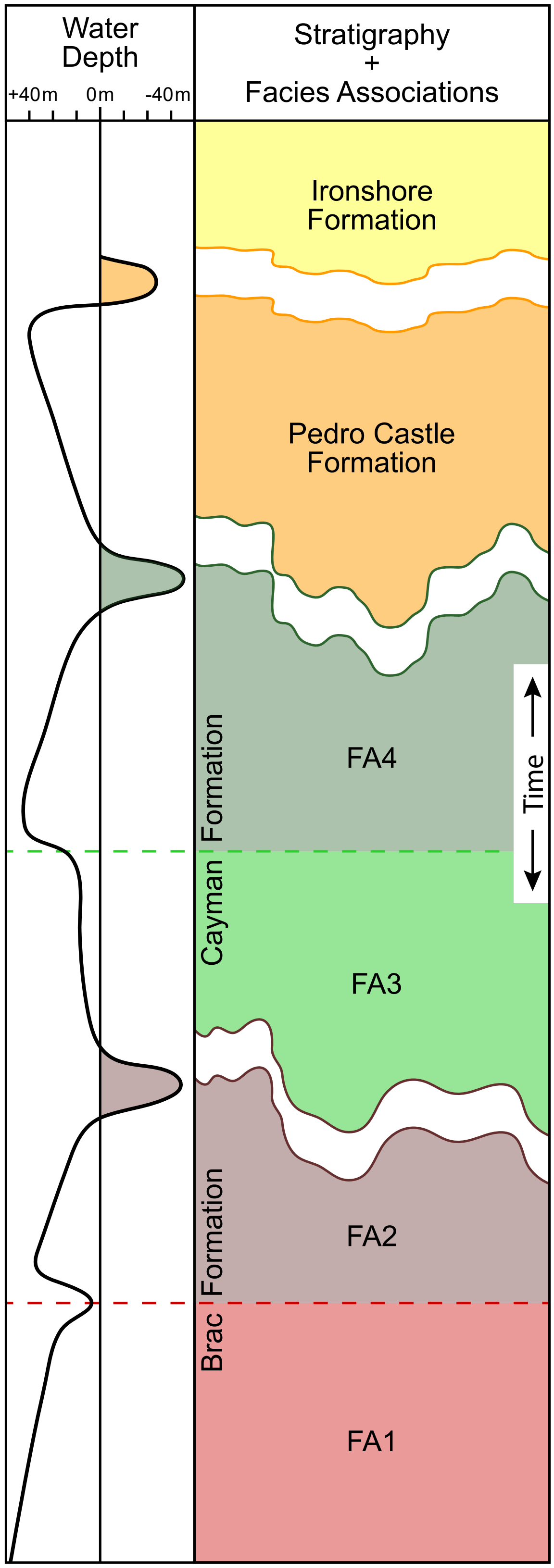

Fig. 30: Idealized water depth curve interpreted from the facies associations and unconformities found in the Paleogene - Neogene succession on Grand Cayman.

(Tortonian - Messinian) age of dolomitization for the Cayman Formation, which indicates that the sediments that now form the formation were deposited prior to the late Miocene (Jones and Luth, 2003a; Wang et al. 2019). Based on the stratigraphic relationship with formations in which the ages are known, it has been suggested that the Cayman Formation is Lower to Middle Miocene (Jones et al. 1994b; Jones and Luth, 2003a). The Cayman Unconformity, which forms the upper boundary of the Cayman Formation, developed over a 2 to 6 million year period during the late Miocene that corresponds to the well-documented Messinian Salinity Crisis in the Mediterranean (Hsü et al. 1977; Jones and Hunter, 1994b; Krijgsman et al. 1999). Based on the stratigraphic relationship with the overlying Pedro Castle Formation, Liang and Jones (2015a) suggested that the Cayman Unconformity developed over two phases: (1) an initial 0.64 to 1.91 million year period during the Messinian that exposed the entire bank and affected all of Grand Cayman, and (2) a 4.3 million year period during the late Pliocene that post-dates the deposition of the sediments that now form the Pedro Castle Formation and that resulted in the Cayman Unconformity being exposed at surface on eastern Grand Cayman.

The Pedro Castle Formation, which stratigraphically overlies the Cayman Formation, is considered to be Pliocene based on limestone $^{87}Sr/^{86}Sr$ isotope ratios and the presence of *Stylophora*, which became extinct in the Caribbean Sea at the end of the Pliocene (Jones and Hunter, 1989; Jones et al. 1994b). The Pedro Castle Unconformity probably formed during the late Pliocene to early Pleistocene (Liang and Jones, 2014; Jones, 2019). Subaerial exposure and the development of the Pedro Castle Unconformity must have terminated prior to the deposition of the sediments that now form the Ironshore Formation, which are accurately dated (Th/U dates from aragonitic corals) to >400 ka to 84 ka (Vezina et al. 1999; Coyne et al. 2007; Jones, 2019).

5.2.2. Facies Association Boundaries

The FA1/FA2 boundary, which is a conformable facies contact on Grand Cayman, has not been recognized on Cayman Brac because the lack of a complete section through the Brac Formation precludes any direction comparison. Although the FA1/FA2 boundary appears to be conformable from the limited available data, the FA1/FA2 boundary may represent a: (1) higher frequency subaerial unconformity, or (2) paraconformity. From the limited core and thin-section data from the Brac Formation on Grand Cayman, however, there is no evidence of paleokarst features associated with the FA1/FA2 boundary (e.g., erosive contacts, dissolution features, speleothems, paleosols, breccias, vadose cements). Furthermore, it is not clear if there is a hiatus across the FA1/FA2 boundary because the precise age of the FA1/FA2 boundary is unknown due to the lack of biostratigraphic data and $^{87}Sr/^{86}Sr$ isotope ratios that have been reset by dolomitization. To resolve this issue, higher resolution petrographic and geochemical data across the FA1/FA2 boundary are required. At this time, the genesis of the FA1/FA2 boundary and its correlation to other Oligocene successions in the Caribbean remains unclear.

The age of the FA3/FA4 boundary on Grand Cayman, which has not been recognized on Cayman Brac, is obscured by the lack of biostratigraphic data and $^{87}Sr/^{86}Sr$ isotope ratios that have been reset by dolomitization. The FA3/FA4 boundary is marked by a rapid transgressive event that, based on the interpretation of facies, may represent a relative sea level rise of 20 m - 30 m that outpaced carbonate productivity and resulted in partial drowning of the bank. Although there is no evidence of phosphogenesis, glauconitisation, and/or ferro-manganese mineralization associated with FA3/FA4 boundary, this contact corresponds to drowning unconformities that have been identified in Lower to Middle Miocene sequences in Italy (Mutti et al. 1997), the Caribbean Sea (Mutti et al. 2005) and the South China Sea (Sattler et al. 2005). Drowning unconformities, as defined by Schlager (1981), represent periods in which sea level rise outpaces carbonate productivity and the platform becomes ‘drowned’ below the euphotic zone. Considering the maximum rate of carbonate productivity is high enough to keep pace with even the most rapid eustatic rises, increased subsidence (Schlager, 1989) or environmental stresses (Wilson, 1998) have been invoked to explain the genesis of drowning unconformities (Godet, 2013). Based on $^{87}Sr/^{86}Sr$ isotope ratios of a phosphatic hardground, Mutti et al. (1997) dated a drowning unconformity on the Maiella platform (Italy) to 21.0 Ma - 20.3 Ma, whereas Mutti et al. (2005) suggested that a drowning unconformity occurred on the Northern Nicaragua Rise (Caribbean Sea) at ~20 Ma.

Furthermore, Sattler et al. (2009) tentatively placed a drowning unconformity that denotes the upper boundary of the Zhujiang Formation (South China Sea) at the end of the Lower Miocene. Although the genesis of these drowning unconformities has been attributed largely to changes in local oceanographic conditions (Mutti et al. 1997; Mutti et al. 2005; Sattler et al. 2005), Godet (2013) suggested that these coeval drowning unconformities, in differing sedimentary basins, may be a response to a more regional environmental phenomenon. Accordingly, the FA3/FA4 boundary, which corresponds to drowning unconformities in the Caribbean Sea (Mutti et al. 2005) and in other basins (Mutti et al. 1997; Sattler et al. 2005), is tentatively placed at ~20 Ma. This interpretation is congruent with proposed sea level curves that show periods of rapid sea level rise during the early Miocene (Vail et al. 1977; Haq et al. 1987; Abreu and Anderson, 1998; Miller et al. 2005). The modern position of the FA3/FA4 boundary, which does not have an erosive component, is located as deep as 60 m bsl and provides a reference for thermal subsidence rates since the time in which it formed (~20 Ma). Estimates of the early Miocene (Aquitanian - Burdigalian) highstand position ranges from ~120 m asl (Haq et al. 1987) to equivalent to modern sea level (Miller et al. 2005). Considering the sediments that now form FA3 were deposited in <10 m water depth, the modern position of the FA3/FA4 boundary suggests that Grand Cayman has subsided 70 m - 190 m since ~20 Ma. This interpretation is congruent with the profile of depth vs. $^{87}Sr/^{86}Sr$ isotope ratio of dolostone from the Cayman Formation, which display a linear decrease with increased depth (Fig. 6). Jones and Luth (2003a) suggested that this relationship indicates that dolomitization was a time-transgressive process that occurred during sea level rise under stable tectonic conditions. This interpretation was plausible because the depth to this dolostone is within the amplitudes of eustatic fluctuations indicated by eustatic curves available at that time (e.g., Haq et al. 1987; ~150 m). More recent eustatic curves (e.g., Miller et al. 2005), however, suggest that the amplitudes of eustatic fluctuations were considerably smaller than the estimates of Haq et al. (1987) and are instead bounded by ±50 m relative to modern sea level. This contention implies that eustatic curves derived from traditional sequence stratigraphic interpretations did not properly account for tectonic effects. The low-amplitude eustatic fluctuations of the Miller et al. (2005) curve support the contention that the modern depth to the Cayman Formation dolostone may be attributed to steady thermal subsidence. Furthermore, Wang et al. (2018, 2019) demonstrated that for the Miocene dolostone on the Xisha Islands, which are located as deep as 525 m bsl, subsidence produced an analogous profile of depth vs. $^{87}Sr/^{86}Sr$ isotope ratio to the dolostone of the Cayman Formation.

5.2.3. Comparison of the Stratigraphy of the Cayman Islands to Paleo-Eustatic Curves

For comparison, numerous eustatic curves and composite isotope records are available (Vail et al. 1977; Haq et al. 1987; Abreu and Anderson, 1998; Miller et al. 2005), each of which is derived from different datasets with variable detail and reliability (Fig. 31). Vail et al. (1977) presented the first relative sea level curve that was derived from seismic stratigraphy. Haq et al. (1987) revised the Vail et al. (1977) curve by integrating supplementary data (e.g., magneto-, chrono-, bio-stratigraphy) with subsurface and outcrop data. Abreu and Anderson (1998) presented a composite $\delta^{18}O$ record for the Cenozoic as an independent comparison to the traditional sequence stratigraphic analysis. Miller et al. (2005) presented a eustatic curve, which was derived from backstripping stratigraphic data, suggesting that the amplitudes of eustatic sea level changes were substantially smaller than the estimates of Vail et al. (1977) and Haq et al. (1987). Although it is not clear which eustatic curve is most accurate, the curve proposed by Miller et al. (2005) appears to be most congruent with the timing and amplitudes of eustatic fluctuations evident in the succession on the Cayman Islands.

Estimates of the highstand position during the early Oligocene (Rupelian) ranges from ~180 m (Haq et al. 1987) to ~20 m asl (Miller et al. 2005). Although the general shapes of each of these eustatic curves are similar, the timing of Oligocene highstand-lowstand boundaries are strikingly different. For example, numerous curves estimate that the early Oligocene highstand was initiated at 33 Ma and extended to 28 Ma (Vail et al. 1977; Abreu and Anderson, 1998; Miller et al. 2005), whereas the Haq et al. (1987) curve suggests that the early Oligocene highstand was initiated at 35 Ma and terminated at 30 Ma. Although the synthesis presented by Haq et al. (1987) is widely used, their timing of the Oligocene highstand-lowstand boundary is not congruent with

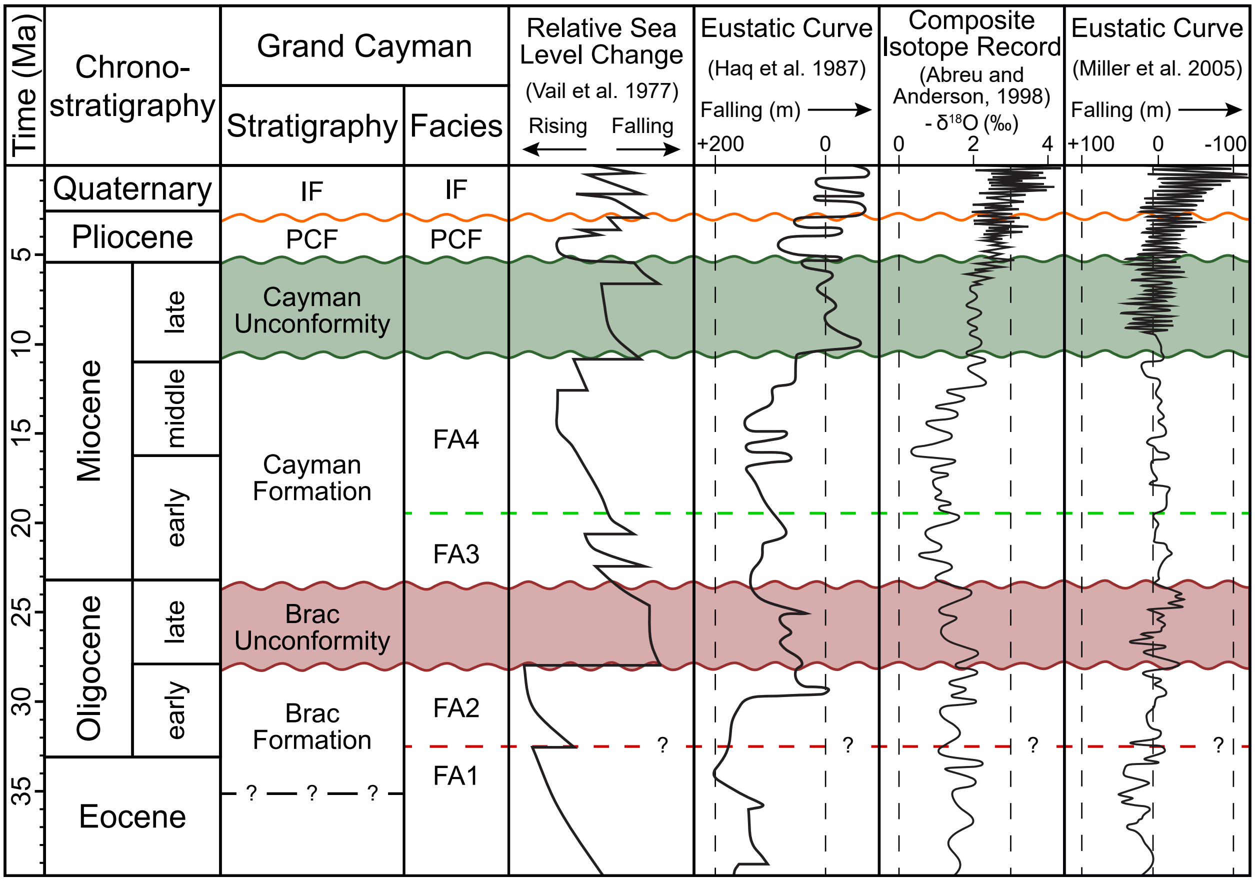

Fig. 31: Correlation of the carbonate sedimentary successions on the Cayman Islands to the interpreted paleo-sea level curves of Vail et al. (1977): Relative sea level curve derived from the sequence stratigraphic interpretation of seismic data; Haq et al. (1987): Eustatic curve derived from the sequence stratigraphic interpretation of seismic, subsurface, and outcrop data; Abreu and Anderson (1998): Composite $\delta^{18}O$ record for the Cenozoic; Miller et al. (2005): Integrated global sea level derived from backstripping data (7.0 Ma - 100 Ma) and $\delta^{18}O$ (0 to 7.0 Ma).

the age of Brac Formation, which was dated to 28 Ma on Cayman Brac (Jones et al. 1994a). Furthermore, the amplitudes of fluctuations in the eustatic curve presented by Haq et al. (1987) are considerably larger than the amplitudes indicated from the stratigraphy on the Cayman Islands. The Brac Unconformity, for example, has at least 57 m of erosional relief on Grand Cayman and is located as deep as 129 m bsl. The modern position of subaerial unconformities represents the maximum lowstand position if the island has experienced no tectonic uplift/subsidence. In contrast, the erosional relief on subaerial unconformities reflects the minimum lowstand position if the modern depth to the unconformity is entirely due to post-erosional subsidence (Fig. 32). Therefore, available information from the Brac Unconformity on Grand Cayman indicates that the

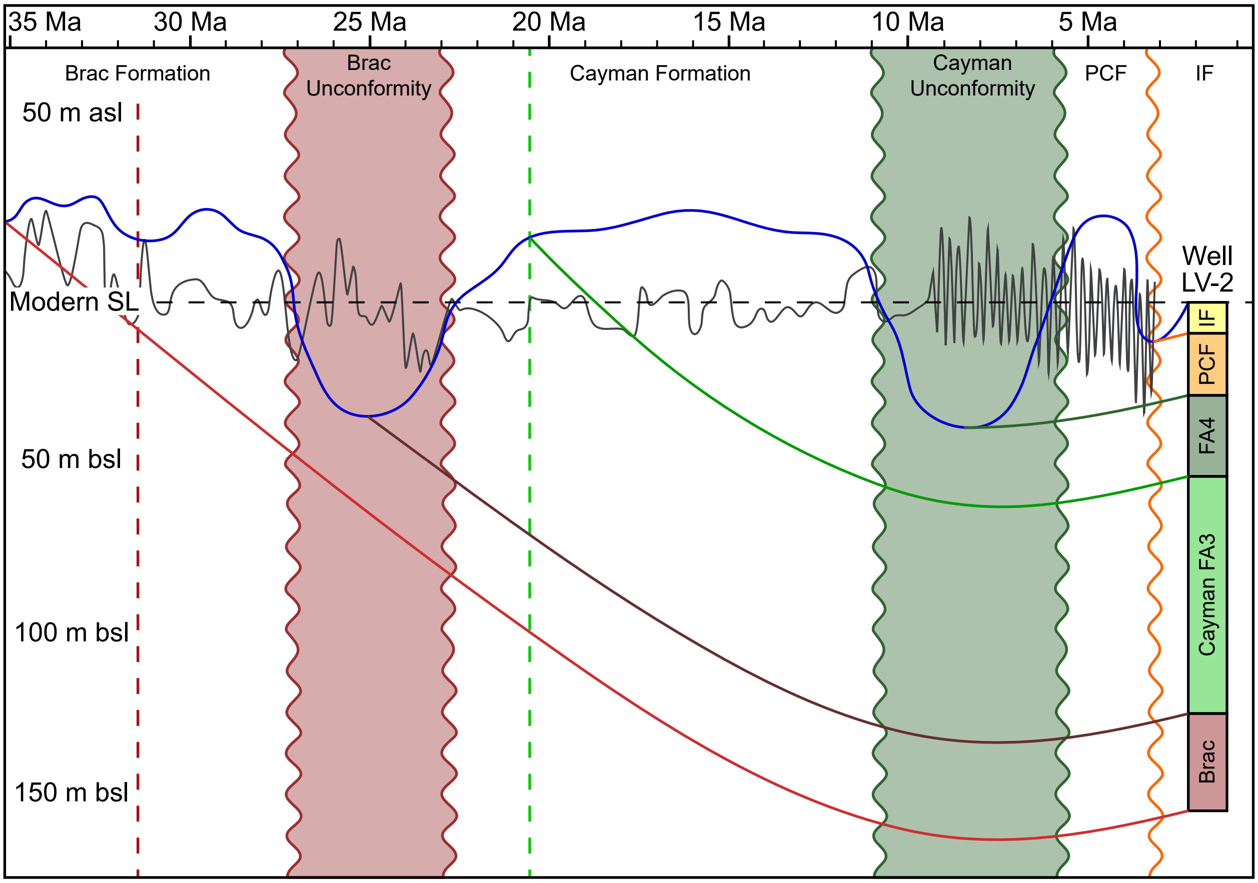

Fig. 32: Idealized diagram showing the minimum subsidence history of the basin floor (light red line) and how the position of the Brac Unconformity (dark red line), the FA3/FA4 boundary (light green line), and the Cayman Unconformity (dark green line) have changed with time to their modern position in LV-2. Black line shows the Miller et al. (2005) eustatic curve. Blue curve line shows the interpreted water depth from facies and unconformities.

late Oligocene (Chattian) lowstand was between 57 m and 129 m bsl. Although these estimates assume that the early Oligocene position of Grand Cayman was not higher than the modern position of the island, evidence from $^{87}Sr/^{86}Sr$ isotope ratios and the stratigraphic framework suggests that the island was tectonically stable during the Oligocene and began to slowly thermally subside during the early Miocene. Estimates from the Haq et al. (1987) curve suggest that sea level fell ~160 m from the early Oligocene to the late Oligocene and was ~20 m asl, whereas the Miller et al. (2005) curve suggest that sea level fell ~60 m from the early Oligocene to the late Oligocene and was ~20 m bsl. These eustatic curves indicate that the late Oligocene lowstand lasted for a 4 to 6 million year period that terminated at the end of the late Oligocene to early Miocene.

Estimates of the highstand position during the early Miocene ranges from ~120 m asl (Haq et al. 1987) to ~10 m bsl (Miller et al. 2005). Each of these eustatic curves indicates that the early Miocene was a period of rapid transgression that reached a maximum highstand position during the middle Miocene. Estimates of the highstand position during the middle Miocene (Langhian - Serravallian) ranges from ~160 m asl (Haq et al. 1987) to equivalent to modern sea level (Miller et al. 2005). Available information from the Cayman Unconformity on Grand Cayman, which has at least 62 m of erosional relief on the island, suggests that the late Miocene (Tortonian - Messinian) lowstand was at least 62 m bsl (Jones and Hunter, 1994b; Liang and Jones, 2014, 2015a). Estimates from the Haq et al. (1987) curve suggest that sea level fell ~150 m from the middle Miocene to the late Miocene and was ~50 m bsl, whereas the Miller et al. (2005) curve suggest that sea level fell ~30 m from the middle Miocene to the late Miocene and was ~15 m bsl. These eustatic curves suggest that the late Miocene lowstand occurred over a 5.5 million year period that terminated in the early Pliocene. The initial 0.64 to 1.91 million year period of subaerial erosion suggested by Liang and Jones (2015a) corresponds to the maximum lowstand position during the Messinian.

Estimates of the highstand position during the Pliocene ranges from ~80 m (Haq et al. 1987) to ~20 m asl (Miller et al. 2005). Although the Pedro Castle Formation is now preserved only in paleo-topographic lows on the underlying Cayman Unconformity, the formation probably covered much of Cayman Brac and Grand Cayman prior to erosion (Zhao and Jones, 2012a; Liang and Jones, 2014). Estimates from the Haq et al. (1987) curve suggest that eustatic sea level fell ~120 m from the middle Pliocene to the early Pleistocene and was ~50 m bsl, whereas the Miller et al. (2005) curve suggest that sea level fell ~60 m from the middle Pliocene to the early Pleistocene and was ~50 m bsl. Due to its poor preservation, the erosional relief on the Pedro Castle Unconformity is not a reliable indicator for the amplitude of eustatic fall during the late Pliocene to early Pleistocene (Liang and Jones, 2014). The Pedro Castle Unconformity was probably initiated at 3 Ma and must have terminated prior to ~400 ka when the sediments that now form unit A of the Ironshore Formation were deposited (Vezina et al. 1999; Jones, 2019).

5.2.4. Paleogene - Neogene Bank Architecture

During the beginning of the early Oligocene (FA1), Grand Cayman was submerged in water depths of 20 m - 40 m, whereas during the latter stages of the early Oligocene (FA2), the bank was submerged in water depths of 10 m - 30 m. There is no evidence that antecedent topography restricted circulation from the surrounding oceanic water and the sediments that now form the Brac Formation were, therefore, deposited in an open bank setting (Fig. 33A; 33B). The biota and textures in the Brac Formation suggest that sedimentation rates during the beginning of the early Oligocene were relatively low, whereas sedimentation rates increased into the latter stages of the early Oligocene. Furthermore, comparison to eustatic curves (Fig. 31) suggest that eustatic sea level was in a stable highstand position during the early Oligocene and it is probable that increasing sedimentation rates are largely responsible for the shallowing-upward succession of facies that comprise the Brac Formation. Although the time when the FA1/FA2 boundary formed is unclear due to the lack of age constraints, this contact is marked by a decrease in water depth of ~10 m. During the late Oligocene, eustatic sea level dropped rapidly and information from the Brac Unconformity suggests that the late Oligocene lowstand was between 57 m and 129 m bsl (Fig. 33C). Eustatic curves suggest that the duration of the late Oligocene lowstand occurred over a 4 to 6 million year period that terminated at the end of the late Oligocene to early Miocene.

During the early Miocene (Aquitanian - Burdigalian), Grand Cayman was submerged in waters <10m in depth. The deepening-upward succession of facies that comprise FA3 of the Cayman Formation, which onlapped and filled antecedent topography on the Brac Unconformity, are indicative of a period of rapid transgression. Antecedent topography restricted circulation from the surrounding oceanic water and the sediments that now form FA3 were, therefore, deposited in a restricted bank to lagoonal setting (Fig. 33D). Regional correlation of facies suggest that bank restriction decreased over time as sedimentation filled the topographic lows on the Brac Unconformity. Sedimentation rates during the early parts of this transgression are high, whereas, relative sea level rise outpaced carbonate productivity during the latter stages of transgression. The FA3/FA4 boundary, which is marked by a relative sea level rise of 20 m - 30 m, probably

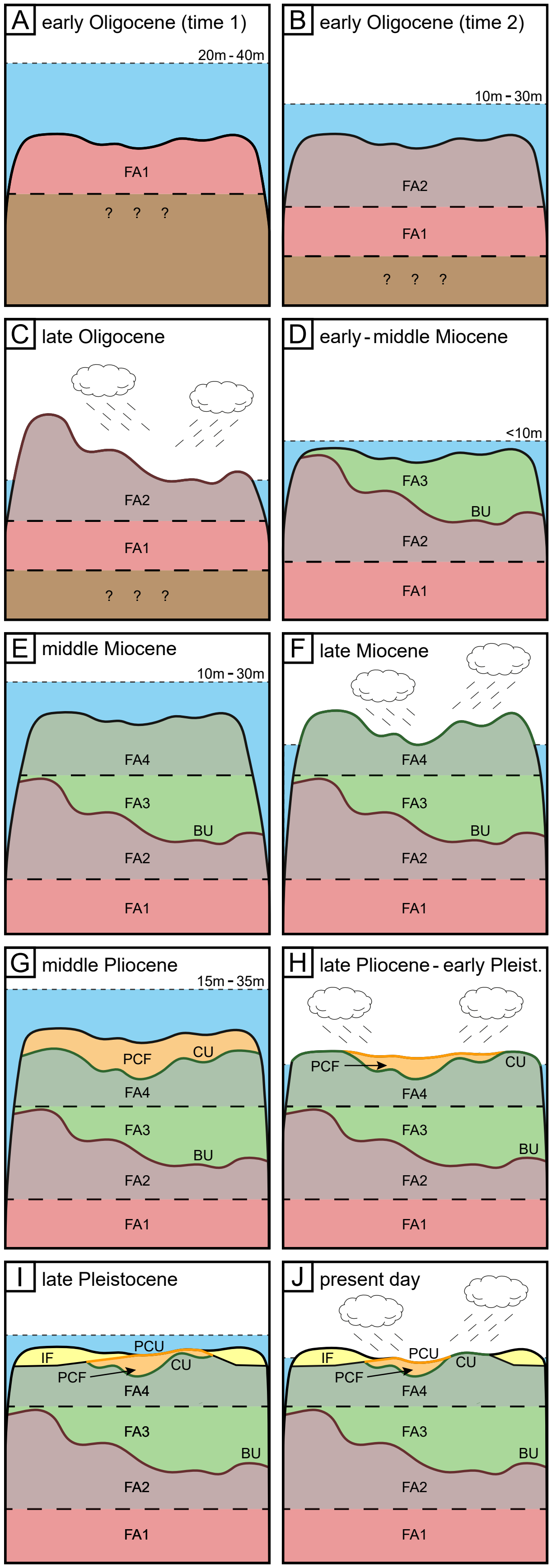

Fig. 33: Evolution of Grand Cayman from the early Oligocene to modern times: (A) early Oligocene (time 1) - deposition of the sediments that now form facies association 1 (FA1); (B) early Oligocene (time 2) - deposition of the sediments that now form facies association 2 (FA2); (C) late Oligocene - subaerial exposure and the development of the Brac Unconformity (BU); (D) early to middle Miocene - deposition of the sediments that now form facies association 3 (FA3); (E) middle Miocene - deposition of the sediments that now form facies association 4 (FA4); (F) late Miocene - subaerial exposure and the development of the Cayman Unconformity (CU); (G) middle Pliocene - deposition of the sediments that now form the Pedro Castle Formation (PCF); (H) late Pliocene to early Pleistocene - subaerial exposure and the development of the Pedro Castle Unconformity (PCU); (I) late Pleistocene deposition of the sediments that now form the Ironshore Formation (IF); (J) Present day subaerial exposure.

formed as a result of partial drowning of the carbonate bank. Following this transgressive event, during the middle Miocene, Grand Cayman was submerged in water depths of 10 m - 30 m (Fig. 33E). Antecedent topography did not restrict circulation from the surrounding oceanic water, because the basal contact with FA3 is sub-horizontal. Based on the biota and textures in FA4 of the Cayman Formation, sedimentation rates during the middle Miocene were moderate to high. Eustatic curves suggest that eustatic sea level was in a stable highstand position during the middle Miocene (Langhian - Serravallian) and it is probable that increasing sedimentation rates were largely responsible for the shallowing-upward succession of facies that comprise FA4. During the late Miocene, eustatic sea level dropped rapidly and information from the Cayman Unconformity suggests that the late Miocene lowstand was at least 62 m bsl (Fig. 33F). Eustatic curves suggest that the late Miocene lowstand occurred over a 5.5 million year period that terminated in the early Pliocene. The maximum lowstand position, however, occurred during a 0.64 to 1.91 million year period during the Messinian (Jones and Hunter, 1994b; Liang and Jones, 2015a).

During the middle Pliocene, Grand Cayman was submerged in water depths of 15 m - 35 m. The deepening-upward succession of facies that comprise the Pedro Castle Formation, which onlapped and filled antecedent topography on the underlying Cayman Unconformity, is indicative of a period of transgression. Antecedent topography restricted circulation from the surrounding oceanic water and the sediments that now form the Pedro Castle Formation were, therefore, deposited in a restricted bank to lagoonal setting (Fig. 33G). During the late Pliocene to early Pleistocene, subaerial exposure led to the development of the Pedro Castle Unconformity (Fig. 33H), which must have terminated prior to ~400 ka when the sediments that now form unit A of the Ironshore Formation were deposited (Vezina et al. 1999; Jones, 2019). Although the Pedro Castle Unconformity is not a reliable indicator for the amplitude of eustatic fall during this period, estimates from eustatic curves suggest that this lowstand was ~50 m bsl. The sediments that now form units A - F of the Ironshore Formation were deposited during the high-frequency eustatic oscillations from >400 ka to 84 ka (Fig. 33I). The most extensive deposition occurred during the Marine Isotope Stage 5e highstand (128 ka - 116 ka) that is estimated to have been 6 m asl and led to the formation of unit D of the Ironshore Formation (Vézina et al. 1999; Coyne et al. 2007). Wave-cut notches, which are found at 6 m asl on Grand Cayman and Cayman Brac, are coeval to unit D of the Ironshore Formation and formed due to coastal erosion (Jones, 2010; Jones et al. 2018; Jones, 2019). Modern karst development on Grand Cayman is due to subaerial exposure that post-dates unit F of the Ironshore Formation (84 ka) (Fig. 33J).

Chapter 6: Discussion

Although a variety of autogenic factors contribute to the development of carbonate sedimentary successions, the interplay between eustasy and tectonism is widely recognized as the key factor in the formation sedimentary sequences (Sarg, 1988; Hunt and Tucker, 1993; Schlager, 1993; Strasser et al. 1999) and the unconformities that bound them (Esteban and Klappa, 1983; James and Choquette, 1984; Choquette and James, 1988; Tucker, 1993; Weidlich, 2010). Decoupling the impact of eustasy from tectonic movement, however, remains obscure unless one of these allogenic controls is well-constrained and treated as a fixed parameter. The carbonate succession that forms the cores of each of the Cayman Islands, which are within 150 km of each other, developed on isolated banks that were surrounded by deep oceanic water. Although each of the Cayman Islands has experienced uniform changes in eustatic sea level, the islands have undergone independent tectonic histories (Perfit and Heezen, 1978; Jones and Hunter, 1994a; Iturralde-Vinent, 2006; Zhao and Jones, 2012a; Boschman et al. 2014; Liang and Jones, 2014). Accordingly, by comparing the successions on each of the Cayman Islands, the impacts of eustasy can be decoupled from the impacts of tectonism.

Although the time in which the Mid-Cayman Rise was initiated is largely unknown, this spreading center, with east-west extension, has been active since at least the Late Eocene (Perfit and Heezen, 1978; Leroy et al. 1996; Pindell and Kennan, 2009; Hayman et al. 2011; Boschman et al. 2014). Throughout the Late Eocene and Oligocene sea-floor spreading in Mid-Cayman Rise facilitated movement on the Oriente Transform Fault and gave rise to the detachment/transportation of the Cayman Islands to their modern-day position (Iturralde-Vinent and Macphee, 1999; Rojas-Agramonte et al. 2005; Iturralde-Vinent, 2006; Pindell and Kennan, 2009). Local extensional features, which began to form on the Cayman Ridge during early to middle Miocene, generated faults perpendicular to the Oriente Transform Fault that divided the Cayman Ridge into a series of fault blocks. (Iturralde-Vinent and Macphee, 1999; Iturralde-Vinent, 2006; Hayman et al. 2011; Boschman et al. 2014). It is possible that these local extensional features gave rise to differential subsidence during the deposition of the sediments that now form the Cayman Formation. Following the segmentation of the Cayman Ridge during the Miocene, transpression along the northern margin of the Cayman Trench resulted in independent tectonic movement on each of these segments (Iturralde-Vinent and Macphee, 1999; Iturralde-Vinent, 2006; Rojas-Agramonte et al. 2005, Mann et al. 2007). Accordingly, each of the Cayman Islands is now situated atop separate fault blocks that have undergone independent tectonic histories. For example, the strata on Cayman Brac dip at 0.5° - 2.0° to the southwest and have clearly been uplifted/tilted, whereas there is no clear evidence of faulting, folding, or tilting of the strata on Grand Cayman which appear to lie horizontal (Jones and Hunter, 1989; Jones et al. 1994b; Zhao and Jones, 2012a; Liang and Jones, 2014; Liang and Jones, 2015a). Although the carbonate succession on Little Cayman is poorly understood due the lack of well data and limited surface exposures, the island appears to have moved independently relative to Cayman Brac and Grand Cayman (Perfit and Heezen, 1978; Stoddart, 1980; Jones, 2019).

Evidence that Cayman Brac has been tectonically uplifted and tilted includes: (1) the Brac Unconformity, which is located up to 33 m asl on the northeast end of the island and is ~50 m bsl on the central parts of the island, (2) the Cayman Unconformity, which is located up to 46 m asl on the northeast end of the island and is close to sea level on the southwest end of the island, (3) evidence that the strata in the Cayman Formation dip at 0.5° - 2.0° to the southwest, and (4) the Pedro Castle Formation, which probably covered most of Cayman Brac after deposition, is now present only on the southwestern part of the island. Based on the stratigraphic relationships between the Pedro Castle Formation (Pliocene), the Ironshore Formation (Pleistocene), and the wave-cut notch at 6 m asl (~125 ka), uplift and tectonic tilting of Cayman Brac probably occurred between the late Pliocene (3.6 Ma) and ~125 ka (Jones et al. 1994b; MacNeil and Jones, 2003; Zhao and Jones, 2012a; Jones et al. 2018). Furthermore, Liang and Jones (2014) suggested that, due to the position of unconformities on each of the Cayman Islands, the axis of rotation for the uplift of Cayman Brac was close to the west end of the island.

Previous work on Grand Cayman has assumed that there has been little, if any, structural impact on the deposition of the sediments that now form the succession (Jones and Hunter, 1989, 1994a, 1994b). This assumption hinged largely on the horizontal appearance of the strata on Grand Cayman and the fact that unconformities in the succession can be matched with global eustatic lowstands (Jones and Hunter, 1994a, 1994b). Evidence that Grand Cayman has not been tectonically uplifted or tilted includes: (1) the facies association boundaries in the Brac Formation (FA1/FA2 boundary) and Cayman Formation (FA3/FA4 boundary) are sub-horizontal, and (2) the 'peripheral ridge' on the Cayman Unconformity is located at similar elevations on each of the coasts of the island. Although there is no clear evidence of faulting, folding, or tilting of the strata on Grand Cayman, it is possible that the island has experienced vertical tectonic movements with no rotational component (e.g. steady thermal subsidence). Although probably negligible, this tectonic component of subsidence may also include some smaller fraction of isostasy. Recent work has acknowledged this possibility but suggested that the recognition of vertical movement is problematic because the product of such a process would be similar to the product of high-amplitude eustatic changes (Jones and Luth 2003a; Liang and Jones, 2014). This interpretation, however, has limited support because: (1) recent eustatic curves (e.g., Miller et al. 2005) have suggested that that the amplitudes of eustatic fluctuations are considerably smaller than the estimates from the traditional sequence stratigraphic methods (e.g., Vail et al. 1977; Haq et al. 1987), (2) Oligocene shallow water limestone on Grand Cayman are found at depths of at least 401 m bsl (Emery and Milliman, 1980), and (3) estimates from even the highest amplitude eustatic curves suggest that sea level was in highstand positions (i.e., above modern-day sea level) during the deposition of the sediments that now form the Brac Formation (Lower Oligocene), Cayman Formation (Middle Miocene), and Pedro Castle Formation (Pliocene). Considering estimates of eustatic sea level are above modern sea level, at what water depth would the sediments that now form this limestone (located at >400 m bsl) have been deposited in if Grand Cayman had undergone no subsidence? Furthermore, the modern position of the FA3/FA4 boundary (as deep as 60 m bsl), suggests that the assumption that Grand Cayman has been tectonically stable since the early to middle Miocene is open to debate.

The use of information from conformable facies boundaries in conjunction with information from subaerial unconformities allows for the interpretation of the effect that eustasy and tectonism had on the development of the succession. This study reveals critical information regarding the development of the Paleogene - Neogene carbonate succession on Grand Cayman, and allows for the following statements regarding the tectonic history of the island:

- The modern position of subaerial unconformities represents the absolute maximum lowstand position if it is assumed that the island has experienced no tectonic uplift/subsidence, whereas the erosional relief on subaerial unconformities reflects the absolute minimum lowstand position, if it is assumed that the depth to the unconformity is entirely due to post-erosional subsidence.
  - For example, available information from the Brac Unconformity suggests that the late Oligocene lowstand was between 57 m and 129 m bsl, whereas available information from the Cayman Unconformity suggests that the late Miocene (Tortonian - Messinian) lowstand was at least 62 m bsl.
- Although the modern position of subaerial unconformities provides a maximum constraint on the magnitude of sea level fall during periods of subaerial exposure, this information is difficult to decouple from the impacts of tectonic uplift/subsidence. The modern position of facies association boundaries, which typically have a negligible erosive component, provide a valuable reference point for thermal subsidence rates since the time in which they formed.
  - For example, information from the FA3/FA4 boundary suggests that Grand Cayman has subsided between 70 m and 190 m since ~20 Ma. This interpretation is supported by the linear decrease of Cayman Formation $^{87}Sr/^{86}Sr$ isotope ratios with increased depth.

Accordingly, by comparing the geologic evolution of the carbonate sedimentary successions on each of the Cayman Islands, this study demonstrates the ability to decouple the impacts of eustasy and tectonism on the development of this carbonate succession.

Chapter 7: Conclusions

The detailed sedimentological and petrographic analysis of samples from 22 wells on west-central Grand Cayman has considerably improved the understanding of the stratigraphic architecture and the development of porosity and permeability in the Paleogene - Neogene succession on the island. Accordingly, the following conclusions are determined from this study:

(1) Each of the Cayman Islands is situated atop separate fault blocks and has therefore undergone independent tectonic histories. Cayman Brac was uplifted and tilted between the late Pliocene and ~125 ka, whereas evidence from the stratigraphic framework and $^{87}Sr/^{86}Sr$ isotope ratios suggests that Grand Cayman has been subsiding since the early Miocene.

(2) Information from the Brac Unconformity suggests that the late Oligocene lowstand was between 57 m and 129 m bsl, whereas the Cayman Unconformity suggests that the late Miocene lowstand was at least 62 m bsl. The modern position of the FA3/FA4 boundary suggests that Grand Cayman has subsided between 70 m and 190 m since ~20 Ma.

(3) FA3 of the Cayman Formation, which is 12 m - 24 m thick on western Grand Cayman and up to 73 m thick on the central parts of the island, consists of a deepening-upwards succession of benthic foraminifera, red algae, bivalve, and domal coral grainstone and rudstone that onlapped and filled paleo-topographic lows on the underlying Brac Unconformity. FA3 has an average porosity of 32.5%, an average K_{max} of 2379 mD, and an average K_{vert} of 1586 mD.

(4) FA4 of the Cayman Formation, which is 26 m - 47 m thick on Grand Cayman, consists of a shallowing-upwards succession of branching coral, rhodolith, green algae, and bivalve wackestone and floatstone. FA4 has an average porosity of 9.3%, an average K_{max} of 1044 mD, and an average K_{vert} of 44.2 mD.

References

Abreu, V.S., Anderson, J.B., 1998. Glacial eustasy during the Cenozoic: sequence stratigraphic implications. AAPG bulletin, 82(7), 1385-1400.

Adey, W.H., Macintyre, I.G., 1973. Crustose coralline algae: a re-evaluation in the geological sciences. Geological Society of America Bulletin, 84(3), 883-904.

Aguirre, J., Riding, R., Braga, J.C., 2000. Diversity of coralline red algae: origination and extinction patterns from the Early Cretaceous to the Pleistocene. Paleobiology, 26(4), 651-667.

Arts, A.E., 2000. Sedimentology and Stratigraphy of the Pedro Castle Formation SW Grand Cayman, BWI. Unpublished M.Sc Thesis, University of Alberta, Edmonton, 107 p.

Ball, M.M., 1967. Carbonate sand bodies of Florida and the Bahamas. Journal of Sedimentary Petrology, 37(2), 556-591.

Bosence, D., 2005. A genetic classification of carbonate platforms based on their basinal and tectonic settings in the Cenozoic. Sedimentary Geology, 175(1-4), 49-72.

Boschman, L.M., van Hinsbergen, D.J., Torsvik, T.H., Spakman, W., Pindell, J.L., 2014. Kinematic reconstruction of the Caribbean region since the Early Jurassic. Earth-Science Reviews, 138, 102-136.

Bosellini, A., Ginsburg, R.N. 1971. Form and internal structure of recent algal nodules (rhodolites) from Bermuda. The Journal of Geology, 79(6), 669-682.

Braga, J.C., Bassi, D., Piller, W.E., 2010. Palaeoenvironmental significance of Oligocene–Miocene coralline red algae – a review. In: Mutti, M., Piller, W.E., Betzler, C., (Eds.). *Carbonate Systems during the Oligocene–Miocene Climatic Transition*. International Association of Sedimentologist Special Publication, 42, 165-182.

Budd, D.A., 1997. Cenozoic dolomites of carbonate islands: their attributes and origin. Earth-Science Reviews, 42(1-2), 1-47.

Burton, F.J., 1994. Climate and tides of the Cayman Islands. In: Brunt M.A., Davies J.E. (Eds.). *The Cayman Islands*. Monographiae Biologicae, 71, 51-60.

Catuneanu, O., Abreu, V., Bhattacharya, J.P., Blum, M.D., Dalrymple, R.W., Eriksson, P.G., Fielding, C.R., Fisher, W.L., Galloway, W.E., Gibling, M.R., Giles, K.A., Holbrook, J.M., Jordan, R., Kendall, C.G.St.C., Macurda,B., Martinsen, O.J., Miall, A.D., Neal, J.E., Nummedal, D., Pomar, L., Posamentier, H.W., Pratt, B.R., Sarg, J.F., Shanley, K.W., Steel, R.J., Strasser, A., Tucker, M.E., Winker, C., 2009. Towards the standardization of sequence stratigraphy. Earth-Science Reviews, 92(1-2), 1-33.

Catuneanu, O., Galloway, W.E., Kendall, C.G.St.C., Miall, A.D., Posamentier, H.W., Strasser, A., Tucker, M.E., 2011. Sequence stratigraphy: methodology and nomenclature. Newsletters on stratigraphy, 44(3), 173-245.

Choquette, P.W., James, N.P., 1988. Introduction. In: James, N.P., Choquette, P.W., (Eds.). *Paleokarst*. Springer-Verlag, Berlin, Germany. 1-21.

Choquette, P.W., Pray, L.C., 1970. Geologic nomenclature and classification of porosity in sedimentary carbonates. AAPG bulletin, 54(2), 207-250.

Corlett, H., Jones, B., 2007. Epiphyte communities on *Thalassia* testudinum from Grand Cayman, British West Indies: Their composition, structure, and contribution to lagoonal sediments. Sedimentary Geology, 194(3-4), 245-262.

Coyne, M.K., Jones, B., Ford, D., 2007. Highstands during marine isotope stage 5: evidence from the Ironshore Formation of Grand Cayman, British West Indies. Quaternary Science Reviews, 26(3-4), 536-559.

Der, A.J., 2012. Deposition and sea level fluctuations during Miocene times, Grand Cayman, British West Indies. Unpublished M.Sc Thesis, University of Alberta, Edmonton, 110 p.

Dixon, T.H., Farina, F., DeMets, C., Jansma, P., Mann, P., Calais, E., 1998. Relative motion between the Caribbean and North American plates and related boundary zone deformation from a decade of GPS observations. Journal of Geophysical Research: Solid Earth, 103(B7), 15157-15182.

Dunham, R.J., 1962. Classification of carbonate rocks according to depositional textures. In: Ham, W.E., (Ed.). *Classification of Carbonate Rocks*. American Association of Petroleum Geologists Memoir, 1, 108-121.

Embry, A.F., Klovan, J.E., 1971. A late Devonian reef tract on northeastern Banks Island, NWT. Bulletin of Canadian Petroleum Geology, 19(4), 730-781.

Emery, K.O., Milliman, J.D., 1980. Shallow-water limestones from slope off Grand Cayman Island. The Journal of Geology, 88(4), 483-488.

Esteban, M., Klappa, C.F., 1983. Subaerial exposure environment. In: Scholle, P.A., Bebout, D.G., Moore, C.H., (Eds.). *Carbonate Depositional Environments*. American Association of Petroleum Geologists, Memoir, 33. American Association of Petroleum Geologists, Tulsa, United States, 1-54.

Etherington, D., 2004. Sedimentology and depositional architecture of the Cayman (Miocene) and Pedro Castle (Pliocene) Formations on Western Grand Cayman, British West Indies. Unpublished M.Sc. Thesis, University of Alberta, Canada, 122 p.

Frost, S.H., Harbour, J.L., Beach, D.K., Realini, M.J., Harris, M., 1983. Oligocene reef tract development, southwestern Puerto Rico (Vol. 9). Sedimenta IX, Comparative Sedimentology Laboratory, Division of Marine Geology and Geophysics, Rosenstiel School of Marine & Atmospheric Science, University of Miami, 1-141.

Frost, S.H., Langenheim, R.L., 1974. Cenozoic reef biofacies. Tertiary larger foraminifera and Scleractinian corals from Chiapus, Mexico. Northern Illinois Univ. Press, Illinois, 1-388.

Ginsburg, R. N., Bosellini, A., 1973. Form and internal structure of recent algal nodules (Rhodolites) from Bermuda: A reply. The Journal of Geology, 81(2), 239-239. Sciences, 91(6), 1054-1070.

Gischler, E., Dietrich, S., Harris, D., Webster, J.M., Ginsburg, R.N., 2013. A comparative study of modern carbonate mud in reefs and carbonate platforms: Mostly biogenic, some precipitated. Sedimentary Geology, 292, 36-55.

Godet, A., 2013. Drowning unconformities: palaeoenvironmental significance and involvement of global processes. Sedimentary Geology, 293, 45-66.

Hallock, P., Glenn, E.C., 1986. Larger foraminifera: a tool for paleoenvironmental analysis of Cenozoic carbonate depositional facies. Palaios, 1, 55-64.

Haq, B.U., Hardenbol, J.A.N., Vail, P.R., 1987. Chronology of fluctuating sea levels since the Triassic. Science, 235(4793), 1156-1167.

Harris, P.M., Purkis, S.J., Ellis, J., Swart, P.K., Reijmer, J.J. 2015. Mapping bathymetry and depositional facies on Great Bahama Bank. Sedimentology, 62(2), 566-589.

Hayman, N.W., Grindlay, N.R., Perfit, M.R., Mann, P., Leroy, S., de Lépinay, B.M., 2011. Oceanic core complex development at the ultraslow spreading Mid-Cayman Spreading Center. Geochemistry, Geophysics, Geosystems, 12(3), 1-21.

Hearty, P.J., Tormey, B.R., 2017. Sea-level change and superstorms; geologic evidence from the last interglacial (MIS 5e) in the Bahamas and Bermuda offers ominous prospects for a warming Earth. Marine Geology, 390, 347-365.

Hills, D.J., Jones, B., 2000. Peyssonnelid Rhodoliths from the Late Pleistocene Ironshore Formation, Grand Cayman, British West Indies. Palaios, 15(3), 212-224.

Holcombe, T.L., Vogt, P.R., Matthews, J.E., Murchison, R.R., 1973. Evidence for sea-floor spreading in the Cayman Trough. Earth and Planetary Science Letters, 20(3), 357-371.

Hollis, C., Vahrenkamp, V., Tull, S., Mookerjee, A., Taberner, C., Huang, Y., 2010. Pore system characterisation in heterogeneous carbonates: An alternative approach to widely-used rock-typing methodologies. Marine and Petroleum Geology, 27(4), 772-793.

Hsü, K. J., Montadert, L., Bernoulli, D., Cita, M. B., Erickson, A., Garrison, R. E., Kidd, R.B., Mèlierés, F., Müller, C., Wright, R., 1977. History of the Mediterranean salinity crisis. Nature, 267(5610), 399.

Hunt, D., Tucker, M.E. 1993. Sequence stratigraphy of carbonate shelves with an example from the mid-Cretaceous (Urgonian) of southeast France. In: Posamentier, H.W., Summerhayes, C.P., Haq, B.U., Allen, G.P., (Eds.). *Sequence Stratigraphy and Facies Associations*. International Association of Sedimentologists Special Publication, 18, 307-341.

Hunter, I.G., (1994). Modern and Ancient Coral Associations of the Cayman Islands. Unpublished Ph.D. Thesis, University of Alberta, Edmonton. 345 p.

Iturralde-Vinent, M.A., MacPhee, R.D., 1999. Paleogeography of the Caribbean region: implications for Cenozoic biogeography. Bulletin of the American Museum of Natural History 238, 1-95.

Iturralde-Vinent, M.A., 2006. Meso-Cenozoic Caribbean paleogeography: implications for the historical biogeography of the region. International Geology Review, 48(9), 791-827.

James, N.P., Choquette, P.W. 1984. Diagenesis 9. Limestones-the meteoric diagenetic environment. Geoscience Canada, 11(4), 161-194.

James, N.P., Jones, B., 2015. *Origin of Carbonate Sedimentary Rocks*. John Wiley & Sons, Oxford, UK. 464 p..

James, N.P., Wood, R., 2010. Reefs. In: James, N.P., Dalrymple, R.W., (Eds.). *Facies Models*, 4th edition, 421-447.

Jones, B., 1992. Caymanite, a cavity-filling deposit in the Oligocene-Miocene Bluff Formation of the Cayman Islands. Canadian Journal of Earth Sciences, 29(4), 720-736.

Jones, B., 1994. Geology of the Cayman Islands. In: Brunt, M.A., Davies, J.E., (Eds.). *The Cayman Islands: Natural History and Biogeography*. Kluwer Academic Publishers. Dordrecht, Netherlands. 13-49.

Jones, B., 2010. Speleothems in a wave-cut notch, Cayman Brac, British West Indies: the integrated product of subaerial precipitation, dissolution, and microbes. Sedimentary Geology, 232(1-2), 15-34.

Jones, B., 2016. Cave-fills in Miocene–Pliocene strata on Cayman Brac, British West Indies: Implications for the geological evolution of an isolated oceanic island. Sedimentary Geology, 341, 70-95.

Jones, B., 2019. Diagenetic processes associated with unconformities in carbonate successions on isolated oceanic islands: Case study of the Pliocene to Pleistocene sequence, Little Cayman, British West Indies. Sedimentary Geology, 386, 9-30.

Jones, B., Hunter, I.G., 1989. The Oligocene - Miocene Bluff Formation on Grand Cayman. Caribbean Journal of Science, 25, 71-85.

Jones, B., Hunter, I.G., 1994a. Evolution of an isolated carbonate bank during Oligocene, Miocene and Pliocene times, Cayman Brac, British West Indies. Facies, 30(1), 25-50.

Jones, B., Hunter, I.G., 1994b. Messinian (late Miocene) karst on Grand Cayman, British West Indies; an example of an erosional sequence boundary. Journal of Sedimentary Research, 64(4b), 531-541.

Jones, B., Hunter, I.G., Kyser, K., 1994a. Stratigraphy of the Bluff Formation (Miocene-Pliocene) and the Newly Defined Brac Formation (Oligocene), Cayman Brac, British West Indies. Caribbean Journal of Science, 30(1-2), 30-51.

Jones, B., Hunter, I.G., Kyser, K., 1994b. Revised Stratigraphic Nomenclature for Tertiary Strata of the Cayman Islands. British West Indies. Caribbean Journal of Science, 30(1-2), 53-68.

Jones, B., Luth, R.W., 2002. Dolostones from Grand Cayman, British West Indies. Journal of Sedimentary Research, 72(4), 559-569.

Jones, B., Luth, R.W., 2003a. Temporal evolution of Tertiary dolostones on Grand Cayman as determined by 87Sr/86Sr. Journal of Sedimentary Research, 73(2), 187-205.

Jones, B., Luth, R.W., 2003b. Petrography of finely crystalline Cenozoic dolostones as revealed by backscatter electron imaging: case study of the Cayman Formation (Miocene), Grand Cayman, British West Indies. Journal of Sedimentary Research, 73(6), 1022-1035.

Jones, B., Luth, R.W., MacNeil, A.J., 2001. Powder X-ray diffraction analysis of homogeneous and heterogeneous sedimentary dolostones. Journal of Sedimentary Research, 71(5), 790-799.

Jones, B., Ng, K.C., Hunter, I.G., 1997. Geology and hydrogeology of the Cayman Islands. In: Vacher, H.L., Quinn, T., (Eds.). *Geology and Hydrogeology of Carbonate Islands*. Developments in Sedimentology (54). 299-326.

Jones, B., Zheng, E., Li, L., 2018. Growth and development of notch speleothems from Cayman Brac, British West Indies: response to variable climatic conditions over the last 125,000 years. Sedimentary Geology, 373, 210-227.

Kindler, P., Hearty, P.J., 1996. Carbonate petrography as an indicator of climate and sea-level changes: new data from Bahamian Quaternary units. Sedimentology, 43(2), 381-399.

Kooistra, W.H.C.F., Coppejans, E.G.G., Payri, C., 2002. Molecular systematics, historical ecology, and phylogeography of *Halimeda* (Bryopsidales). Molecular Phylogenetics and

Krijgsman, W., Hilgen, F.J., Raffi, I., Sierro, F.J., Wilson, D.S., 1999. Chronology, causes and progression of the Messinian salinity crisis. Nature, 400(6745), 652.

Kuznetsov, A.B., Semikhatov, M.A., Gorokhov, I.M., 2018. Strontium isotope stratigraphy: principles and state of the art. Stratigraphy and Geological Correlation, 26(4), 367-386.

Leroy, S., de Lepinay, B.M., Mauffret, A., Pubellier, M., 1996. Structural and tectonic evolution of the eastern Cayman Trough (Caribbean Sea) from seismic reflection data. AAPG bulletin, 80(2), 222-247.

Li, C., Jones, B., 1997. Comparison of foraminiferal assemblages in sediments on the windward and leeward shelves of Grand Cayman, British West Indies. Palaios, 12, 12-26.

Li, R., Jones, B., 2013. Heterogeneous diagenetic patterns in the Pleistocene Ironshore Formation of Grand Cayman, British West Indies. Sedimentary Geology, 294, 251-265.

Liang, T., Jones, B., 2014. Deciphering the impact of sea-level changes and tectonic movement on erosional sequence boundaries in carbonate successions: A case study from Tertiary strata on Grand Cayman and Cayman Brac, British West Indies. Sedimentary Geology, 305, 17-34.

Liang, T., Jones, B., 2015a. Ongoing, long-term evolution of an unconformity that originated as a karstic surface in the Late Miocene: A case study from the Cayman Islands, British West Indies. Sedimentary Geology, 322, 1-18.

Liang, T., Jones, B., 2015b. Petrographic and geochemical features of sinkhole-filling deposits associated with an erosional unconformity on Grand Cayman. Sedimentary Geology, 315, 64-82.

Lucia, J.L., 1999. *Carbonate Reservoir Characterization*. Springer-Verlag. 226 p.

Macdonald, K.C., Holcombe, T.L., 1978. Inversion of magnetic anomalies and sea-floor spreading in the Cayman Trough. Earth and Planetary Science Letters, 40(3), 407-414.

MacNeil, A., Jones, B., 2003. Dolomitization of the Pedro Castle Formation (Pliocene), Cayman Brac, British West Indies. Sedimentary Geology, 162(3-4), 219-238.

Mann, P., Demets, C., Wiggins-Grandison, M., 2007. Toward a better understanding of the Late Neogene strike-slip restraining bend in Jamaica: geodetic, geological, and seismic constraints. In: Cunningham, W.D., Mann, P., (Eds.). *Tectonics of Strike-Slip Restraining and Releasing Bends*. Geological Society of London, Special Publications, 290, 239-253.

Matley, C.A., 1924. Reconnaissance geological survey of Cayman Islands, British West Indies. Pan-Amer. Geol. 42, 313-315.

Matley, C.A., 1926. The geology of the Cayman Islands (British West Indies), and their relation to the Bartlett Trough. Quarterly Journal of the Geological Society, 82(1-4), 352-387.

McArthur, J.M., Howarth, R.J., Bailey, T.R., 2001. Strontium isotope stratigraphy: LOWESS version 3: best fit to the marine Sr-isotope curve for 0–509 Ma and accompanying look-up table for deriving numerical age. The Journal of Geology, 109(2), 155-170.

McArthur, J.M., Howarth, R.J., Shields, G.A., 2012. Chapter 7 – Strontium Isotope Stratigraphy. In: Gradstein, F., Ogg, J., Schmitz, M., Ogg, G., (Eds.). *The Geologic Time Scale*, 1, 127-144.

Merino, E., Banerjee, A., 2008. Terra rossa genesis, implications for karst, and eolian dust: A geodynamic thread. The Journal of Geology, 116(1), 62-75.

Miller, K.G., Kominz, M.A., Browning, J.V., Wright, J.D., Mountain, G.S., Katz, M.E., Sugarman, P.J., Cramer, B.S., Christie-Blick, N., Pekar, S.F., 2005. The Phanerozoic record of global sea-level change. Science, 310(5752), 1293-1298.

Montpetit, J.C., 1998. Sedimentology, depositional architecture, and diagenesis of the Cayman Formation at Tarpon Springs Estates, Grand Cayman, British West Indies. Unpublished M.Sc. Thesis, University of Alberta, Edmonton, 133 p.

Muhs, D.R., Budahn, J.R., 2009. Geochemical evidence for African dust and volcanic ash inputs to terra rossa soils on carbonate reef terraces, northern Jamaica, West Indies. Quaternary International, 196, 13-35.

Murray, J.W., 1991. *Ecology and Palaeoecology of Benthic Foraminifera*. Longman Scientific and Technical, London. 397 p.

Mutti, M., Bernouilli, D., Stille, P., 1997. Temperate carbonate platform drowning linked to Miocene oceanographic events: Maiella platform margin, Italy. Terra Nova 9 (3), 122-125.

Mutti, M., Droxler, A.W., Cunningham, A.D., 2005. Evolution of the Northern Nicaragua Rise during the Oligocene–Miocene: drowning by environmental factors. Sedimentary Geology, 175(1-4), 237-258.

Ng, K.C., Jones, B., Beswick, R., 1992. Hydrogeology of Grand Cayman, British West Indies: a karstic dolostone aquifer. Journal of Hydrology, 134(1-4), 273-295.

Pemberton, S.G., Jones, B., 1988. Ichnology of the Pleistocene Ironshore Formation, Grand Cayman Island, British West Indies. Journal of Paleontology, 495-505.

Perfit, M.R., Heezen, B.C., 1978. The geology and evolution of the Cayman Trench. Geological Society of America Bulletin, 89(8), 1155-1174.

Pindell, J.L., Kennan, L., 2009. Tectonic evolution of the Gulf of Mexico, Caribbean and northern South America in the mantle reference frame: an update. In: James, K.H., Lorente, M.A., Pindell, J.L., (Eds.). *The Origin and Evolution of the Caribbean Plate*. Geological Society, London, Special Publications, 328(1), 1-55.

Pleydell, S.M., Jones, B., Longstaffe, F.J., Baadsgaard, H., 1990. Dolomitization of the Oligocene – Miocene Bluff Formation on Grand Cayman, British West Indies. Canadian Journal of Earth Sciences, 27(8), 1098-1110.

Pomar, L., 2001. Types of carbonate platforms: a genetic approach. Basin Research, 13(3), 313-334.

Pomar, L., Kendall, C.G.St.C., 2008. Architecture of carbonate platforms: a response to hydrodynamics and evolving ecology. In: Simo, A., Lukasik, J., (Eds.). *Controls on Carbonate Platform and Reef Development*. SEPM Special Publication, 89, 187-216.

Reid, R.P., Macintyre, I.G., 1988. Foraminiferal-algal nodules from the eastern Caribbean: growth history and implications on the value of nodules as paleoenvironmental indicators Palaios, 424-435.

Ren, M., Jones, B., 2016. Diagenesis in limestone-dolostone successions after 1 million years of rapid sea-level fluctuations: A case study from Grand Cayman, British West Indies. Sedimentary Geology, 342, 15-30.

Ren, M., Jones, B., 2017. Spatial variations in the stoichiometry and geochemistry of Miocene dolomite from Grand Cayman: Implications for the origin of island dolostone. Sedimentary Geology, 348, 69-93.

Ren, M., Jones, B., 2018. Genesis of island dolostones. Sedimentology, 65(6), 2003-2033.

Rojas-Agramonte, Y., Neubauer, F., Handler, R., García-Delgado, D.E., Friedl, G., and Delgado-Damas, R., 2005. Variation of palaeostress patterns along the Oriente transform wrench corridor, Cuba: significance for Neogene–Quaternary tectonics of the Caribbean realm. Tectonophysics, 396(3-4), 161-180.

Sarg, J.F., 1988. Carbonate sequence stratigraphy. In: Wilgus, C.K., Hastings, B.S., Kendall, C.G.St.C., Posamentier, H.W., Ross, C.A., van Wagoner, J.C., (Eds.). *Sea-Level Changes: an Integrated Approach*. SEPM Special Publication, 42, 155–181.

Sattler, U., Immenhauser, A., Schlager, W., Zampetti, V., 2009. Drowning history of a Miocene Carbonate platform (Zhujiang Formation, South China Sea). Sedimentary Geology, 219(1-4), 318-331.

Semesi, I.S., Beer, S., Björk, M., 2009. Seagrass photosynthesis controls rates of calcification and photosynthesis of calcareous macroalgae in a tropical seagrass meadow. Marine Ecology Progress Series, 382, 41-47.

Schlager, W., 1981.The paradox of drowned reefs and carbonate platforms. Geological Society of America Bulletin 92, 197-211.

Schlager, W., 1989. Drowning unconformities on carbonate platforms. In: Crevello, P.D., Wilson, J.L., Sarg, J.F., Read, J.F. (Eds.). *Controls on Carbonate Platform and Basin Development*. SEPM Special Publication, 44. SEPM, Oklahoma, U.S.A., 15-25.

Schlager, W., 1993. Accommodation and supply - a dual control on stratigraphic sequences. In: Cloetingh, S., Sassi, W., Horvath F., Puigdefabregas C., (Eds.). *Basin Analysis and Dynamics of Sedimentary Basin Evolution*. Sedimentary Geology, 86(1-2), 111-136.

Strasser, A., Pittet, B., Hillgärtner, H., Pasquier, J. B., 1999. Depositional sequences in shallow carbonate-dominated sedimentary systems: concepts for a high-resolution analysis. Sedimentary Geology, 128(3-4), 201-221.

Stoddart, D.R., 1980. Geology and Geomorphology of Little Cayman. Geography and Ecology of Little Cayman. Atoll Research Bulletin, 242, 11-16.

Swart, P.K., Ruiz, J., Holmes, C.W., 1987. Use of strontium isotopes to constrain the timing and mode of dolomitization of upper Cenozoic sediments in a core from San Salvador, Bahamas. Geology, 15(3), 262-265.

Swart, P.K., Elderfield, H., Beets, K., 2001. The 87Sr/86Sr ratios of carbonates, phosphorites, and fluids collected during the Bahamas Drilling Project Cores Clino and Unda: implications for dating and diagenesis. In: Ginsburg, R.N. (Ed.). *Subsurface Geology of a Prograding Carbonate Platform: Results of the Bahamas Drilling Project*. Special Publication, 70, 175-186.

ten Brink, U.S., Coleman, D.F., Dillon, W.P., 2002. The nature of the crust under Cayman Trough from gravity. Marine and Petroleum Geology, 19(8), 971-987.

Todd, P.A., 2008. Morphological plasticity in scleractinian corals. Biological reviews, 83(3), 315-337.

Triffleman, N.J., Hallock, P., Hine, A.C., 1992. Morphology, sediments, and depositional environments of a small carbonate platform; Serranilla Bank, Nicaraguan Rise, Southwest Caribbean Sea. Journal of Sedimentary Research, 62(4), 591-606.

Tucker, M.E., 1993. Carbonate diagenesis and sequence stratigraphy. In: Wright, V.P., (Ed.). *Sedimentology Review*. Blackwell, Oxford, 51-72.

Uzelman, B.C., 2009. Sedimentology, diagenesis, and dolomitization of the Brac Formation (Lower Oligocene), Cayman Brac, British West Indies. Unpublished M.Sc. Thesis, University of Alberta, Edmonton, 120 p.

Vahrenkamp, V.C., Swart, P.K., Ruiz, J., 1988. Constraints and interpretation of 87Sr/86Sr ratios in Cenozoic dolomites. Geophysical Research Letters, 15(4), 385-388.

Vahrenkamp, V.C., Swart, P.K., Ruiz, J., 1991. Episodic dolomitization of late Cenozoic carbonates in the Bahamas; evidence from strontium isotopes. Journal of Sedimentary Research, 61(6), 1002-1014.

Vail, P.R., Mitchum, R.M., Thompson, S., 1977. Seismic stratigraphy and global changes of sea level, part IV: global cycles of relative changes in sea level. In: Payton, C., (Ed.). *Stratigraphic Interpretation of Seismic Data*. American Association of Petroleum Geologists, 83-97.

Van der Land, C., Wood, R., Wu, K., van Dijke, M.I., Jiang, Z., Corbett, P.W., Couples, G. 2013. Modelling the permeability evolution of carbonate rocks. Marine and Petroleum Geology, 48, 1-7.

Vaughan, T.W., 1926. Species of *Lepidocyclina* and *Carpentaria* from the Cayman Islands, and their geological significance. Quarterly Journal of the Geological Society of London, 82, 388-400.

Vecsei, A., 2004. Carbonate production on isolated banks since 20 ka BP: climatic implications. Palaeogeography, Palaeoclimatology, Palaeoecology, 214(1-2), 3-10.

Veron, J.E.N., 2010a. Family Agariciidae: genus *Leptoseris*. In: Stafford-Smith, M., (Ed.). *Corals of the World*. Volume 2 edn, 202-220.

Veron, J.E.N., 2010b. Family Pocilloporidae: genus *Stylophora*. In: Stafford-Smith, M., (Ed.). *Corals of the World*. Volume 2 edn, 56-65.

Veron, J.E.N., 2010c. Family Poritidae: genus *Porites*. In: Stafford-Smith, M., (Ed.). *Corals of the World*. Volume 3 edn, 276-345.

Veron, J.E.N., 2010d. Family Faviidae: genus *Montastrea*. In: Stafford-Smith, M., (Ed.). *Corals of the World*. Volume 3 edn, 212-225.

Veron, J.E.N., 2010e. Family Trachyphylliidae: genus *Trachyphyllia*. In: Stafford-Smith, M., (Ed.). *Corals of the World*. Volume 3 edn, 272-273.

Vezina, J., Jones, B., Ford, D., 1999. Sea-level highstands over the last 500,000 years; evidence from the Ironshore Formation on Grand Cayman, British West Indies. Journal of Sedimentary Research, 69(2), 317-327.

Wang, R., Jones, B., Yu, K., 2019. Island dolostones: Genesis by time-transgressive or event dolomitization. Sedimentary Geology, 390, 15-30.

Wang, R., Yu, K., Jones, B., Wang, Y., Zhao, J., Feng, Y., Bian, L., Xu, S., Fan, T., Jiang, W., Zhang, Y., 2018. Evolution and development of Miocene “island dolostones” on Xisha Islands, South China Sea. Marine Geology, 406, 142-158.

Weidlich, O., 2010. Meteoric diagenesis in carbonates below karst unconformities: heterogeneity and control factors. Geological Society, London, Special Publications, 329(1), 291-315.

Wheeler, C.W., Aharon, P., 1991. Mid-oceanic carbonate platforms as oceanic dipsticks: examples from the Pacific. Coral Reefs, 10(2), 101-114.

Wignall, B.D., 1995. Sedimentology and diagenesis of the Cayman and Pedro Castle formations at Safe Haven, Grand Cayman, B.W.I. Unpublished M.Sc. Thesis, University of Alberta, Edmonton, 110 p.

Willson, E.A., 1998. Depositional and diagenetic features of the Middle Miocene Cayman Formation, Roger’s Wreck Point, Grand Cayman, British West Indies. Unpublished M.Sc. Thesis, University of Alberta, Edmonton, 104 p.

Wilson, B., 2004. Benthonic foraminiferal paleoecology across a transgressive-regressive cycle in the Brasso Formation (Early-Middle Miocene) of Central Trinidad. Caribbean Journal of Science, 40(1), 126-138.

Wilson, P.A., Jenkyns, H.C., Elderfield, H., Larson, R.L., 1998. The paradox of drowned carbonate platforms and the origin of Cretaceous Pacific guyots. Nature, 392(6679), 889-894.

Woodroffe, C.D., 1981. Mangrove swamp stratigraphy and Holocene transgression, Grand Cayman Island, West Indies. Marine Geology, 41(3-4), 271-294.

Woodroffe, C.D., Stoddart, D.R., Giglioli, M.E.C., 1980. Pleistocene patch reefs and holocene swamp morphology, Grand Cayman Island, West Indies. Journal of Biogeography, 103-113.

Zhao, H., Jones, B., 2012a. Origin of "island dolostones": A case study from the Cayman Formation (Miocene), Cayman Brac, British West Indies. Sedimentary Geology, 243, 191-206.

Zhao, H., Jones, B., 2012b. Genesis of fabric-destructive dolostones: A case study of the Brac Formation (Oligocene), Cayman Brac, British West Indies. Sedimentary Geology, 267, 36-54.

Well ID	Depth (m)	Sample Type	Thin Section Samples	XRD Samples	Sr Ratio Samples	ϕ and K_{max} Samples
TW-1	49	Core/Cuttings	-	-	-	10
TW-2	117	Core/Cuttings	-	15	15	18
SH-3	40	Core	38	-	-	-
SH-4	15	Core	2	-	-	-
SH-5	50	Core	1	-	-	-
SH-12	31	Core	11	-	-	-
GTH-1	117	Core/Cuttings	-	68	24	13
BH-10	28	Core	-	-	-	5
SHT-4	146	Core/Cuttings	15	58	26	26
RG-1	91	Cuttings	-	54	28	-
RG-4	91	Cuttings	-	55	-	-
CUC-1	114	Core/Cuttings	-	28	14	-
CUC-3	110	Cuttings	-	63	17	-
CUC-4	122	Cuttings	-	74	25	-
GET-1	113	Core/Cuttings	8	48	15	22
LV-1	21	Core/Cuttings	9	-	-	-
LV-2	155	Core/Cuttings	28	72	35	20
WMF-1	64	Core/Cuttings	3	10	-	5
WMF-2	28	Core/Cuttings	-	-	-	4
WMF-4	12	Core/Cuttings	-	-	-	3
WMF-12	30	Core	-	-	-	11
RTR-1	139	Cuttings	25	91	24	-
Total			140	636	223	137

Appendix 1: List of samples and data from the wells on western and central Grand Cayman used for this study (see Fig. 2A, 2C for locations), including the maximum depth reached from drilling.

Well ID	Pedro Castle Formation	Cayman Formation - FA4	Cayman Formation - FA3	Brac Formation - FA2	Brac Formation - FA1
TW-1	not present	7 m	n/a	n/a	n/a
TW-2	8 m	10 m	59 m	83 m	100 m
SH-3	6 m	28 m	n/a	n/a	n/a
SH-4	6 m	14 m	n/a	n/a	n/a
SH-5	7 m	30 m	n/a	n/a	n/a
SH-12	8 m	15 m	n/a	n/a	n/a
GTH-1	12 m	16 m	56 m	79 m	106 m
BH-10	10 m	14 m	n/a	n/a	n/a
SHT-4	10 m	19 m	62 m	77 m	104 m
RG-1	6 m	22 m	–	74 m	–
RG-4	8 m	18 m	–	–	–
CUC-1	9 m	21 m	–	–	110 m
CUC-3	14 m	24 m	–	74 m	96 m
CUC-4	8 m	27 m	–	72 m	101 m
GET-1	3 m	12 m	61 m	73 m	–
LV-1	0 m	n/a	n/a	n/a	n/a
LV-2	n/a	25 m	50 m	123 m	–
WMF-1	not present	0 m	35 m	n/a	n/a
WMF-2	not present	0 m	–	n/a	n/a
WMF-4	not present	0 m	–	n/a	n/a
WMF-12	not present	0 m	–	n/a	n/a
RTR-1	not present	0 m	48 m	129 m	n/a

Appendix 2: Depth to the top of each formation and facies association identified in this study on western and central Grand Cayman. Note that the top of FA4 of the Cayman Formation is formed by the Cayman Unconformity and the top of FA2 of the Brac Formation is formed by the Brac Unconformity. Depth is relative to modern sea level.

Well ID	Depth (m)	87Sr / 86Sr	2 Std Error	Formation
TW-2	10.7	0.709125	0.000016	Pedro Castle
TW-2	19.8	0.709065	0.000015	Cayman
TW-2	29.0	0.709061	0.000019	Cayman
TW-2	38.1	0.709052	0.000015	Cayman
TW-2	47.2	0.709075	0.000016	Cayman
TW-2	56.4	0.709035	0.000015	Cayman
TW-2	64.0	0.709037	0.000029	Cayman
TW-2	68.9	0.709064	0.000031	Cayman
TW-2	73.8	0.709021	0.000024	Cayman
TW-2	76.8	0.709032	0.000026	Cayman
TW-2	88.4	0.708967	0.000014	Brac
TW-2	94.5	0.708979	0.000017	Brac
TW-2	103.6	0.708940	0.000017	Brac
TW-2	108.2	0.708965	0.000012	Brac
TW-2	115.8	0.708992	0.000012	Brac
GTH-1	13.9	0.709032	0.000016	Pedro Castle
GTH-1	20.0	0.709122	0.000009	Pedro Castle
GTH-1	26.1	0.709024	0.000014	Cayman
GTH-1	30.6	0.709036	0.000009	Cayman
GTH-1	35.2	0.709020	0.000014	Cayman
GTH-1	38.3	0.709016	0.000014	Cayman
GTH-1	42.8	0.708993	0.000011	Cayman
GTH-1	50.4	0.709035	0.000017	Cayman
GTH-1	56.5	0.709066	0.000011	Cayman
GTH-1	61.1	0.709008	0.000008	Cayman
GTH-1	62.6	0.709042	0.000011	Cayman
GTH-1	68.7	0.709127	0.000006	Cayman
GTH-1	74.8	0.709055	0.000007	Cayman
GTH-1	77.9	0.709015	0.000017	Cayman
GTH-1	82.4	0.708951	0.000009	Brac
GTH-1	87.0	0.708964	0.000017	Brac
GTH-1	91.6	0.708933	0.000007	Brac
GTH-1	93.1	0.709058	0.000011	Brac
GTH-1	94.6	0.708985	0.000010	Brac
GTH-1	96.2	0.709014	0.000011	Brac
GTH-1	102.3	0.708969	0.000008	Brac
GTH-1	106.8	0.709004	0.000013	Brac
GTH-1	111.4	0.708944	0.000006	Brac
GTH-1	116.0	0.709013	0.000018	Brac
SHT-4	8.8	0.709052	0.000010	Pedro Castle
SHT-4	15.8	0.709052	0.000014	Pedro Castle
SHT-4	19.7	0.709035	0.000013	Cayman
SHT-4	24.2	0.709012	0.000017	Cayman
SHT-4	29.7	0.709025	0.000013	Cayman
SHT-4	34.3	0.708991	0.000017	Cayman
SHT-4	39.8	0.709028	0.000009	Cayman
SHT-4	45.9	0.708987	0.000011	Cayman
SHT-4	52.0	0.709031	0.000014	Cayman
SHT-4	58.1	0.708995	0.000011	Cayman
SHT-4	64.8	0.709022	0.000010	Cayman
SHT-4	72.4	0.709024	0.000017	Cayman
SHT-4	75.7	0.709048	0.000016	Cayman
SHT-4	80.6	0.709000	0.000014	Brac
SHT-4	85.5	0.708941	0.000011	Brac
SHT-4	90.2	0.708920	0.000014	Brac
SHT-4	92.4	0.708945	0.000011	Brac
SHT-4	93.7	0.708948	0.000013	Brac
SHT-4	98.3	0.708961	0.000013	Brac

Appendix 3: List of all average $^{87}Sr/^{86}Sr$ isotope ratios used for this study from the wells on western and central Grand Cayman showing sample locations and depths, as well as the 2 standard error of the mean for the analysis.

Well ID	Depth (m)	87Sr / 86Sr	2 Std Error	Formation
SHT-4	102.9	0.708951	0.000009	Brac
SHT-4	111.1	0.708963	0.000010	Brac
SHT-4	117.5	0.709046	0.000013	Brac
SHT-4	123.3	0.708997	0.000017	Brac
SHT-4	127.7	0.708927	0.000009	Brac
SHT-4	136.7	0.709015	0.000017	Brac
SHT-4	146.3	0.708936	0.000014	Brac
RG-1	6.9	0.709023	0.000027	Pedro Castle
RG-1	9.9	0.709104	0.000011	Pedro Castle
RG-1	13.0	0.709086	0.000017	Pedro Castle
RG-1	16.0	0.709068	0.000017	Pedro Castle
RG-1	19.1	0.709094	0.000030	Pedro Castle
RG-1	22.1	0.709057	0.000014	Cayman
RG-1	25.1	0.709007	0.000017	Cayman
RG-1	28.2	0.709052	0.000017	Cayman
RG-1	31.2	0.709033	0.000017	Cayman
RG-1	34.3	0.709054	0.000011	Cayman
RG-1	37.3	0.709054	0.000011	Cayman
RG-1	40.4	0.709071	0.000014	Cayman
RG-1	45.0	0.709054	0.000016	Cayman
RG-1	48.0	0.709021	0.000018	Cayman
RG-1	51.1	0.709029	0.000011	Cayman
RG-1	54.1	0.709038	0.000014	Cayman
RG-1	57.2	0.708966	0.000017	Cayman
RG-1	60.2	0.709072	0.000023	Cayman
RG-1	63.2	0.708997	0.000011	Cayman
RG-1	66.3	0.708977	0.000010	Cayman
RG-1	69.3	0.708970	0.000013	Cayman
RG-1	72.4	0.708966	0.000017	Cayman
RG-1	75.4	0.708947	0.000013	Brac
RG-1	78.5	0.708945	0.000016	Brac
RG-1	81.5	0.708973	0.000017	Brac
RG-1	84.6	0.708975	0.000017	Brac
RG-1	87.6	0.708984	0.000014	Brac
RG-1	90.7	0.709013	0.000013	Brac
CUC-1	14.3	0.709015	0.000013	Pedro Castle
CUC-1	29.6	0.709009	0.000012	Cayman
CUC-1	41.8	0.708993	0.000012	Cayman
CUC-1	56.4	0.708990	0.000013	Cayman
CUC-1	62.5	0.709013	0.000014	Cayman
CUC-1	65.5	0.709027	0.000014	Cayman
CUC-1	70.9	0.708952	0.000014	Brac
CUC-1	76.2	0.709021	0.000014	Brac
CUC-1	81.1	0.708961	0.000016	Brac
CUC-1	90.2	0.709017	0.000013	Brac
CUC-1	93.0	0.709008	0.000013	Brac
CUC-1	102.1	0.708990	0.000011	Brac
CUC-1	111.3	0.708995	0.000012	Brac
CUC-1	114.3	0.708922	0.000014	Brac
CUC-3	16.0	0.709014	0.000011	Pedro Castle
CUC-3	22.1	0.709106	0.000011	Pedro Castle
CUC-3	28.2	0.709008	0.000011	Cayman
CUC-3	34.3	0.709026	0.000013	Cayman
CUC-3	40.4	0.709002	0.000010	Cayman
CUC-3	46.5	0.709016	0.000014	Cayman
CUC-3	52.6	0.709008	0.000011	Cayman
CUC-3	58.7	0.708954	0.000013	Cayman
CUC-3	64.8	0.708984	0.000014	Cayman